Studies on metal complexes with acylhydrazones based on heterocyclic carbonyl compounds

Thesis submitted to

Cochin University of Science and Technology

in partial fulfillment of the requirements

for the award of the degree of

Doctor of Philosophy

in

Chemistry

by

Sheeja S. R.

Department of Applied Chemistry
Cochin University of Science and Technology
Kochi - 682 022

July 2010

Studies on metal complexes with acylhydrazones based on heterocyclic carbonyl compounds

Ph. D. thesis under the Faculty of Science

Author:

Sheeja S. R.
Research Fellow, Department of Applied Chemistry
Cochin University of Science and Technology
Kochi, India 682 022
Email: sheejasr@cusat.ac.in

Research Advisor:

Dr. M.R. Prathapachandra Kurup
Professor
Department of Applied Chemistry
Cochin University of Science and Technology
Kochi, India 682 022
Email: mrp@cusat.ac.in

Department of Applied Chemistry
Cochin University of Science and Technology
Kochi, India 682 022

July 2010

Front cover: Crystal structure of quinoline-2-carbaldehyde benzoyl hydrazone monohydrate

Back cover: Supramolecular chain mediated by intermolecular hydrogen bonding interactions in the crystal structure of quinoline-2-carbaldehyde benzoyl hydrazone monohydrate

---

.... to my beloved

Achan & Amma

DEPARTMENT OF APPLIED CHEMISTRY
COCHIN UNIVERSITY OF SCIENCE AND TECHNOLOGY
KOCHI - 682 022, INDIA

Phone Off. 0484-2575804
Phone Res. 0484-2576904
Telex: 885-5019 CUIN
Fax: 0484-2577595
Email: mrp@cusat.ac.in
mrp_k@yahoo.com

Dr. M.R. Prathapachandra Kurup
Professor

06-07-2010

Certificate

     This is to certify that the thesis entitled "**Studies on metal complexes with acylhydrazones based on heterocyclic carbonyl compounds**" submitted by Ms. Sheeja S.R., in partial fulfillment of the requirements for the degree of Doctor of Philosophy, to the Cochin University of Science and Technology, Kochi-22, is an authentic record of the original research work carried out by her under my guidance and supervision. The results embodied in this thesis, in full or in part, have not been submitted for the award of any other degree.

M. R. Prathapachandra Kurup
(Supervisor)

DECLARATION

I hereby declare that the work presented in this thesis entitled "**Studies on metal complexes with acylhydrazones based on heterocyclic carbonyl compounds**" is entirely original and was carried out independently under the supervision of Prof. M.R. Prathapachandra Kurup, Department of Applied Chemistry, Cochin University of Science and Technology and has not been included in any other thesis submitted previously for the award of any other degree.

06-07-2010   **Sheeja S. R.**
Kochi-22

PREFACE

Coordination chemistry has evolved as an important subject area in current research activities. Coordination complexes show diversity in structures depending on the metal ion, its coordination number and the denticity of the ligands used. This has led to their usage as sensors, medicines etc. The presence of more electronegative nitrogen and oxygen on the ligand is established to enhance the coordinating possibilities of ligands. In this aspect, a great deal of attention has been focused on the complexes formed by transition metal ions with hydrazones. Recent years witnessed an intensive investigation of the coordination chemistry of Schiff bases due to their interesting coordination properties and diverse applications.

The chemistry of hydrazones has received considerable attention due to their proliferate applications. The transition metal complexes of them found applications in biology, medicine and industry.

The present work deals with the complexation of hydrazones with various transition metal ions. Complexes of vanadium(IV), manganese(II), cobalt(II), copper(II) and zinc(II) have been prepared. Various spectral techniques are employed for characterization.

The work is presented in seven chapters and the last section deals with summary and conclusion. The studies reveal that the acylhydrazones coordinate in different modes depending on the reaction conditions, resulting in complexes with varying geometrical configurations.

The work in this thesis was carried out by the author in the Department of Applied Chemistry during 2006-2010. The primary aim of these investigations was to probe the physicochemical studies of hydrazones and their transition metal complexes.

Acknowledgement

The work presented in this thesis could not have been accomplished without the help of several individuals. There are many people who made this journey easier with words of encouragement, invaluable support and friendship. It is a pleasure to thank them all who have helped and inspired me all through this period.

I am deeply indebted to my supervising guide Prof. M.R. Prathapachandra Kurup for his patience, motivation, enthusiasm and immense knowledge throughout the entire course of this work. His stimulating suggestions and encouragement helped me in all the time of research and writing of the thesis.

I express my sincere thanks to Prof. K.K. Mohammed Yusuff for his encouragement and support as my doctoral committee member. I am very much thankful to Prof. K. Sreekumar, Head, Department of Applied Chemistry, CUSAT for the support and cooperation during the period of this work. I extend my gratitude to Prof. K. Girish Kumar, Former Head, for providing necessary help and valuable suggestions. I am thankful for the support received from all the teaching and non-teaching staff of the Department of Applied Chemistry, CUSAT.

I would like to extend my gratitude to the Council of Scientific and Industrial Research (CSIR), New Delhi, India for the financial support offered. I deeply acknowledge the head of the institutions of SAIF Kochi, IISc Bangalore, IIT Roorkee and IIT Bombay for the services rendered in sample analyses. I express my thanks to Dr. Chitrapriya N., Bharathiar University, Coimbatore, India and Dr. C. Jayabalakrishnan, Sri Ramakrishna Mission Vidyalaya College of Arts and Science, Coimbatore, India for helping me to record cyclic voltammograms of the compounds.

I am grateful to my seniors Dr. Suni V, Dr. P.F. Rapheal, Dr. Mini Kuriakose, Dr. Bessy Raj, Dr. Sreesha Sasi, Dr. Manoj E., Dr. Binu Varghese and Dr. Suja Krishnan for their help and cooperation during my research work. It is a pleasure to thank Dr. Seena E.B. for all the help offered throughout my research work. My special thanks to my friend Dr. Leji Latheef for her valuable advices and motivation. I am thankful to all my labmates Laly miss, Jessy miss, Renjusha, Prem, Reena chechi, Dhanya, Sarika, Roji, Jayakumar sir, Annie miss, Shimi, Sarika, Bibitha, Asokan sir, Anju and Nisha for their whole-hearted support during this period. Particularly I am thankful to Jinsa who helped me a lot during the final stages of the manuscript preparation. I express my profound gratitude to Eesan sir and Jinsa for doing EPR simulation work for me. I cherish the moments with Litha which make CUSAT life quite memorable.

Contents

Chapter **3**

VANADIUM(IV) COMPLEXES OF ACYLHYDRAZONES: SYNTHESES AND SPECTRAL INVESTIGATIONS

Chapter **4**

SYNTHESES AND SPECTRAL INVESTIGATIONS OF MANGANESE(II) COMPLEXES OF ACYLHYDRAZONES

Chapter **5**

SYNTHESES AND CHARACTERIZATION OF
COBALT(II) COMPLEXES OF ACYLHYDRAZONES

Chapter **6**

SYNTHESES OF COPPER(II) COMPLEXES OF
ACYLHYDRAZONES AND THEIR CHARACTERIZATION

Chapter **7**

SYNTHESES AND CHARACTERIZATION OF ZINC(II) COMPLEXES OF ACYLHYDRAZONES

SUMMARY AND CONCLUSION

…..ഇരു…..

A CONCISE OF ACYLHYDRAZONES AND THEIR METAL COMPLEXES

1.1. Introduction

Coordination chemistry is a challenging field in inorganic chemistry and has evolved as an important subject area in current research activities. Coordination compounds have been known for well over a century and the scientific interest in these compounds increased dramatically. The field of coordination chemistry has been widely explored. The recent surge in the popularity of coordination compounds is their perceived applications in many areas such as catalysis, analytical chemistry and medicine [1].

Coordination complexes show diversity in structures depending on the metal ion, its coordination number and the denticity of the ligands used and therefore, the selection of ligand is crucial in determining the properties and structures of coordination compounds. The presence of more electronegative nitrogen and oxygen on the ligand is established to enhance the coordinating possibilities of ligands. Hence

1

the coordination chemistry of nitrogen-oxygen donor ligands is an interesting area of research. In this aspect, a great deal of attention has been focused on the complexes formed by transition metal ions with acylhydrazones. In view of their applicability in various fields, acylhydrazones, with triatomic >C=N–N< linkage, take the forefront position in the development of coordination chemistry [2].

1.2. Acylhydrazones

Hydrazides with general formula, $NH_2–NH–R$, are derived from hydrazines ($NH_2–NH_2$) by suitable substitution. Hydrazones are compounds obtained by the reaction of hydrazides with aldehydes or ketones (Scheme I). If the substituent R is an acyl group, then it is called acylhydrazone. The –C=O group provides the possibility for the electron delocalization within the hydrazone moiety and also, increases the denticity of these compounds (Fig. 1.1).

| Hydrazine | Hydrazide | Hydrazone |
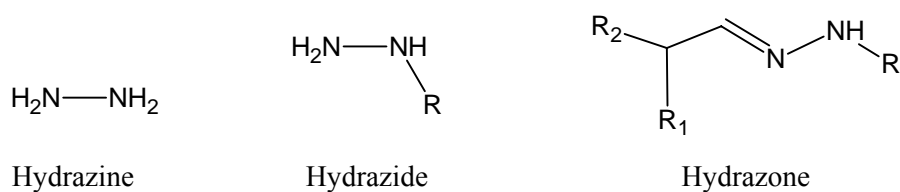
Scheme I
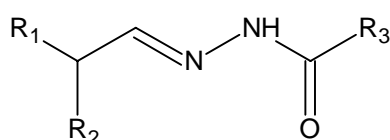
Fig. 1.1. General formula of a substituted acylhydrazone.

The amide oxygen and azomethine nitrogen are the available donor sites present in the acylhydrazone compounds. Further, the number of coordination sites can be increased by the suitable substitution on the hydrazone framework. Consequently, the acylhydrazones can chelate to various metal ions, forming complexes with flexible stereochemistries, applications and with enhanced bioactivity compared to the parental ligands. The acylhydrazones attribute more

than two coordination sites, the number of which depends on the carbonyl compound and on their tautomeric equilibrium [3,4].

One important facet of acylhydrazones is their ability to exist in tautomeric forms (Fig. 1.2). The existence of tautomeric equilibrium in these compounds makes it possible to obtain coordination compounds containing either neutral keto form or deprotonated enol form. The tautomerism as well as the renowned transition metal chelating properties of these compounds allows various structural possibilities for the corresponding metal complexes [5].

Keto form (I)   Enol form (II)
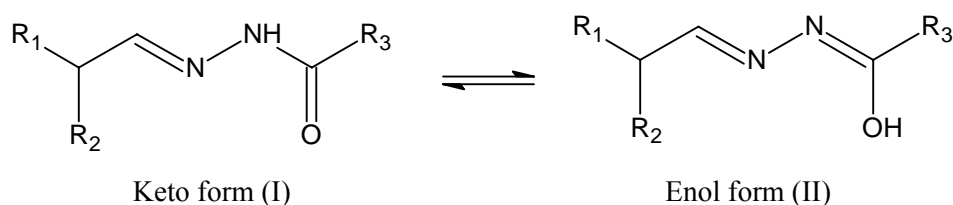
Fig. 1.2. Tautomerism in acylhydrazones.

The synthesis of transition metal complexes with ligands of nitrogen and oxygen donors has stimulated interest due to their vast variety of biological activities such as pharmacological, antitumor, fungicide, bactericide, anti-inflammatory and antiviral. These effects are based on their tendency to form metal chelates with transition metal ions. The reaction of acylhydrazones with transition metal ions can proceed according to two pathways attaining the ketonic or enolic structure of the hydrazide part of the molecule.

1.3. Importance of acylhydrazones

In the last two decades, much interest has been focused on compounds containing hydrazide and hydrazone moieties and their complexes with first row transition metal ions. Such interest has been growing due to their use in medicine (for treatment of tuberculosis), biological systems and analytical chemistry [6-9].

The coordination chemistry of acylhydrazones is an intensive area of study and numerous transition metal complexes of these ligands have been investigated.

Many researchers have synthesized a number of new acylhydrazones because of their ease of synthesis.

Interest in coordination chemistry of acylhydrazones is connected with their wide using as drugs, photo-thermochromic compounds and precursors for organic synthesis [10-13]. In the case of acylhydrazones, the presence of the carbonyl oxygen atom promotes the formation of a chelate binding center [3]. Acylhydrazones and their metal complexes possess pronounced biological and pharmaceutical activities as antitumor [14-16], antimicrobial [17], antituberculosis [18] and antimalarial agents [19]. Patole *et al.* have screened the 2-acetylpyridine benzoyl hydrazone and its copper complex for their antitubercular activity [18]. The results were found to be comparable with the drug Ciprofloxacin. The antituberculous activity of hydrazides and hydrazones was ascribed to their ability to form more or less stable chelates with the transition metal ions. Hydrazones play an important role in improving the antitumor selectivity and toxicity profile of antitumor agents by forming drug carrier systems employing suitable carrier proteins [20].

Furthermore, some hydrazones are used as quantitative analytical reagents, especially in colorimetric and fluorimetric determinations of metal ions. Salicylaldehyde formyl hydrazone is one of the most sensitive reagents for the fluorimetric determination of aluminium. They are also employed as extracting agents in spectrophotometric determination of some ions [21-23] and spectrophotometric determination of some species in pharmaceutical formulations [24], as well as used in catalytic processes [25,26] and waste water treatment [27]. The 2,2'-bipyridyl-2-pyridyl hydrazone (BPPH) can be used as a reagent for the spectrophotometric determination of cyanocobalamine and of cobalt in sea water and brine.

Hydrazones, such as pyridoxal isonicotinoyl hydrazone, salicyladehyde benzoyl hydrazone and 2-pyridyl carboxaldehyde-2-thiophene carboxaldehyde hydrazone, act as orally effective drugs for the treatment of iron overload diseases or

genetic diseases such as β-thalassemia [28,29]. Metal complexes of acylhydrazones have found applications in various chemical processes like nonlinear optics, sensors etc. [30] and have been used in the separation and concentration of palladium and platinum in road dust [31].

Hydrazones have found wide applications in synthetic chemistry [32], to be used as indicators. Hydrazones are now being used extensively in detection and quantitative determination of several metals, for the preparation of compounds having diverse structures, analytical chemistry for the identification and isolation of carbonyl compounds [33].

The hydrazones have been used for different purposes such as herbicides, insecticides, nematocides, rodenticides and plant growth regulators [34]. The hydrazones are also important for their use as plasticizers and stabilizers for polymers [35], polymerization initiators and antioxidants [36].

Quinolines are heterocyclic compounds, which are worth to study for many reasons, chief among them being their prevalence among biologically active molecules. Derivatives of quinoline have been widely used in the synthesis of antibacterial, antihypertensive and antifungal drugs [37].

These molecules possess non-centrosymmetry and hence they are widely used in the synthesis of molecules having non-linear responses [37,38]. Molecular based second-order nonlinear optical (NLO) chromophores have recently attracted much interest because of their potential applications in emerging optoelectronic technologies. As for molecular design of new non-linear optical materials based on quinoline, the pyridine ring can be thought of as an acceptor group within the molecule, with the benzene ring as a donor. Increasing the acceptor character of the pyridine ring and/or increasing the donor character of the benzene ring would, therefore, substantially increase the non-linearity of this class of compounds [39].

More recently, 8-hydroxyquinoline aluminum has been widely used as the emissive and electron transporting material in organic light emitting devices [40,41].

El-Sonabati et al. [42] reported the supramolecular structures and stereochemical versatility of azoquinoline containing novel rare earth metal complexes.

Schiff bases containing the RC=N– group constitute an interesting class of chelating agents capable to coordinate with one or more metal ions giving mononuclear or polynuclear metal complexes, which serve as models for metalloproteins [43]. It has been suggested that monoamine oxidase enzyme inhibition occurs via metal Schiff base complex formation [44]. Copper(II) salicylaldehyde benzoyl hydrazone [45] and 2-pyridine carboxaldehyde–2-pyridyl hydrazone [46] have been reported to produce significant inhibition of tumor growth [47].

Recently, complexes of zinc(II) with di-2-pyridyl ketone benzoyl hydrazone and complexes of nickel(II) with di-2-pyridyl ketone salicyloyl hydrazone were used to develop a highly sensitive spectrophotometric method [48,49]. Selective Zn^{2+} fluorescent sensors, di(2-quinolinecarbaldehyde)-2,2$^{'}$-bibenzoyl hydrazone and di(2-quinolinecarbaldehyde)-6,6$^{'}$-dicarboxylic acid hydrazone-2,2$^{'}$-bipyridine, have been designed and prepared. Zinc binding red shifts the emission band and also enhances the fluorescence intensity by an order of magnitude based on the deprotonization strategy *via* self-assembly.

The most widely used fluorescent probes for Zn^{2+} are *N*-(6-methoxy-8-quinolyl)-*p*-toluenesulfonamide and its congeners, which are quinoline derivatives bearing sulfonamide groups that give substantial fluorescence enhancement upon Zn(II) bonding [50]. Richardson *et al.* have designed and patented a novel class of ligands based on 2-pyridinecarbaldehyde isonicotinoyl hydrazone (HPCIH), that have shown great promise *in vitro*, demonstrating a high iron chelation efficacy [51,52].

1.4. Bonding and coordination strategy of acylhydrazones

The mode of bonding depends on the nature of both the ligand and metal ions, the anion of the metal salt and the solvent used. Based on the previous studies, the extent of $p\pi$-$d\pi$ interaction between the hydrazone group and the

central metal ion is determined by the type and position of the different substituents relative to the parent hydrazine compound.

Also, the stability of the hydrazone chelates is higher than that of the corresponding hydrazine compounds and depends on the different substituents. For the same metal ion, the stability of the chelates is highly affected by the nature of the donor atoms and the medium of the reaction.

Depending on the reaction conditions and the stability of the metal complex formed, the acylhydrazones show a variety of coordination modes with the metal. The number and type of the substituents also influence the coordination mode.

If the carbonyl compound contains a pyridine ring or derivatives of pyridine *viz*. 2-benzoylpyridine, pyridine-2-carbaldehyde and quinoline-2-carbaldehyde, then the acylhydrazone can act as a tridentate ligand. The expected coordination sites are azomethine nitrogen, amide oxygen and the ring nitrogen in the carbonyl compound.

The amide oxygen can coordinate to the metal either in enolate form (Structure I) or in keto form (Structure II). If the medium of the reaction is acidic, then the deprotonation will not be easy and therefore, in such cases, coordination with neutral keto form is expected. In some cases, along with the principal ligand, coligands such as anions may be present in order to make the complex neutral.

Structure I   Structure II
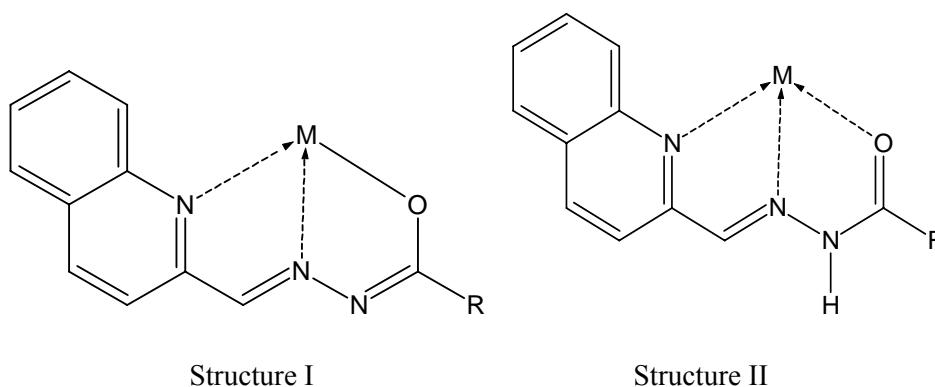
Sometimes, two ligands may coordinate to the same metal and six coordinate tetragonal geometry is expected (Structure III).
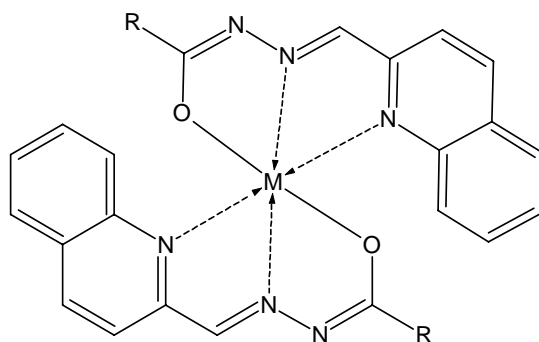
Structure III

In some other cases, an atom or group may act as a bridging ligand and the resulting complex will be a dimer (Structure IV).
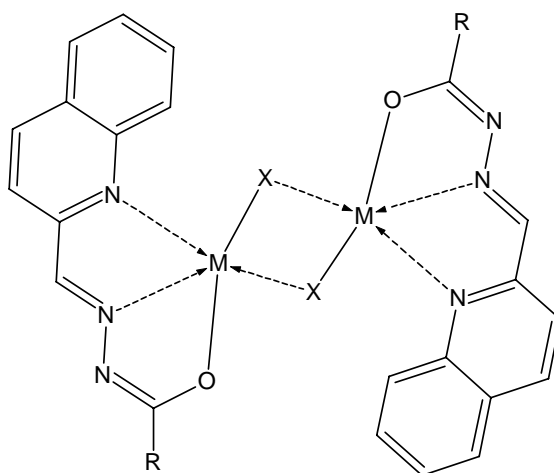
Structure IV

If the hydrazide part of the ligand contains a heteroatom, it may also involve in coordination. If it is a nicotinoyl derivative, the presence of nitrogen at the meta position of the ring will provide an additional coordination site. Usually this donor atom does not involve in coordination to the metal in the same molecule, but it can coordinate to the adjacent metal centre giving a polymeric compound (Structure V).
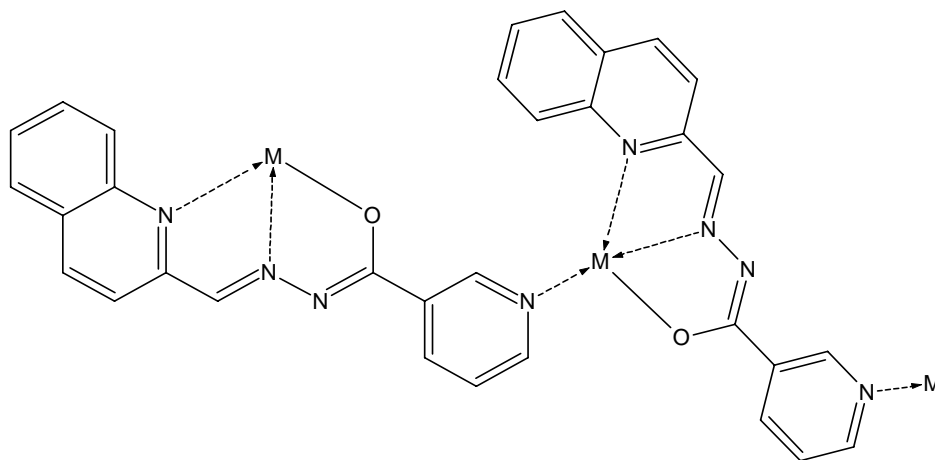
Structure V

1.5. Objectives of the present work

Acylhydrazones and their coordination compounds are well known to be biologically important and interest in studying this class of compounds lies in their antibacterial, antitumour and antitubercular activities. Also, they have been used as analytical reagents and also as polymer-coatings, inks, pigments and fluorescent materials. So acylhydrazones constitute an important class of nitrogen-oxygen donor ligands.

The versatile applications of metal complexes of acylhydrazones in various fields prompted us to synthesize the tridentate NNO-donor hydrazones and their metal complexes. As part of our studies on transition metal complexes with these ligands, we undertook the current work with the following objectives:

The present work is mainly concerned with the studies on metal complexes of acylhydrazones derived from quinoline-2-carbaldehyde. Here, quinoline-2-carbaldehyde benzoyl hydrazone (HQb) and quinoline-2-carbaldehyde nicotinic hydrazone (HQn) were selected as the ligands.

The composition of these hydrazones was determined by the partial elemental analyses. For the characterization of these compounds, IR, UV and

9

NMR spectroscopy were used. The molecular structure of HQb·H_2O was obtained by single crystal XRD studies.

The coordination modes of the ligands with transition metals have been investigated by using different physicochemical techniques.

In the present study, oxovanadium(IV), manganese(II), cobalt(II), copper(II) and zinc(II) complexes of these ligands were prepared. They were characterized by various spectroscopic techniques, magnetic studies and cyclic voltammetry. Single crystals of some of the metal complexes were isolated, but due to the low quality, they did not diffract and the XRD studies were failed.

This thesis is divided into seven chapters.

Chapter I, entitled 'a concise of acylhydrazones and their metal complexes' describes importance of acylhydrazones, their mode of coordination and the relevance of present investigation. Brief introduction to the different analytical techniques for the characterization is also presented in this chapter

Chapter II explains the preparation of the acylhydrazones and their physicochemical investigations.

Chapters III, IV, V, VI and VII discuss the procedure followed for the preparation of the complexes of oxovanadium(IV), manganese(II), cobalt(II), copper(II) and zinc(II) and their physicochemical investigations.

1.6. Physical measurements

The physicochemical methods adopted during the present investigation are discussed below:

1.6.1. Partial elemental analyses

Elemental analyses were carried out using Vario EL III CHNS analyzer at the Sophisticated Analytical Instruments Facility, Kochi, India.

1.6.2. Conductivity measurements

The molar conductivities of the complexes in dimethylformamide (DMF) solutions (10^{-3} M) at room temperature were measured using a direct reading conductivity meter at the Department of Applied Chemistry, CUSAT, Kochi, India.

1.6.3. Magnetic susceptibility measurements

The magnetic susceptibility measurements were done in the polycrystalline state at room temperature on a PAR model 155 Vibrating Sample Magnetometer at 5 kOe field strength at the Indian Institute of Technology, Roorkee, India.

1.6.4. Infrared spectroscopy

IR spectra were recorded on a Thermo Nicolet AVATAR 370 DTGS model FT-IR Spectrophotometer in the range 4000-400 cm^{-1} with KBr pellets and ATR technique at the SAIF, Kochi, India. The far IR spectra were recorded using polyethylene pellets in the 500-100 cm^{-1} region on a Nicolet Magna 550 FTIR instrument at the SAIF, Indian Institute of Technology, Bombay, India.

1.6.5. Electronic spectroscopy

UVD-3500, UV-vis Double Beam Spectrophotometer was used to record the electronic spectra from acetonitrile/DMF solutions in the range 50000-11000 cm^{-1} at the Department of Applied Chemistry, CUSAT, Kochi, India.

1.6.6. NMR spectroscopy

^{1}H NMR, ^{13}C NMR, ^{1}H-^{1}H COSY and HSQC spectra were recorded using Bruker AMX 400 FT-NMR Spectrometer with DMSO-d_6 as solvent and TMS as the internal standard at the Sophisticated Instrumentation Facility, Indian Institute of Science, Bangalore, India.

1.6.7. EPR spectroscopy

The EPR spectra of the polycrystalline samples at 298 K and DMF solution at 77 K were recorded in the X-band, using 100 kHz modulation; g factors were quoted relative to the standard marker TCNE (g = 2.00277), at the SAIF, IIT Bombay, Mumbai, India.

1.6.8. X-ray crystallography

The data were collected using Oxford Diffraction Xcalibur-S diffractometer, equipped with graphite-monochromated Mo Kα (λ = 0.71073 Å) radiation at the National Single Crystal X-ray Facility, IIT Bombay, Mumbai, India. The intensity data were collected at 120(2) K by the ω/q-scan mode. The cell refinement was done using the CrysAlis RED software [53]. The structure was solved by direct methods with the program SHELXS-97 and refined by full matrix least squares on F^2 using SHELXL-97 [54]. The graphical tool used were Diamond version 3.1f [55] and Mercury [56].

1.6.9. Cyclic voltammetry

Cyclic voltammograms were recorded on a CHI II20A electrochemical analyzer with a three electrode compartment consisting of a platinum disc working electrode, platinum wire counter electrode and Ag/Ag$^+$ reference electrode, at the Department of Chemistry, Bharathiar University, Coimbatore, India. The solutions of complexes in DMF have been used to study the electrochemical properties using TBAP (tetrabutylammonium phosphate) as the supporting electrolyte. The voltammogram is run between the potentials of –200 and +200 mV at a scan speed of 100 mV/s.

1.6.10. Thermogravimetric Analysis

TG-DTA-DTG analyses of the hydrazones and their complexes were carried out under nitrogen at a heating rate of 10 °C min^{-1} using a Perkin Elmer Pyris Diamond TG/DTA analyzer.

References

[1]   J.C. Craliz, J.C. Rub, D. Willis, J. Edger, Nature 34 (1955) 176.

[2]   A. Rana, R. Dinda, P. Sengupta, S. Ghosh, L.R. Falvello, Polyhedron 21 (2002) 1023.

[3]   S.S. Tandon, S. Chander, L.K. Thompson, Inorg. Chim. Acta 300-302 (2000) 683.

[4]   H. Oshio, K. Toriumi, Y. Maeda, Y. Takashima, Inorg. Chem. 30 (1991) 4252.

[5]   J.C. Jeffery, P. Thornton, M.D. Ward, Inorg. Chem. 33 (1994) 3612.

[6]   T.R. Rao, M. Sahay, R.C. Aggarwal, Synth. React. Inorg. Met-Org. Chem. 15 (1985) 209.

[7]   S. Sridhar, M. Saravanan, A. Ramesh, Eur. J. Med. Chem. 36 (2001) 615.

[8]   B. Bottari, R. Maccari, F. Monforte, R. Ottana, E. Rotondo, M. Vigorita, Bioorg. Med. Chem. Lett. 10 (2000) 657.

[9]   E. Ainscough, A. Brodie, J. Ranford, M. Waters, Inorg. Chim. Acta 236 (1995) 83.

[10]   E. Schmidt, Hydrazine and its Derivatives: Preparation, Properties, Applications, second ed. Wiley, New York 2001.

[11]   P.V. Bernhardt, P. Chin, D.R. Richardson, J. Biol. Inorg. Chem. 6 (2001) 801.

[12]   V. Kogan, V. Zelentsov, G. Larin, V. Lhukov, Complexes of Transitional Metals with Hydrazones, Nauka, Moscow, 1990.

[13]   U. Ragnarsson, Chem. Soc. Rev. 30 (2001) 205.

[14]   N. Terzioglu, A. Gürsoy, Eur. J. Med. Chem. 38 (2003) 781.

[15]   M.T. Cocco, C. Congiu, V. Lilliu, V. Onnis, Bioorg. Med. Chem. 14 (2006) 366.

[16]   J. Easmon, G. Puerstinger, T. Roth, H.-H. Fiebig, M. Jenny, W. Jaeger, G. Heinisch, J. Hofmann, Int. J. Cancer 94 (2001) 89.

[17]   P. Vicini, F. Zani, P. Cozzini, I. Doytchinova, Eur. J. Med. Chem. 37 (2002) 553.

[18]   J. Patole, U. Sandbhor, S. Padhye, D.N. Deobagkar, C.E. Anson, A. Powell, Bioorg. Med. Chem. Lett. 13 (2003) 51.

[19] A. Walcourt, M. Loyevsky, D.B. Lovejoy, V.R. Gordeuk, D.R. Richardson, Int. J. Biochem. Cell Biol. 36 (2004) 401.

[20] F. Kratz, U. Beyer, T. Roth, N. Tarasova, P. Collery, F. Lechenault, A. Cazabat, P. Schumacher, C. Unger, U. Falken, J. Pharm. Sci. 87 (1998) 338.

[21] S. Sivaramaiah, P.R. Reddy, J. Anal. Chem. 60 (2005) 828.

[22] S.H. Babu, K. Suvardhan, K.S. Kumar, K.M. Reddy, D. Rekha, P. Chiranjeevi, J. Hazard Mater. 120 (2005) 213.

[23] S.A. Berger, J. Microchem. 47 (1993) 317.

[24] A.A. El-Emam, F.F. Belal, M.A. Moustafa, S.M. El-Ashry, D.T. El-Sherbiny, S.H. Hansen, Farmaco 58 (2003) 1179.

[25] M.S. Niasari, A. Amiri, Appl. Catal. A 290 (2005) 46.

[26] P. Pelagatti, M. Carcelli, C. Pelizzi, M. Costa, Inorg. Chim. Acta 342 (2003) 323.

[27] M.G. El-Meligy, Sh. El-Rafie, K.M. Abu-Zied, Desalination 173 (2005) 33.

[28] T.B. Chaston, D.R. Richardson, Am. J. Hematol. 73 (2003) 200.

[29] P.V. Bernhardt, P. Chin, P.C. Sharpe, J.-Y.C. Wang, D.R. Richardson, J. Biol. Inorg. Chem. 10 (2005) 761.

[30] M. Bakir, I. Hassan, T. Johnson, O. Brown, O. Green, C. Gyles, M.D. Coley, J. Mol. Struct. 688 (2004) 213.

[31] X. Ge, I. Wendler, P. Schramel, A. Kettrup, React. Funct. Polymer 61 (2004) 1.

[32] A.V. Xavier (Ed.), Frontiers in Bioinorganic Chemistry, VCH, 1985.

[33] M. Fabian, G. Palmer, Biochemistry 40 (2001) 1867.

[34] I. Pozdnyakova, P.W. Stafshede, Biochemistry 40 (2001) 13728.

[35] U. Kühn, S. Warzeska, H. Pritzkow, R. Krämer, J. Am. Chem. Soc. 123 (2001) 8125.

[36] K.D. Karlin, J. Zubieta, Copper Coordination Chemistry: Biochemical and Inorganic Perspectives, Adenine Press Guilderland, New York 1983.

[37] A.G. Mac Diarmid, A.J. Epstein, in:S.A.Jenekhe, K.J.Wynne (Edn), Photonic and Optoelectronic Polymers, American Chemical Society, Washington DC, 1997.

[38] A.J. Epstein, Mater. Res. Soc. Bull. 22 (1997) 16.

[39] G. Purohit, G.C. Joshi, Indian J. Pure Appl. Phys. 41 (2003) 922.

[40] H.D. Burrows, M. Fernandes, J. Seixas de Melo, A.P. Monkman, S. Navaratnam, J. Am. Chem. Soc. 125 (2003) 15310.

[41] G.M. Credo, D.L. Winn, S.K. Buratto, Chem. Mater. 13 (2001)1258.

[42] A.Z. El-Sonbati, R.M. Issa, A.M. Abd El-Gawad, Spectrochim. Acta 68A (2007) 134.

[43] E.I. Solomon, R.K. Szilagyi, S.D. George, L. Basumallick, Chem. Rev. 104 (2004) 419.

[44] S. Bernard, C. Paillat, T. Oddos, M. Seman, R. Milcent, Eur. J. Med. Chem. 30 (1995) 471.

[45] L. Pickart, W.H. Goodwin, T.B. Murphy, D.K. Johnson, J. Cell Biochem. Suppl. 6 (1982) L-42.

[46] J.R.J. Sorenson, Chem. Ber. 20 (1984) 1110.

[47] M. Mohan, A. Kumar, M. Kumar, N.K. Jha, Inorg. Chim. Acta 136 (1987) 65.

[48] I. Gaubeur, M.C.C. Areias, L.H.S.A. Terra, M.E.V. Suárez-Iha, Spectrosc. Lett. 35 (2002) 455.

[49] I. Gaubeur, M. Guekezian, L.H.S.A. Terra, M.C.B. Moraes, C.L. Lago, J.R. Matos, M.E.V. Suárez-Iha, Polyhedron 23 (2004) 2095.

[50] D.-Y. Wu, L.-X. Xie, C.-L. Zhang, C.-Y. Duan, Y.-G. Zhao, Z.-J. Guo, J. Chem. Soc. Dalton Trans. (2006) 3528.

[51] D.R. Richardson, E. Becker, P.V. Bernhardt, Acta Cryst. C55 (1999) 2102.

[52] E. Becker, D.R. Richardson, J. Lab. Clin. Med. 134 (1999) 510.

[53] CrysAlis CCD and CrysAlis RED Versions 1.171.29.2 (CrysAlis 171. NET), Oxford Diffraction Ltd., Abingdon, Oxfordshire, England, 2006.

15

[54] G.M. Sheldrick, Acta Cryst. A64 (2008) 112.

[55] K. Brandenburg, Diamond Version 3.1f, Crystal Impact GbR, Bonn, Germany, 2008.

[56] C.F. Macrae, P.R. Edgington, P. McCabe, E. Pidcock, G.P. Shields, R. Taylor, M. Towler, J. van de Streek, J. Appl. Cryst. 39 (2006) 453.

…..ဆလ…..

Chapter 2

SYNTHESES AND CHARACTERIZATION OF ACYLHYDRAZONES

Contents

2.1 Introduction

2.2 Quinoline-2-carbaldehyde benzoyl hydrazone sesquihydrate (HQb·1.5H$_2$O)

2.3 Quinoline-2-carbaldehyde nicotinic hydrazone sesquihydrate (HQn·1.5H$_2$O)

References

2.1. Introduction

The hydrazones are formed by the condenzation of hydrazides with aldehydes or ketones. Acylhydrazones of heterocyclic ketones and aldehydes have prospective importance because they possess a broad spectrum of potentially useful biological activities. Hydrazide and hydrazone derivatives have interesting ligation properties with transition metal ions. Acylhydrazones and their metal complexes were widely studied due to their versatile applications in the field of analytical and medicinal chemistry [1-6]. The metal complex is found to be more active than the free ligand and some side effects may decrease upon complexation. The biological activities of many of these compounds were shown to be related to their metal chelating abilities.

Hydrazones have similarities in their donor properties with unsymmetrical salen (condensation product of salicylaldehyde and 1,2-diaminoethane) type ligands. Recently it was reported that such ligands, like non-symmetrical salens, can act as effective catalysts towards alkene epoxidation [7].

In analytical chemistry, hydrazones find wide applications as transition metal binders [8,9]. Studies have also shown that the azomethine nitrogen, which

17

has a lone pair of electrons in an sp^2 hybridized orbital, has considerable biological importance [10].

Acylhydrazone complexes of transition metal ions are known to provide useful models for the elucidation of the mechanism of enzyme inhibition by hydrazine derivatives [11,12] and for their possible pharmacological applications [13,14].

This chapter describes the synthesis and characterization of acylhydrazones. We synthesized two heteroacylhydrazones, which are derived from quinoline-2-carbaldehyde.

They are

    a)   Quinoline-2-carbaldehyde benzoyl hydrazone (HQb)

    b)   Quinoline-2-carbaldehyde nicotinic hydrazone (HQn)

Both the hydrazones consist of two nitrogen and one oxygen atoms, capable of coordination with the metal ion.

They were characterized by IR, electronic and NMR spectroscopy. Also, the crystal structure of quinoline-2-carbaldehyde benzoyl hydrazone monohydrate is reported.

2.2. Quinoline-2-carbaldehyde benzoyl hydrazone sesquihydrate (HQb·1.5H$_2$O)

The compound quinoline-2-carbaldehyde benzoyl hydrazone (Fig. 2.1) was prepared by refluxing equimolar solutions of benzhydrazide and quinoline-2-carbaldehyde in methanol.
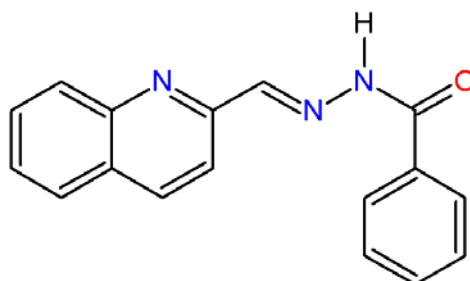
Fig. 2.1. Quinoline-2-carbaldehyde benzoyl hydrazone (HQb).

2.2.1. Experimental

2.2.1a. *Materials*

All the chemicals and solvents used for the syntheses were of analytical grade. Quinoline-2-carbaldehyde (Sigma Aldrich) and benzhydrazide (Sigma Aldrich) were used as received.

2.2.1b. *Synthesis*

Benzhydrazide (0.272 g, 2 mmol) dissolved in methanol (20 ml) was added to a hot solution of quinoline-2-carbaldehyde (0.314 g, 2 mmol) in the same solvent (20 ml). Two drops of glacial acetic acid were added to the reaction mixture. Then the above solution was refluxed for 4 hours and cooled to room temperature. The pale yellow product formed was filtered off, washed with methanol and dried over P_4O_{10} *in vacuo*. Yield – 84%, m.p. 143-145 °C. Elemental Anal. Found (Calcd) %: C, 67.81 (67.54); H, 4.86 (5.33); N, 14.40 (13.90) for $C_{17}H_{13}N_3O \cdot 1\frac{1}{2}H_2O$. % H_2O 8.50 (8.91) from TG data.

Colorless needle-like single crystals suitable for X-ray diffraction studies were obtained by the slow evaporation of its solution in ethanol.

The reaction scheme is depicted in the Scheme I.
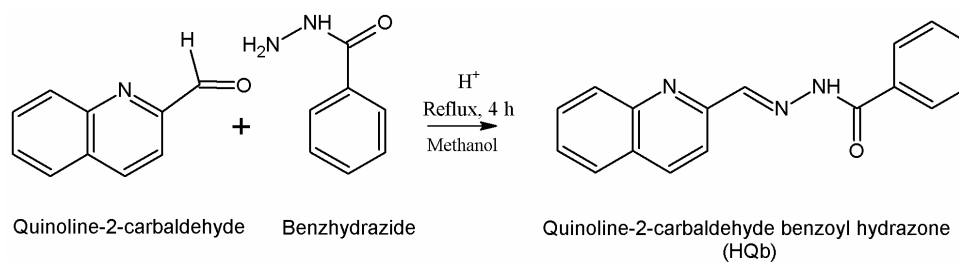
Scheme I.

2.2.2. Infrared spectrum

Infrared spectral data give details about the characteristic groups present in the compound. IR spectral analysis was done using KBr on Thermo Nicolet AVATAR 370 DTGS FT-IR spectrophotometer.

The band at 1655 cm^{-1} is attributable to the presence of carbonyl group in the compound which authenticates the existence of keto form in solid state and the crystal structure confirms this assignment. The amide-II band which occurs due to interaction between the N–H bending and the C–N stretching of the C–N–H group is found at 1542 cm^{-1}. The C=N stretching band appears at 1593 cm^{-1}. The band at 3193 cm^{-1} is assigned for the N–H stretching frequency. Aromatic C–H stretching bands occur around 3055 cm^{-1}. Carbon to carbon stretching vibrations within the ring occur at 1461 cm^{-1}. The O–H stretching vibration of the water molecule is observed as a distinct peak at 3380 cm^{-1} and the decrease in the value is due to the involvement of the water molecule in intermolecular hydrogen bonding [15-17]. IR spectrum of HQb·1.5H$_2$O is shown in Fig. 2.2.
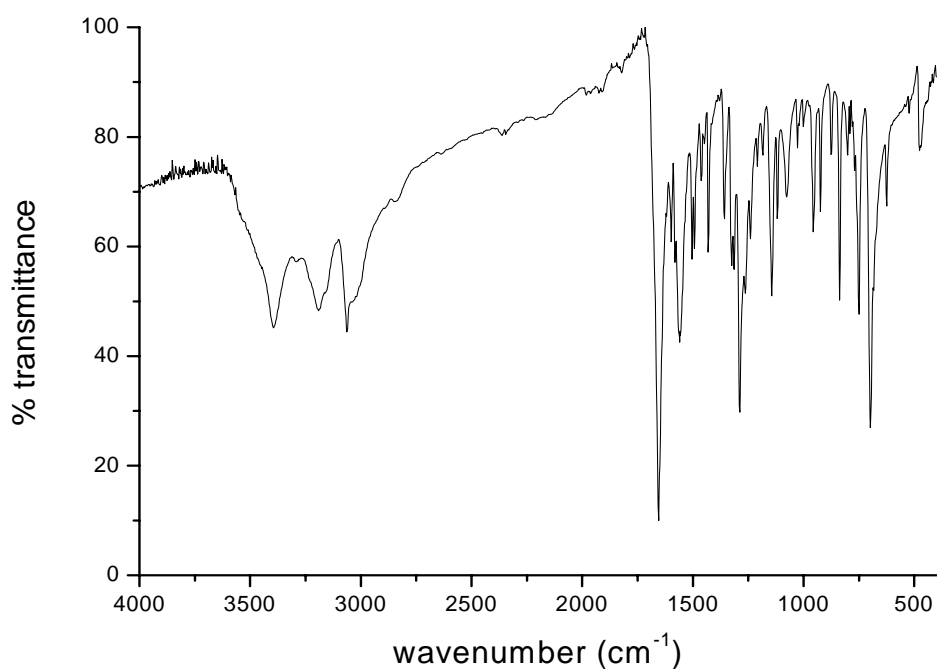
Fig. 2.2. IR spectrum of HQb·1.5H$_2$O.

2.2.3. Electronic spectrum

The electronic spectrum of the compound was recorded in acetonitrile solution on a UVD-3500 UV-vis Double Beam Spectrophotometer. The spectrum is presented in Fig. 2.3.

20

The $\pi \rightarrow \pi^*$ transitions are observed in the 32000-44000 cm^{-1} region and the $n \rightarrow \pi^*$ transitions are observed in the region of 32000-29000 cm^{-1} [17,18].

λmax (cm^{-1})
43790
41640
35860
32580
31690
30430
29130
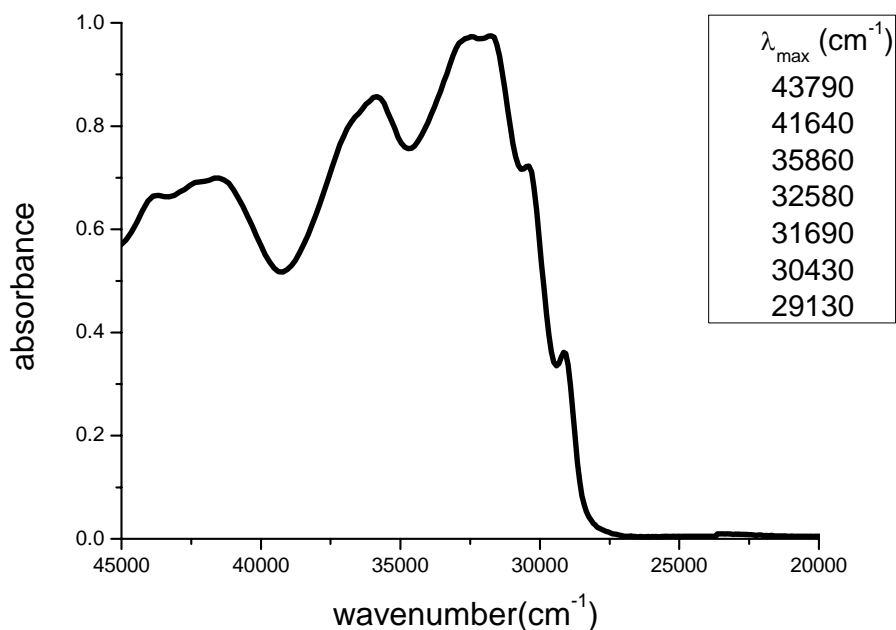
Fig. 2.3. Electronic spectrum of HQb·1.5H$_2$O.

2.2.4. NMR spectral studies

Nuclear magnetic resonance spectroscopy is a helpful tool for the identification of organic compounds in conjugation with other spectrometric information.

The ^{1}H NMR, ^{13}C NMR, COSY and HSQC spectra were recorded with DMSO-d$_6$ as solvent and TMS as the internal standard at the Sophisticated Instruments Facility, Indian Institute of Science, Bangalore, India. The numbering scheme adopted for the NMR spectral assignments is shown in Scheme II.
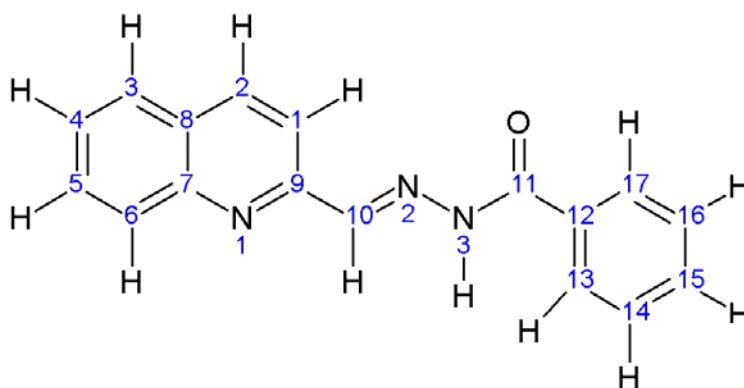
Scheme II.

2.2.4a. ^1H NMR spectrum

A sharp singlet, which integrates as one hydrogen at δ = 12.21 ppm is assigned to the proton attached to the nitrogen atom N(3). From the crystal structure, it is evident that this proton is involved in hydrogen bonding with water molecule. The hydrogen bonding decreases the electron density around the proton and thus moves the proton absorption to a lower field [15].

Upon addition of D_2O, the intensity of this signal significantly decreases, which suggests that this proton is easily exchangeable and confirm the assignment. Absence of any coupling interactions by N(3)–H due to the unavailability of protons on neighboring atoms render singlet peak for the imine proton. The presence of electron withdrawing azomethine group near to the C(10)–H proton leads to its resonance as a singlet at 8.62 ppm.

Aromatic protons resonate in the range of 8.42-7.55 ppm [15,19]. The doublet at δ = 7.95 ppm, which integrates as two hydrogens, is assigned to the ortho protons C(13)–H and C(17)–H in the phenyl ring. Coupling of these protons with the neighboring protons, C(14)–H and C(16)–H respectively, splits their signals into doublets. A triplet at δ = 7.55 ppm corresponds to the meta protons and the para proton C(15)–H resonates as a triplet at δ = 7.63 ppm. The

two triplets at δ = 7.63 and 7.78 ppm are assigned to the protons C(4)–H and C(5)–H respectively.

The resonances for C(1)–H and C(2)–H protons, due to coupling with each other, appear as doublets at δ = 8.13 and 8.42 ppm respectively. These protons are shifted lower field due to the presence of ring nitrogen. Two doublets at δ = 8.00 ppm and δ = 8.04 ppm are assigned to the C(3)–H and C(6)–H protons respectively [15,20]. The ^{1}H NMR spectrum of HQb·1.5H₂O in DMSO is given in Fig. 2.4.
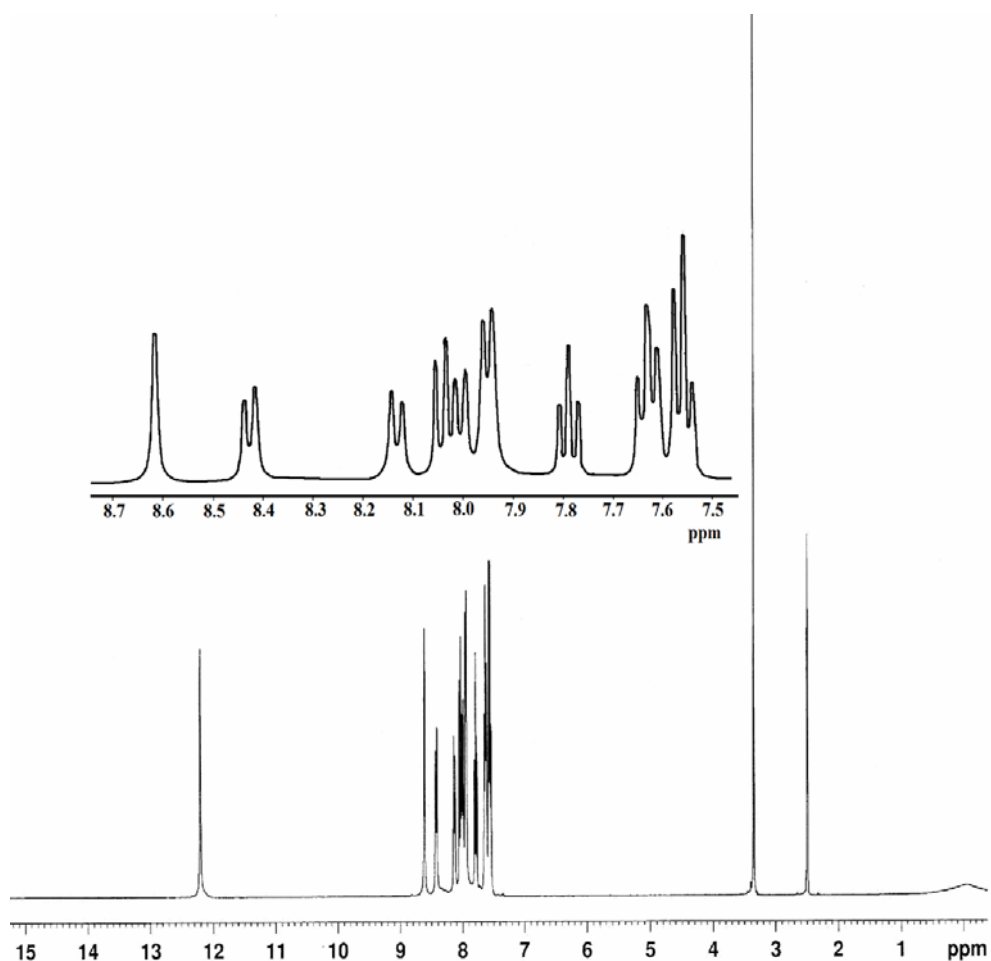
Fig. 2.4. ^{1}H NMR spectrum of HQb·1.5H₂O.

23

2.2.4b. ^1H–^1H COSY

The COSY spectrum reveals the ^1H–^1H coupling interactions in a molecule. It is usually plotted as three-dimensional contours, where the conventional spectrum is represented along the diagonal.

The cross-peaks along both the sides of the diagonal identify the nuclei that are coupled to each other, while the protons that are decoupled from the adjacent ones due to the lack of α-protons will show no correlation in the spectrum. Thus N(3)–H and C(10)–H protons do not show cross peaks in the COSY spectrum of HQb·1.5H$_2$O.

The above assignments of proton NMR spectrum are confirmed by ^1H–^1H correlation spectroscopy. The absence of any off-diagonal peaks at δ = 12.21 and 8.62 ppm confirms their assignments to N(3)–H and C(10)–H protons respectively. COSY spectrum turns out very helpful in the accurate assignments of proton resonances in the aromatic region.

The doublet of the protons C(13)–H and C(17)–H (7.95 ppm) show coupling interactions with the triplet at δ = 7.55 ppm [C(14)–H and C(16)–H]. Resonances at 8.13 ppm [C(1)–H] and 8.42 ppm [C(2)–H] show some interaction with each other, which means that they are attached to the neighboring carbon atoms. However, extending horizontal and vertical straight lines drawn from δ = 8.00 ppm [C(3)–H] encounter cross-peaks at δ = 7.63 ppm [C(4)–H]. Also the triplet at δ = 7.78 ppm [C(5)–H] show coupling interaction with the doublet at δ = 8.04 ppm [C(6)–H].

The schematic contour plot of ^1H-^1H COSY experiment of the hydrazone along with the observed ^1H / ^1H couplings is given in Fig. 2.5.
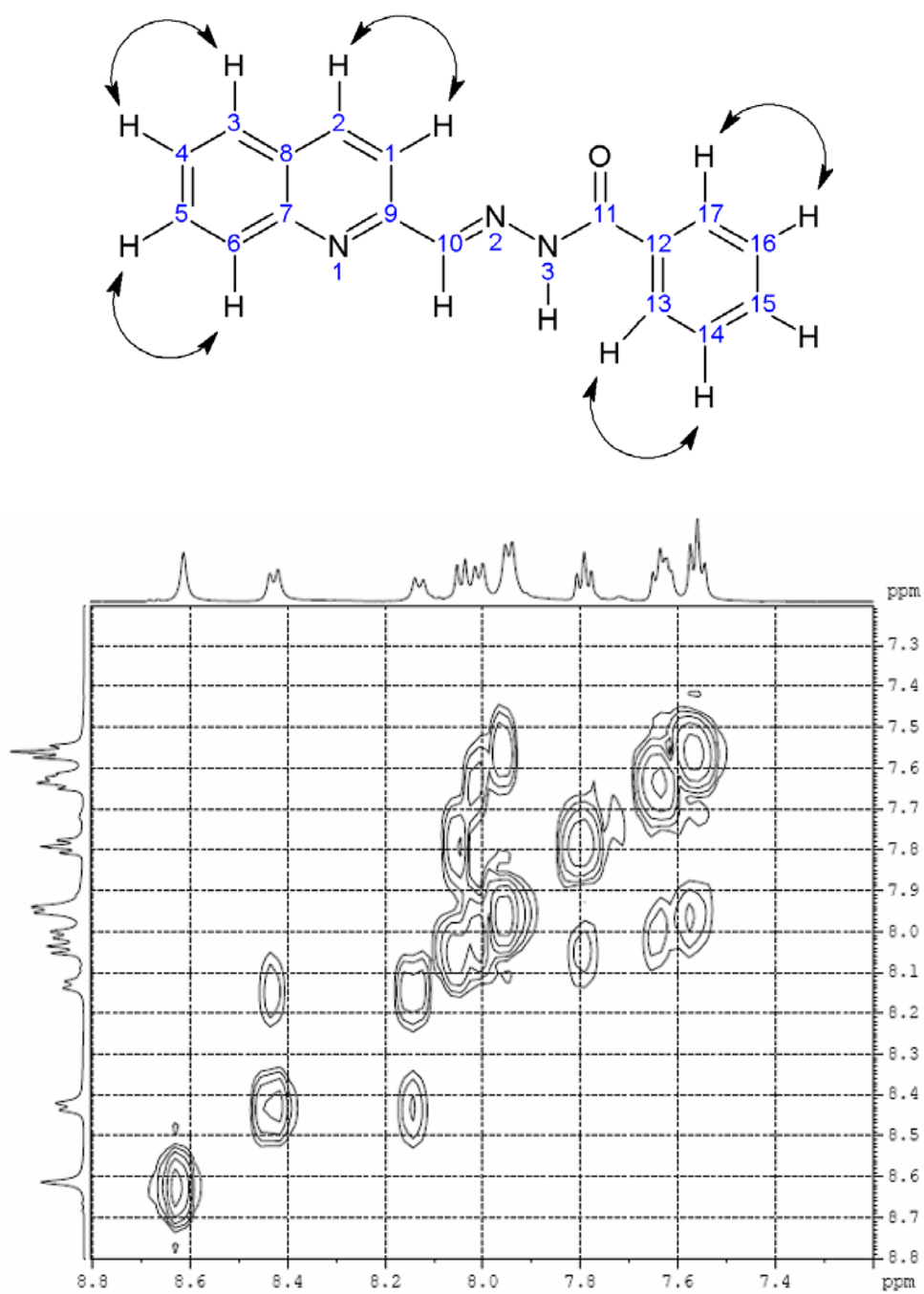
Fig. 2.5. ^{1}H–^{1}H COSY spectrum of HQb·1.5H$_2$O along with the observed ^{1}H / ^{1}H couplings.

Based on ^{1}H NMR and ^{1}H–^{1}H COSY spectra, the different protons of HQb are assigned as shown in Fig. 2.6.
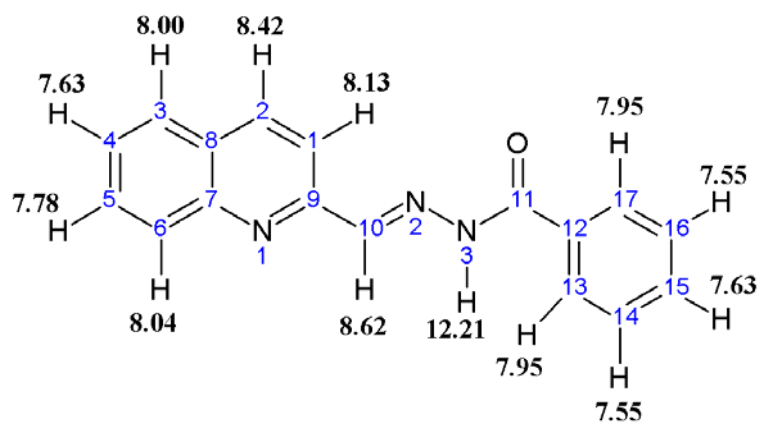
Fig. 2.6. ^{1}H NMR spectral assignments of HQb.

2.2.4c. ^{13}C NMR

The ^{13}C NMR spectrum provides the direct information about the carbon skeleton of the molecule. The ^{13}C NMR spectrum was assigned on the basis of proton decoupled ^{13}C spectrum. The ^{13}C NMR spectrum of HQb (Fig. 2.7) contains 17 peaks corresponding to the 17 magnetically unique carbon atoms.
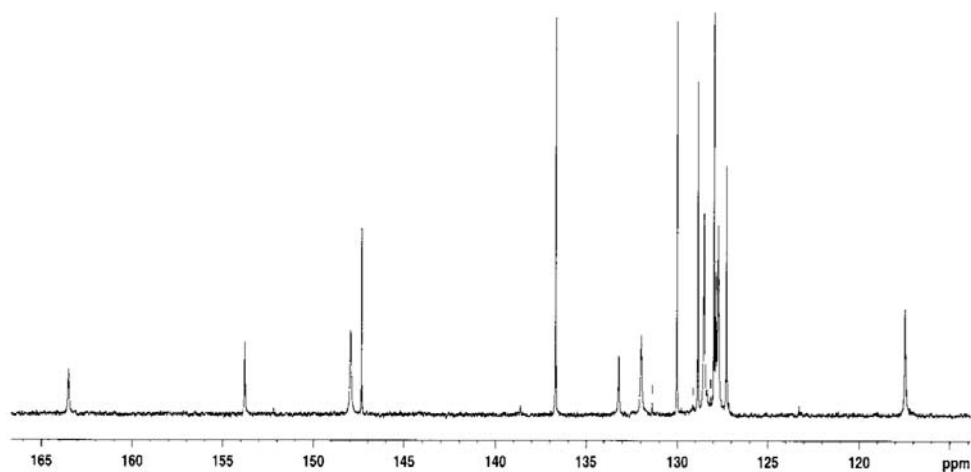
Fig. 2.7. ^{13}C NMR spectrum of HQb·1.5H$_2$O.

The carbonyl carbon C(11) resonates at 163.50 ppm and the azomethine carbon C(10) at 147.94 ppm. These two carbons are identified as more deshielded because of the extensive π electron delocalization along the conjugated framework of the carbon skeleton, which reduces the electron density around the carbon atom. Due to the presence of adjacent carbonyl group, which is a π electron acceptor, the nonprotonated carbon C(12) also resonates at lower field (153.77 ppm).

In the substituted phenyl ring, three different types of aromatic carbons are clearly distinguishable in the ^{13}C NMR spectrum. The phenyl resonances are 127.96 [C(13) and C(17)], 128.87 [C(14) and C(16)] and 127.73 ppm [C(15)].

The nonprotonated carbon C(9) adjacent to the ring nitrogen resonates at 147.34 ppm. The δ values assigned for the quinoline carbons are C(1), 117.46; C(2), 136.70; C(3), 128.52; C(4), 131.98; C(5), 130.03; C(6), 128.87; C(7), 133.18; and C(8), 127.27 ppm. The carbon atom positioned *para* to the ring nitrogen [C(2), 136.70 ppm] is found to resonate at lower field value than the carbon atom at the *meta* position [C(1), 117.46 ppm].

2.2.4d. ^{1}H–^{13}C HSQC

Heteronuclear chemical shift correlation experiments correlate the chemical shift of one nucleus with the chemical shift of another. HSQC can be performed as either a ^{1}H–^{15}N or ^{1}H–^{13}C correlation experiment. The carbon skeleton of the molecule was identified by recording ^{13}C NMR and HSQC (Heteronuclear Single Quantum Coherence) ^{1}H-^{13}C correlation spectrum.

The ^{1}H–^{13}C HSQC spectrum provides information regarding the interactions between the protons and the carbon atoms to which they are directly attached. Contrary to the COSY spectrum, only the resultant interactions are plotted as contour peaks in the HSQC spectrum. The vertical dimensions represent the ^{13}C chemical shifts scale and the horizontal

correspond to those of the protons. The interpretations made by ^{1}H and ^{13}C spectroscopy can be confirmed by [1]H-^{13}C connectivity made on the basis of HSQC spectrum.

The absence of any contours at 133.18, 127.27, 147.34, 163.50 and 153.77 ppm in the HSQC spectrum suggests that these absorptions are due to nonprotonated carbons. These peaks are assigned to C(7), C(8), C(9), C(11) and C(12) respectively.

The singlet at δ 8.62 ppm shows contour peak at δ 147.94 ppm which confirms its assignment to C(10). The peaks observed at δ 117.46 and 136.70 ppm are assigned to C(1) and C(2) respectively, due to their interactions with ^{1}H resonances at δ 8.13 and 8.42 ppm. The peak at δ 7.63 ppm shows two different resultant contour peaks at 131.98 and 127.73 ppm, which are assigned to C(4) in the quinoline ring and C(15) in the phenyl ring.

The doublet at 7.95 ppm and the triplet at 7.55 ppm show contours at 127.96 and 128.87 ppm respectively, which can be assigned respectively to ortho carbons and meta carbons in the phenyl ring. The remaining ^{13}C peaks δ 128.52, 130.03 and 128.87 ppm show interaction with ^{1}H resonances δ 8.00, 7.78 and 8.04 ppm respectively in HSQC and these are assigned to C(3), C(5) and C(6). These assignments are in agreement with one-dimensional spectral assignments. The HSQC spectrum of the hydrazone and the observed ^{1}H/^{13}C couplings are shown in Fig. 2.8.
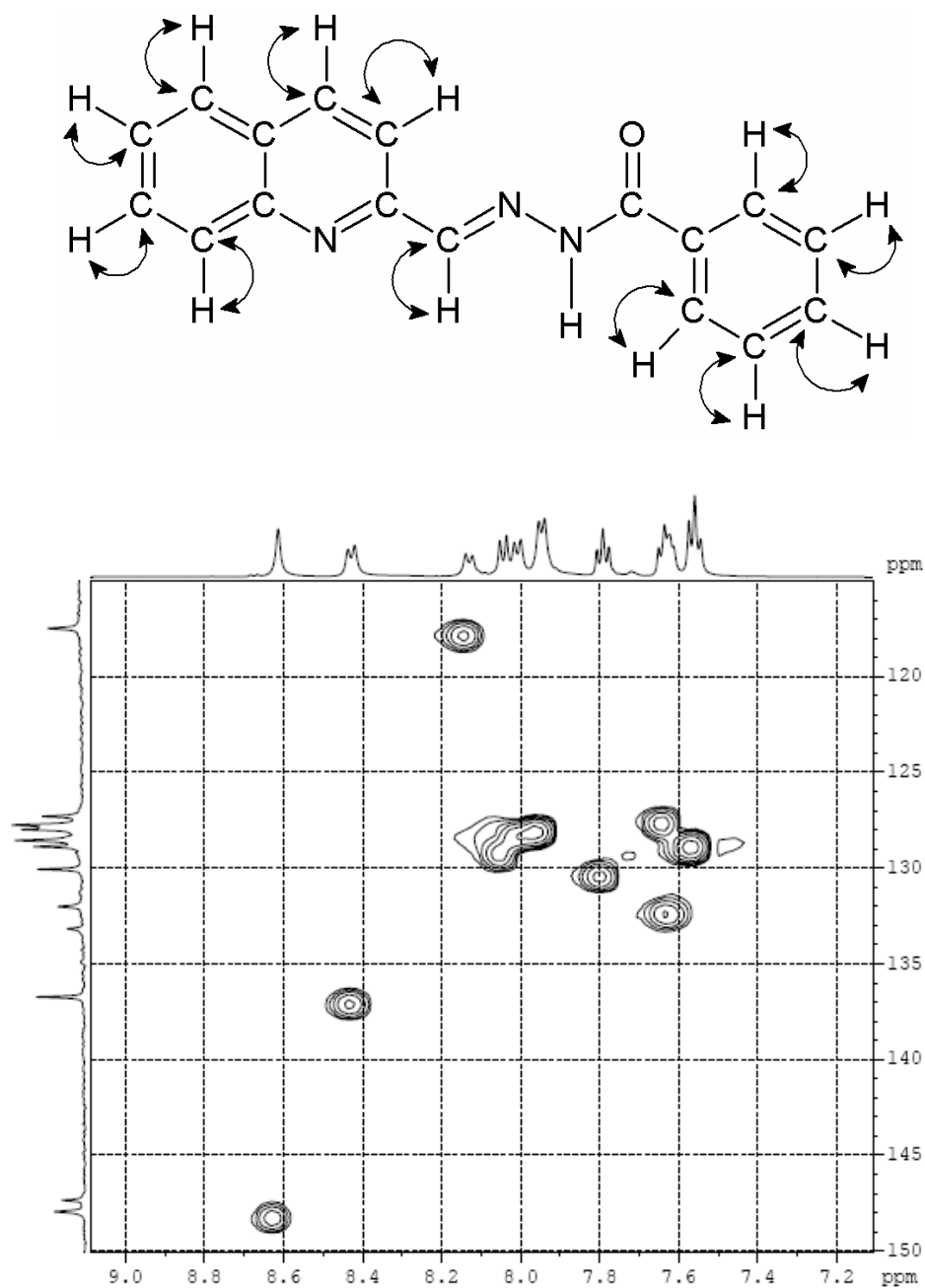
Fig. 2.8. $^1H–^{13}C$ HSQC spectrum and observed $^1H/^{13}C$ couplings of HQb·1.5H$_2$O.

Based on the above findings, the assignment of different resonant peaks to respective carbon atoms are presented in Fig. 2.9.
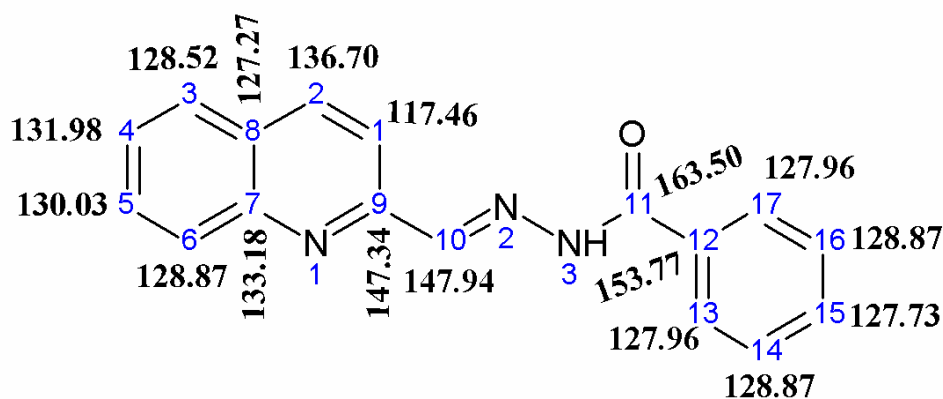
Fig. 2.9. ^{13}C NMR spectral assignments of HQb.

2.2.5. X-ray crystallography

Colorless block shaped crystals of quinoline-2-carbaldehyde benzoyl hydrazone monohydrate, suitable for X-ray diffraction studies, were grown from a solution of the compound in a mixture of DMF and ethanol (1:1 v/v). The lattice is monoclinic in nature with $P2_1/n$ symmetry. The crystal data and structural refinement parameters are given in Table 2.1.

The data were collected using Oxford Diffraction Xcalibur-S diffractometer, equipped with graphite-monochromated Mo Kα ($\lambda = 0.71073$ Å) radiation at the National Single Crystal X-ray Facility, IIT Bombay, Mumbai, India. The intensity data were collected at 120(2) K by the ω/q-scan mode. The cell refinement was done using the CrysAlis RED software [21]. The structure was solved by direct methods with the program SHELXS-97 and refined by full matrix least squares on F^2 using SHELXL-97 [22]. The graphical tool used were Diamond version 3.1f [23] and mercury [24]. Full crystallographic data (cif file) relating to the crystal structure have been deposited with the Cambridge Crystallographic Data Centre as CCDC 743681.

Table 2.1. Summary of crystal data and structure refinement for HQb·H_2O.

Formula	$C_{17}H_{15}N_3O_2$
Formula weight	293.32
Color; shape	Colorless, block
Temperature (T) K	150(2)
Wavelength (Mo Kα) (Å)	0.71073
Crystal system	Monoclinic
Space group	$P2_1/n$
Lattice constants	
a (Å)	6.4221(4)
b (Å)	32.7824(18)
c (Å)	7.0736(4)
α (°)	90.00
β (°)	104.047(6)
γ (°)	90.00
Volume V ($Å^3$)	1444.69(15)
Z	4
Calculated density (ρ) (Mg m^{-3})	1.349
Absorption coefficient, μ (mm^{-1})	0.091
F(000)	616
Crystal size (mm^3)	0.23 x 0.18 x 0.15
θ range for data collection	3.03 to 25.0
Limiting indices	$-6 \leq h \leq 7$; $-38 \leq k \leq 35$; $-8 \leq l \leq 8$
Measured/Unique Data	9072/2546 [$R_{(int)}$ = 0.064]
Observed Data [I > 2σ(I)]	1416
Data / restraints / parameters	2540 / 0 / 211
Final R indices	R1 = 0.0475, wR2 = 0.0680
R indices (all data)	R1 = 0.1179, wR2 = 0.0806

The molecule as a whole is roughly planar with a maximum dihedral angle of 4.82(11)° between the rings formed by the atoms C1, C2, C3, C4, C5, C6 and C12, C13, C14, C15, C16, C17 respectively. The C11–O1 bond length of 1.228(3) Å indicates the molecule exists in the keto form in the solid-state. The C10–N2 bond length of 1.279(2) Å confirms its significant double-bond character. The values of the N2–N3 and N3–C11 bond distances of 1.379(2) and 1.362(3) Å, respectively, are greater than the value for a double bond and less than the value for a single bond, which indicate significant delocalization of π-electron density over the hydrazone portion of the molecule. Due to the short N–N bond length, the HQb acts mostly as tridentate moieties though they have the potential to act as bridging tetradentate ligands. The significant bond lengths and bond angles are given in Table 2.2.

Table 2.2. Selected bond lengths (Å) and bond angles (°) of HQb·H_2O

Bond lengths (Å)		Bond angles (°)	
C10–N2	1.279(2)	C10–N2–N3	115.50(19)
C11–O1	1.228(3)	N2–N3–C11	118.1(2)
N2–N3	1.379(2)	N3–C11–O1	121.9(2)
C11–N3	1.362(3)	C9–C10–N2	119.9(2)
C9–C10	1.460(3)	N3–C11–C12	117.0(2)
C11–C12	1.495(3)		

The torsion angle values, −179.54(19)° and 1.9(3)° attained by N3–N2–C10–C9 and N2–N3–C11–O1, suggest the existence of the ligand in *trans* configuration along the C10–N2 bond and in *cis* form along the C11–N3 bond [25-27]. The existence of C10–N2 bond in *trans* configuration rules out the possibility of intramolecular N3–H···N1 hydrogen bonding. The structure of the compound is given in Fig. 2.10.
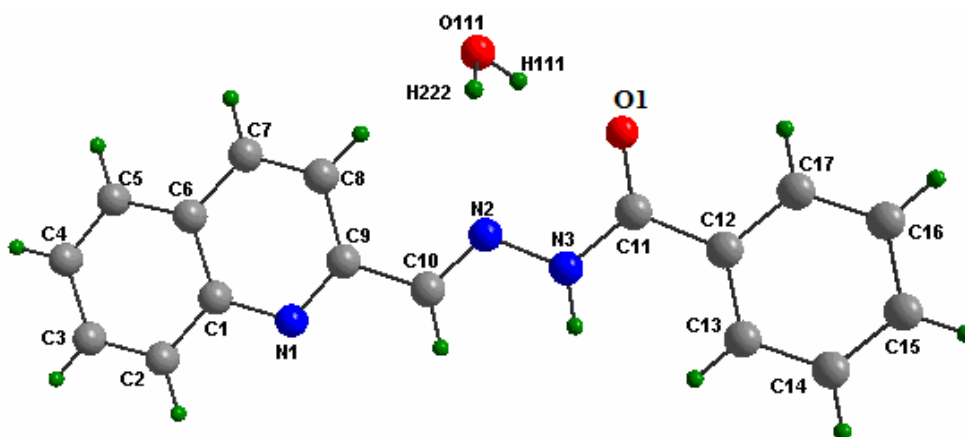
Fig. 2.10. Crystal structure of quinoline-2-carbaldehyde benzoyl hydrazone monohydrate.

The packing of molecules in the crystal lattice is shown in Fig. 2.11. The unit cell is viewed down the 'a' axis. The molecules are arranged in a zig-zag manner in the unit cell.
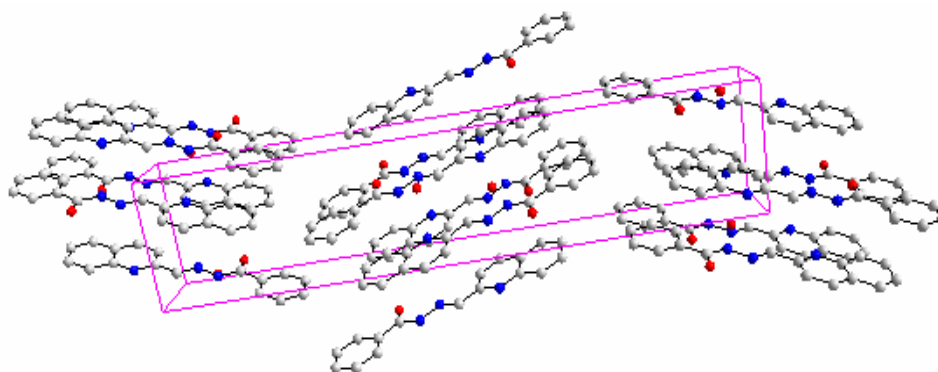
Fig. 2.11. Unit cell packing diagram of quinoline-2-carbaldehyde benzoyl hydrazone monohydrate viewed along the 'a' axis. Hydrogen atoms are excluded for clarity.

An interesting feature of the crystal packing is the formation of a supramolecular chain mediated by a network of hydrogen bonds. The residual water molecule in the crystal lattice interconnects adjacent molecules in the lattice through intermolecular hydrogen bonds. The two protons in the water molecule form hydrogen bonds with amide oxygen and quinoline nitrogen of

33

different hydrazone moieties and the oxygen in the same water molecule forms hydrogen bond with N–H proton of the third hydrazone molecule. Finally, these chains are linked into highly ribbed 3D array by extensive hydrogen bonding interactions. The supramolecular chain stabilized by hydrogen bonding between the hydrazone and water molecule is illustrated in Fig. 2.12. The important interaction parameters are given in Table 2.3.
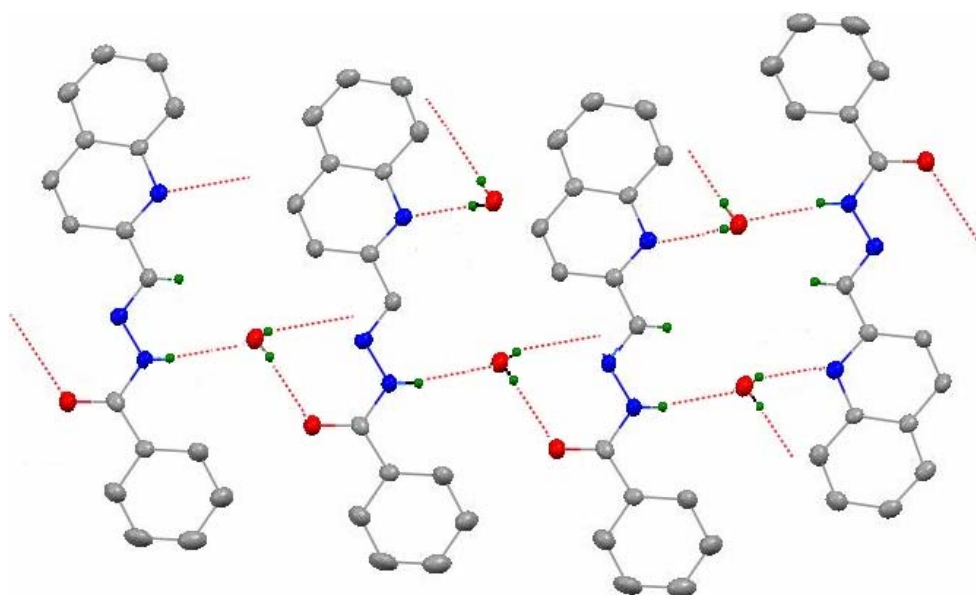
Fig. 2.12. Supramolecular chain stabilized by hydrogen bonding between the hydrazone and water molecule.

The orientation of the molecules in the crystal lattice is in such a manner that $\pi\cdots\pi$ stacking interactions are present between Cg(2) [C1, C2, C3, C4, C5, C6] and Cg(3) [C12, C13, C14, C15, C16, C17] at an average distance of 3.8931(14) Å. In addition, C11–O1$\cdots$Cg(2) interaction is also observed with O1$\cdots$Cg distance of 3.9025(19) Å and C11$\cdots$Cg distance of 3.481(2) Å. The molecules in the adjacent layers within the unit cell are held together by these interactions, which reinforce the packing.

34

Table 2.3. Interaction parameters of the hydrazone.

Hydrogen bonding

D–H⋯A	D–H (Å)	H⋯A (Å)	D⋯A (Å)	∠D–H⋯A(º)
N3–H(3N)⋯O111[a]	0.91(3)	2.00(3)	2.879(3)	161.4(18)
O111–H111⋯O1	0.92(3)	1.91(3)	2.796(2)	161(2)
O111–H222⋯N1[b]	0.84(3)	2.14(3)	2.948(3)	160(3)

Short ring interaction

Cg(I)⋯Cg(J)	Cg-Cg (Å)	α (º)	β (º)	γ (º)
Cg(2)⋯Cg(3)[b]	3.8931(14)	4.82	20.70	25.52

Pi-ring interaction

Y–X(I)⋯Cg(J)	X⋯Cg (Å)	Y–X⋯Cg	Y⋯Cg
C(11)–O(1)⋯Cg(2)[c]	3.9025(19)	61.19(12)	3.481(2)

Note:

Equivalent position codes: a = 1+x, y, z; b = 1-x, -y, 2-z; c = 1-x, -y, 1-z

Cg (2) = C1, C2, C3, C4, C5, C6; Cg (3) = C12, C13, C14, C15, C16, C17

α (º) = Dihedral Angle between Planes I and J;

β (º) = Angle between Cg(I)-Cg(J) vector and normal to plane I;

γ (º) = Angle between Cg(I)-Cg(J) vector and normal to plane J.

2.3. Quinoline-2-carbaldehyde nicotinic hydrazone sesquihydrate (HQn·1.5H₂O)

The compound quinoline-2-carbaldehyde nicotinic hydrazone (Fig. 2.13) was prepared from quinoline-2-carbaldehyde and nicotinic hydrazide.
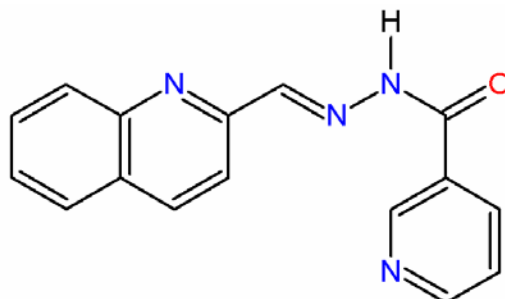
Fig. 2.13. Quinoline-2-carbaldehyde nicotinic hydrazone (**HQn**).

2.3.1. Experimental

2.3.1a. *Materials*

    All the chemicals and solvents used for the syntheses were of analytical grade. Quinoline-2-carbaldehyde (Sigma Aldrich) and nicotinic hydrazide (Sigma Aldrich) were used as received.

2.3.1b. *Synthesis*

    The hydrazone HQn·1.5H$_2$O was synthesized by a procedure similar to that of HQb·1.5H$_2$O except with the use of nicotinic hydrazide (0.274 g, 2 mmol) instead of benzhydrazide. The colorless product formed was filtered off, washed with methanol and dried over P$_4$O$_{10}$ *in vacuo*. Yield – 89%, m.p. 140-142 °C. Elemental Anal. Found (Calcd) %: C, 63.16 (63.36); H, 4.59 (4.98); N, 18.58 (18.47) for C$_{16}$H$_{12}$N$_4$O·1½ H$_2$O. % H$_2$O 9.18 (8.91) from TG data.

    The reaction scheme is depicted in the Scheme III.

Quinoline-2-carbaldehyde   Nicotinichydrazide   Quinoline-2-carbaldehyde nicotinic hydrazone (HQn)
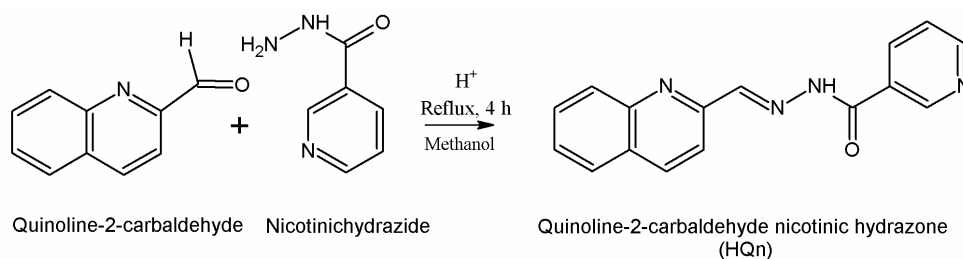
Scheme III

2.3.2. Infrared spectrum

    Infrared spectral analyses were done using KBr on Thermo Nicolet AVATAR 370 DTGS FT-IR spectrophotometer. The IR spectrum of the hydrazone is shown in Fig. 2.14.
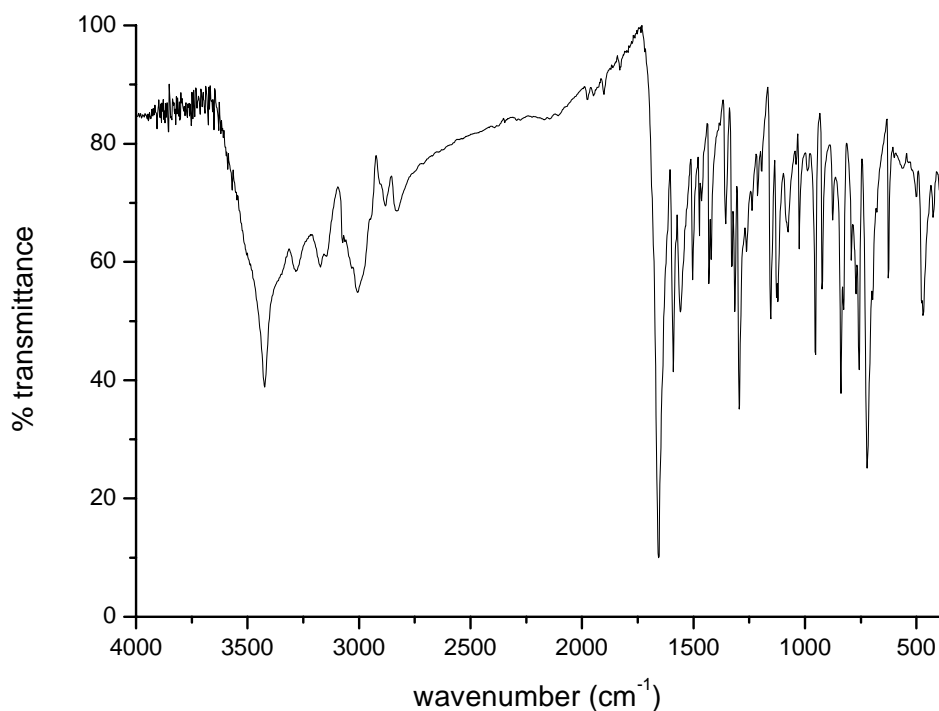
Fig. 2.14. IR spectrum of HQn·1.5H$_2$O.

The band at 1656 cm^{-1} is characteristic of stretching frequency of carbonyl group. This band confirms the existence of hydrazone in keto form in solid state. The azomethine band, ν(C=N), is observed at 1591 cm^{-1} and ν(N–N) at 1195 cm^{-1}. The peak at 3173 cm^{-1} is assigned to the N–H stretching frequency. The amide-II band is found at 1558 cm^{-1}. Aromatic C–H stretching bands occur nearly at 3074 cm^{-1}. Carbon to carbon stretching vibrations within the ring occur at 1473 cm^{-1}. The O–H stretching vibration of the water molecule is observed as a distinct peak at 3426 cm^{-1}.

2.3.3 Electronic spectrum

The electronic spectrum of the compound was recorded in acetonitrile solution on a UVD-3500 UV-vis Double Beam Spectrophotometer. Electronic spectrum HQn·1.5H$_2$O is shown in Fig. 2.15.

37
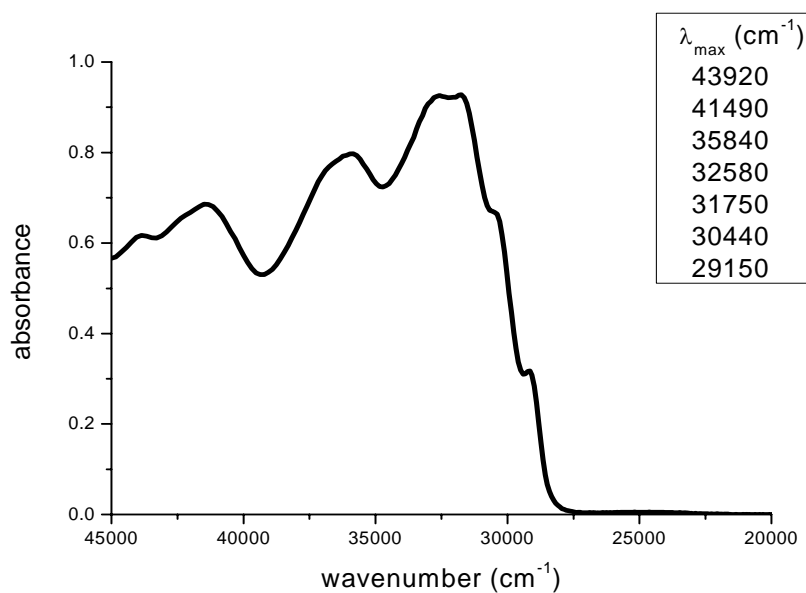
Fig. 2.15. Electronic spectrum of HQn·1.5H$_2$O.

The bands in the region 32000-44000 cm^{-1} are assigned to $\pi \rightarrow \pi^*$ transitions. The absorption bands in the region 29000-32000 cm^{-1} are attributed to $n \rightarrow \pi^*$ transitions.

2.3.4. NMR spectral studies

The NMR spectral assignments were done on the basis of ^{1}H NMR, ^{13}C NMR, COSY and HSQC. The one dimensional and two dimensional nuclear magnetic resonance spectra were used in resolving the carbon and hydrogen atoms of HQn and the assignments are based on the structure shown in Fig. 2.13. The numbering scheme adopted for the NMR spectral assignments is shown in Scheme IV.
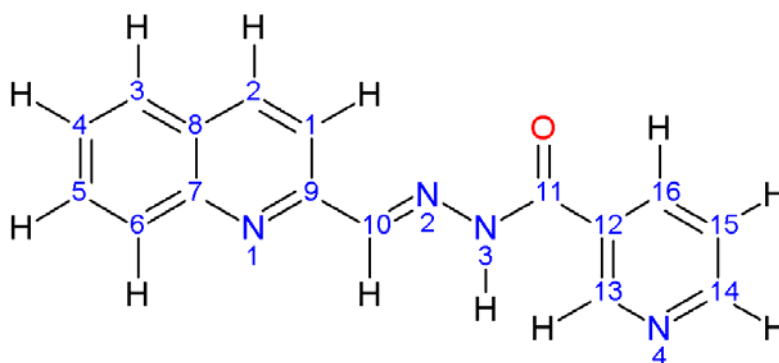
Scheme IV.

The ^{1}H resonances were assigned on the basis of chemical shift values, multiplicities and connectivity from ^{1}H NMR and [1]H-^{1}H correlation experiments [15,18]. These give insight into the average effective magnetic fields present, interaction of the nuclear spin with the adjacent atoms and the number of equivalent protons.

The assignment of the -NH proton was made by comparison with the spectra recorded using deuterium exchange.   Assignments of protonated carbons were made by two dimensional HSQC experiments.

2.3.4a. *^{1}H NMR spectrum*

In the ^{1}H NMR spectrum of HQn·1.5H_2O (Fig. 2.16), the N(3)–H proton due to hydrogen bonding is shifted downfield to resonate at 12.40 ppm.   This assignment was confirmed by deuterium exchange, in which the intensity of this band was considerably decreased.
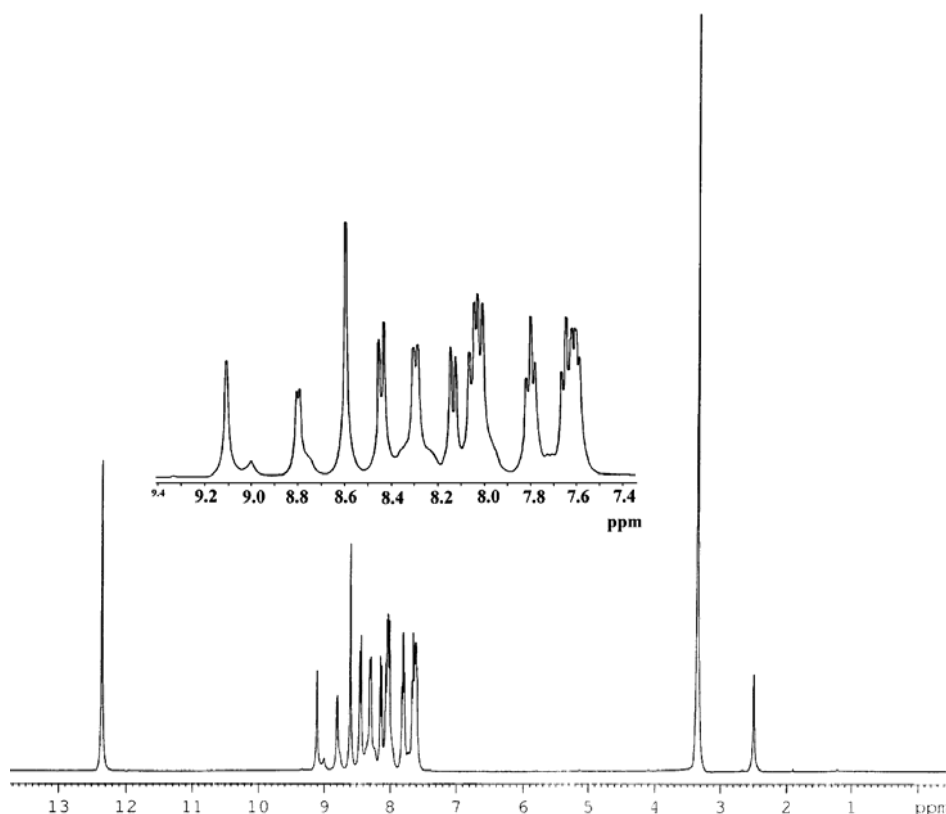
Fig. 2.16. ^{1}H NMR spectrum of HQn·1.5H_2O.

The singlet peak at 9.11 ppm corresponds to C(13)–H proton which is highly deshielded by the adjacent ring nitrogen and the carbonyl group attached to C(11). The proton attached to C(10) resonates as a singlet in the ^{1}H NMR spectrum at δ = 8.59 ppm. These two singlets are retained in deuterium exchange NMR spectrum.

Two doublets observed at δ = 8.13 and 8.44 ppm are assigned to C(1)–H and C(2)–H protons respectively. The higher δ value of C(2)–H proton compared to C(1)–H proton is explained by its position *para* to the ring nitrogen. The C(3)–H and C(6)–H protons resonate as doublets at δ = 8.00 and 8.03 ppm respectively.

The two triplets observed at δ = 7.63 and 7.79 ppm correspond to C(4)–H and C(5)–H protons respectively. The C(14)–H and C(16)–H protons resonate as doublets at δ = 8.79 and 8.28 ppm respectively due to coupling with C(15)–H proton, while C(15)–H proton resonates as a triplet at δ = 7.6 ppm. The C(14)–H proton is more deshielded due to the presence of electronic effects exerted by the adjacent nitrogen atom N(4) directly attached to them.

2.3.4b. ^{1}H–^{1}H COSY

The above assignments of proton NMR spectrum are confirmed by ^{1}H-^{1}H correlation spectroscopy. In this contour plot, both dimensions represent the ^{1}H chemical shift scale and the ^{1}H NMR spectrum appears on the diagonal where as the off diagonal peaks prove the existence of spin-spin couplings.

There is no correlation for the peaks at δ 8.59, 12.40 and 9.11 ppm, which indicate the absence of interaction of these protons with any other protons. Contours are observed in the aromatic region only.

In the COSY spectrum of HQn, the horizontal and vertical straight lines drawn from the doublet at δ = 8.13 ppm [C(1)–H] encounter off-diagonal peak at the doublet at δ = 8.44 ppm [C(2)–H]. The resonance at δ 7.60 ppm [C(15)–H] shows considerable interaction with 8.28 ppm [C(16)–H] and 8.79 ppm [C(14)–H]. This makes sure that these protons belong to the *meta* substituted pyridine ring and

the higher value is assigned to the C(14)–H proton due to the presence of nitrogen atom adjacent to it. Also, the peak at δ 8.00 ppm makes a good contour with δ 7.63 ppm and the absorption at δ 7.79 ppm with δ 8.03. The COSY spectrum and ^{1}H/^{1}H couplings observed are shown in Fig. 2.17.
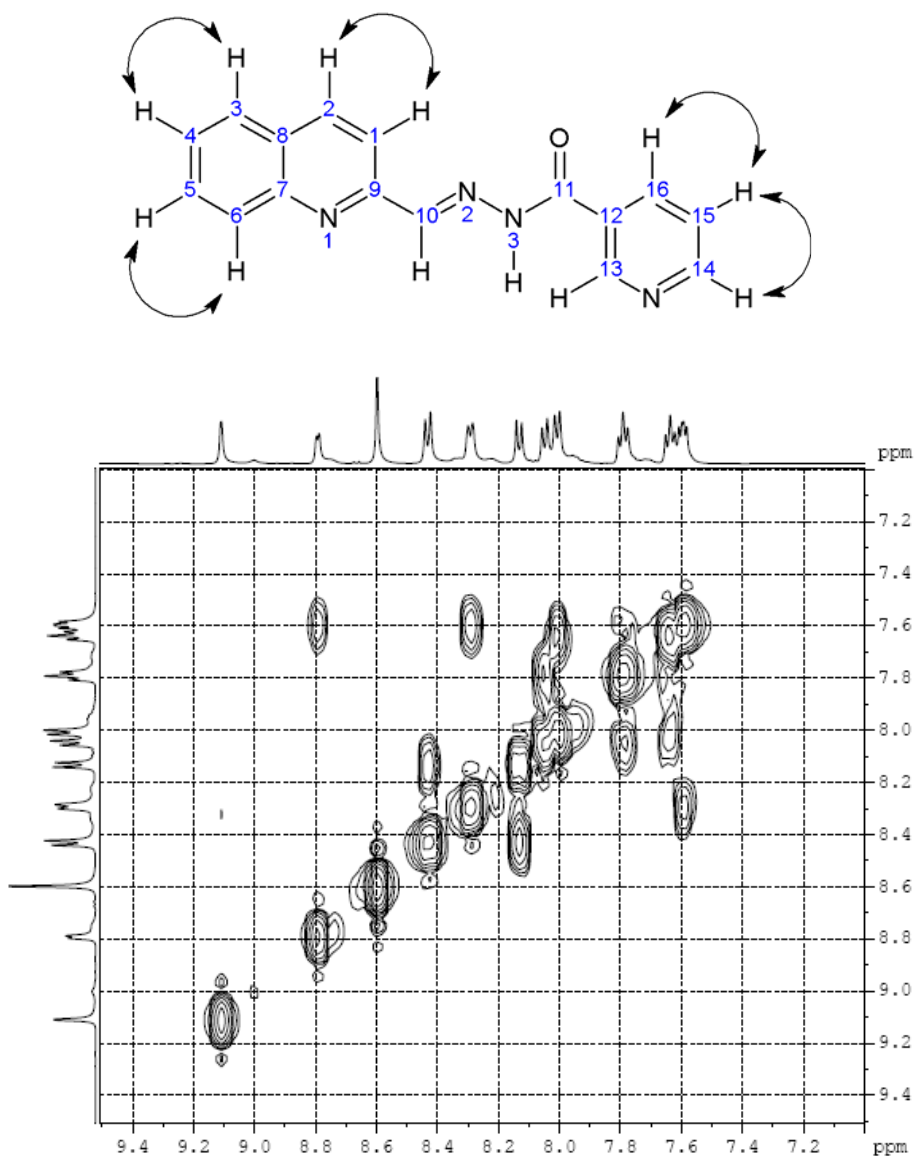
Fig. 2.17. ^{1}H–^{1}H COSY spectrum of HQn·1.5H$_2$O along with the observed ^{1}H/^{1}H couplings.

41

Based on ¹H NMR and ¹H–¹H COSY spectra, the different protons of HQn are assigned as shown in Fig. 2.18.
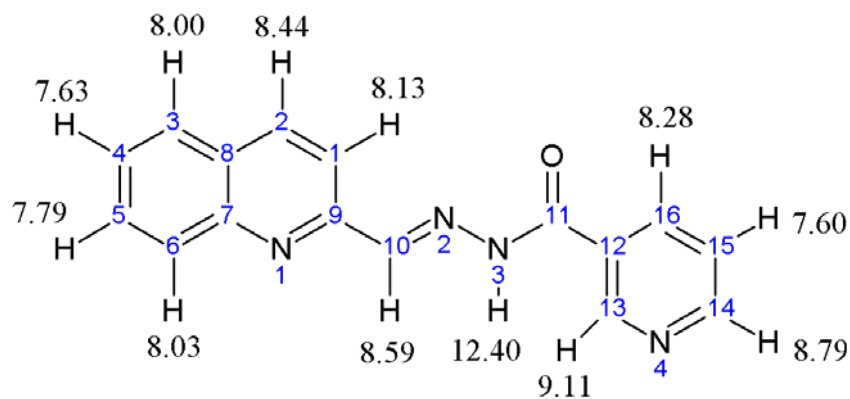
Fig. 2.18. ¹H NMR spectral assignments of HQn.

2.3.4c. *¹³C NMR*

The carbon skeleton of the molecule was identified by recording proton decoupled ¹³C NMR (Fig. 2.19). The carbonyl carbon C(11) appears at a δ value of 162.07 ppm, which indicates the downfield shifting due to conjugative effect of the N(2)–N(3)–C(11)–O1 core in the hydrazone.
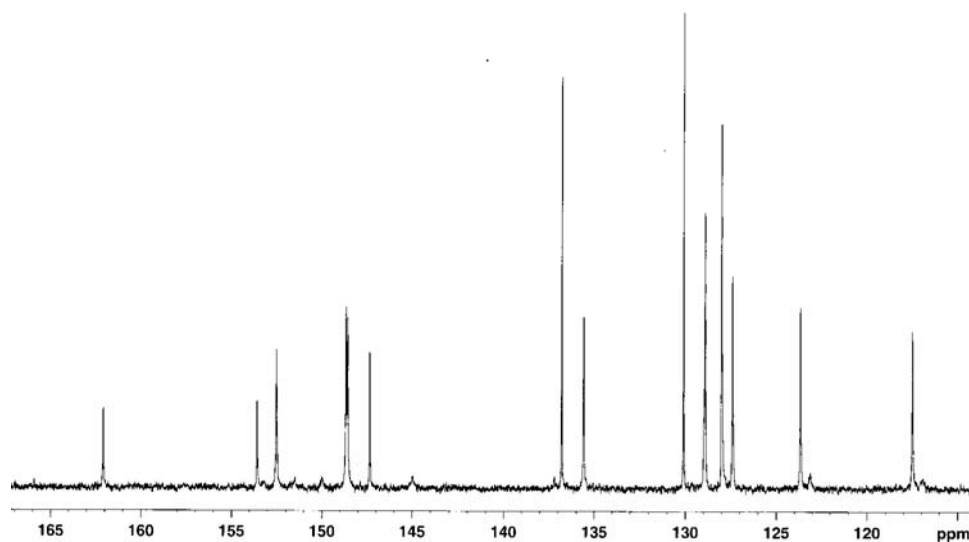
Fig. 2.19. ¹³C NMR spectrum of HQn·1.5H₂O.

In the pyridyl ring, the carbon atoms *viz*. C(13) (148.65 ppm) and C(14) (152.50 ppm) adjacent to the electronegative nitrogen are found to resonate at lower field. The lower field value of the carbon atom C(10) (δ = 148. 56 ppm) is due to the extensive π electron delocalization of the C(10)=N(2) bond.

The resonances assigned to quinoline carbons are C(1), 117.49; C(2), 136.79; C(3), 128.90; C(4), 127.98; C(5), 130.09; C(6), 128.96; C(7), 127.94; C(8), 127.38 and C(9), 147.34 ppm. In the present compound, the carbon positioned *para* to the ring nitrogen C(16) is observed at higher δ value (135.58 ppm) than the corresponding *meta* positioned carbon, C(15), 123.64 ppm.

The nonprotonated carbon C(12) is found to be downfield shifted and resonates at 153.56 ppm. This is due to the electronic effects exerted by the adjacent carbonyl group directly attached to it.

2.3.4d. ^{1}H–^{13}C HSQC

The ^{1}H-^{13}C correlation spectrum was recorded to confirm the above assignments. The vertical dimensions in the spectrum represent the ^{13}C NMR chemical shifts scale and horizontal that of the proton NMR. The cross peaks indicate one-bond correlation, (^{1}H-^{13}C bond) i.e. they correlate proton and carbon signals of atoms directly attached. ^{1}H–^{13}C HSQC spectrum of HQn·1.5H$_2$O is shown in Fig. 2.20 along with observed ^{1}H/^{13}C couplings.

The ^{1}H-^{13}C connectivity made on the basis of HSQC spectrum is in agreement with the ^{1}H and ^{13}C spectral assignments. The ^{13}C peaks at δ 162.07, 153.56, 147.34, 127.94 and 127.38 ppm do not make any correlation pattern in HSQC suggesting that these peaks are made by non-protonated carbons.

Based on the above discussions, the assignment of different resonant peaks to respective carbon atoms are presented in Fig. 2.21.
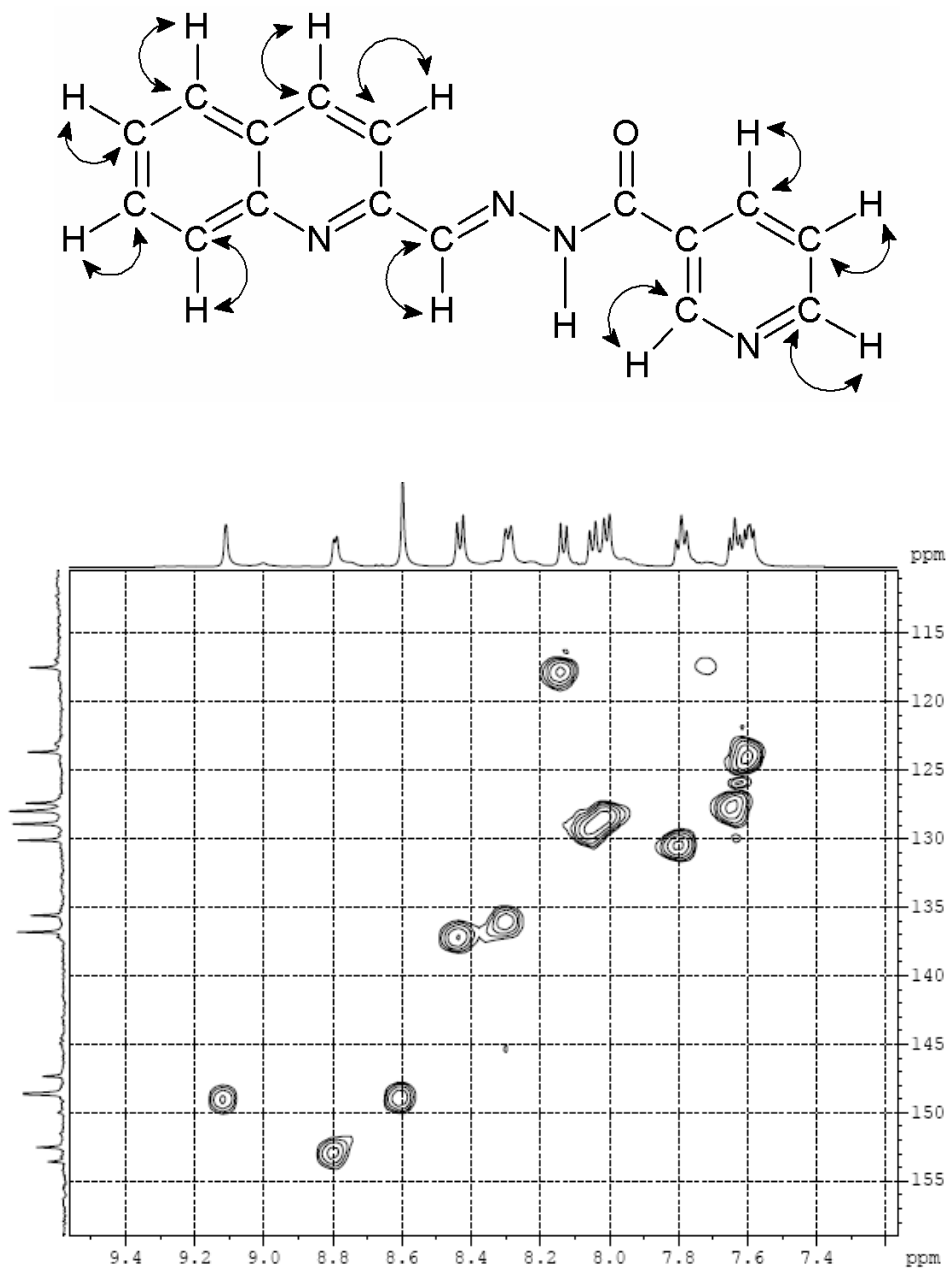
Fig. 2.20. ^{1}H-^{13}C HSQC spectrum of HQn·1.5H$_2$O and the observed ^{1}H/^{13}C couplings.
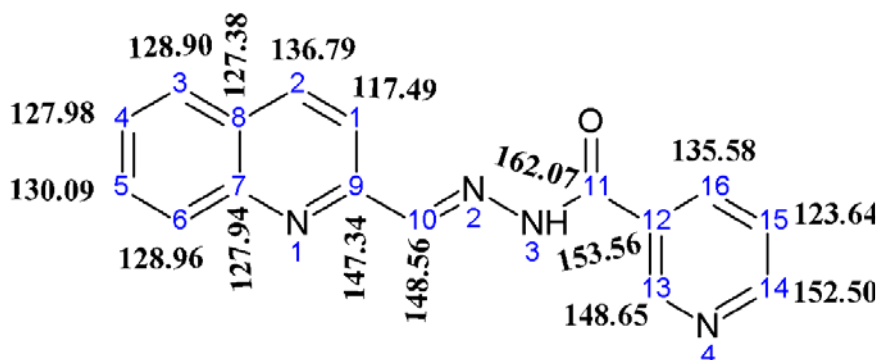
Fig. 2.21. ^{13}C NMR spectral assignments of HQn.

References

[1]   H. Adams, D.E. Fenton, G. Minardi, E. Mura, M. Angelo, Inorg. Chem. Commun. 3 (2000) 4.

[2]   Z.Y. Yang, R.D. Yang, F.S. Li, K.B. Yu, Polyhedron 19 (2000) 2599.

[3]   P. Ponka, D. Richardson, E. Baker, H.M. Schulman, J.T. Edward, Biochim, Biophys. Acta 967 (1988) 122.

[4]   M.F. Iskander, L. Sayed, A.F.M. Hefny, S.E. Zayan, J. Inorg. Nucl. Chem. 38 (1976) 2209.

[5]   R.L. Dutta, M.M. Hossain, J. Sci. Ind. Res. 44 (1985) 635.

[6]   E. Baker, M.L. Vitolo, J. Webb, Biochim. Pharmacol 34 (1985) 3011.

[7]   O. Pouralimardan, A.C. Chamayou, C. Janiak, H.H. Monfared, Inorg. Chim. Acta 360 (2007) 1599.

[8]   I.H.A. Suez, S.O. Pehkonen, M.R. Hoffmann, Sci. Technol. 28 (1994) 2080.

[9]   L.H. Terra, A.M.C. Areias, I. Gaubeur, M.E.V. Suez-Iha, Spectrosc. Lett. 32 (1999) 257.

[10]   S. Patai, The Chemistry of Carbon–Nitrogen Double Bond, Interscience, New York (1970).

[11]   J.C. Galiz, J.C. Rub, J. Edger, Nature 34 (1955) 176.

[12] M.F. Iskander, S.E. Zayan, M.A. Khalifa, L. Elsayed, J. Inorg. Nucl. Chem. 36 (1974) 556.

[13] J.R. Marchent, D.S. Clothia, J. Med. Chem. 13 (1970) 335.

[14] J.R. Dilworth, Coord. Chem. Rev. 21 (1976) 29.

[15] R.M. Silverstein, G.C. Bassler, T.C. Morrill, Spectrometric Identification of Organic Compounds, 4th Ed., Wiley, New York (1981).

[16] M. Kuriakose, M.R.P. Kurup, E. Suresh, Polyhedron 26 (2007) 2713.

[17] P.B. Sreeja, M.R.P. Kurup, Spectrochim. Acta A 61 (2005) 331.

[18] W. Kemp, Organic Spectroscopy, 3rd Ed., Macmillan, Hampshire (1996).

[19] S. Sen, P. Talukder, G. Rosair, S. Mitra, Struct. Chem. 16 (2005) 605.

[20] V. Suni, M.R.P. Kurup, M. Nethaji, J. Mol. Struct. 749 (2005) 183.

[21] CrysAlis CCD and CrysAlis RED Versions 1.171.29.2 (CrysAlis 171. NET), Oxford Diffraction Ltd., Abingdon, Oxfordshire, England (2006).

[22] G.M. Sheldrick, Acta Crystallogr. A64 (2008) 211.

[23] K. Brandenburg, Diamond Version 3.1f, Crystal Impact GbR, Bonn, Germany (2008).

[24] C.F. Macrae, P.R. Edgington, P. McCabe, E. Pidcock, G.P. Shields, R. Taylor, M. Towler, J. van de Streek, J. Appl. Crystallogr. 39 (2006) 453.

[25] V. Suni, M.R.P. Kurup, M. Nethaji, Spectrochim. Acta A 63 (2006) 174.

[26] M. Joseph, V. Suni, M.R.P. Kurup, M. Nethaji, A. Kishore, S.G. Bhat, Polyhedron 23 (2004) 3069.

[27] R.P. John, A. Sreekanth, M.R.P. Kurup, A. Usman, I.A. Razak, H.-K. Fun, Spectrochim. Acta A 59 (2003) 1349.

…..ಬಚ…..

VANADIUM(IV) COMPLEXES OF ACYLHYDRAZONES: SYNTHESES AND SPECTRAL INVESTIGATIONS

3.1. Introduction

Hydrazones constitute an interesting class of chelating agents capable to coordinate with one or more metal ions giving mononuclear or polynuclear metal complexes, which serve as models for metalloproteins [1,2]. Hydrazones take the forefront position in the development of coordination chemistry, owing to their diverse applications in various fields [3]. The chemistry of transition metal complexes of hydrazones continues to be of interest on account of the remarkable structural features presented by this class of compounds and also because of their biological importance [4-11].

During the last twenty years or so, chemistry has witnessed the tremendous development of vanadium chemistry because of the discovery of enzymatic and physiological activities of its compounds. The discovery, in 1985, that a simple vanadium salt, sodium orthovanadate, added to drinking water, could reverse most of the diabetic symptomatology of experimentally-diabetic rats, was exceptionally enticing [12].

Structural and/or functional models for vanadate-dependent haloperoxidases, vanadium nitrogenases and other biologically active vanadium compounds have encouraged further study on vanadium coordination chemistry [13,14]. Moreover, the acylhydrazone can coordinate the metal through oxygen and nitrogen atoms and are similar to the coordination environments of the biological system. The study of the biochemical role of vanadium has received much interest particularly due to the presence of this element in significant amounts in some organisms and its involvement in both promotory and inhibitory enzymatic processes in biological systems [15-17].

A number of vanadium complexes have been shown to be insulin mimetic, that is, they diminish blood glucose levels, when administered as therapeutic agents. More recent studies have shown that these complexes do not actually mimic insulin, but merely enhance the effects of the small quantities of insulin that are present. A variety of coordination complexes containing combinations of N/S/O donor sets found to be effective in reducing blood glucose levels regardless of which donor set is employed. Bis (picolinato)oxovanadium(IV) (VO(pico)$_2$) is one of the most effective coordination complexes being investigated for use in diabetic therapy.

This chapter describes the syntheses and spectral characterization of oxovanadium(IV) complexes of acylydrazones.

3.2. Experimental

3.2.1. Materials

All the chemicals and solvents used for the syntheses were of analytical grade. Quinoline-2-carbaldehyde (Aldrich), Benzhydrazide (Aldrich), nicotinic hydrazide (Aldrich), vanadyl sulfate (Aldrich) and vanadyl acetylacetonate (E-Merck) were used as received. Solvents were purified by standard procedures before use.

3.2.2. Syntheses of ligands

Preparation of the acylhydrazones HQb and HQn were done as described previously in Chapter 2.

3.2.3. Syntheses of oxovanadium(IV) complexes
3.2.3a. *Synthesis of [VO(Qb)(OMe)]·1.5H$_2$O (1)*

To a solution of HQb·1.5H$_2$O (0.303 g, 1 mmol) in methanol (20 ml), a DMF–methanol mixture (1:1 v/v, 20 ml) of VO(acac)$_2$ (0.265 g, 1 mmol) was added. The resulting solution was refluxed for 6 h. and then kept at room temperature. The green crystalline precipitate of **1** that separated out was filtered, washed with ether and dried over P$_4$O$_{10}$ *in vacuo*. Yield: 89%, m.p. >300 °C. λ_m (DMF): 20 ohm^{-1} cm^2 mol^{-1}. Elemental Anal. Found (Calcd) %: C, 53.73 (54.14); H, 4.41 (4.54); N, 10.63 (10.52) for [VO(Qb)(OMe)]·1.5H$_2$O. % H$_2$O 6.23 (6.75) from TG.

3.2.3b. *Synthesis of [(VO)$_2$(HQn)$_2$(µ-SO$_4$)]SO$_4$·4H$_2$O (2)*

Vanadyl sulfate (0.163 g, 1 mmol) in methanol (20 ml) was added to a solution of HQn·1.5H$_2$O (0.303 g, 1 mmol) in methanol (20 ml) and refluxed for 5 h. A green crystalline precipitate of **2** obtained was filtered off, washed with ether and dried over P$_4$O$_{10}$ *in vacuo*. Yield: 63%, m.p. 225–227 °C. λ_m (DMF): 62 ohm^{-1} cm^2 mol^{-1}, Elemental Anal. Found (Calcd) %: C, 40.44 (40.43); H, 3.81 (3.39); N, 11.72 (11.79) for [(VO)$_2$(HQn)$_2$(µ-SO$_4$)]SO$_4$·4H$_2$O. % H$_2$O 7.02 (7.58) from TG.

3.3. Results and discussion

Vanadium can exist in different oxidation states; commonly found oxidation states in naturally occurring vanadium compounds are +3, +4 and +5. Complexes of vanadium usually adopt five coordinate square pyramidal or six-coordinate distorted octahedral geometries and the electronic and steric requirements rule out the possibility of the trigonal bipyramidal stereochemistry.

Here, the reaction of equimolar ratio of the tridentate ligand and the metal salt yielded corresponding oxovanadium (IV) complex. Based on the elemental analyses, conductivity measurements and spectral investigations, the complexes were formulated.

The hydrazones discussed here are NNO donors and they can coordinate either in the keto form or in enolate form. Infrared spectral evidence supports the presence of coordination of the respective hydrazones through the enolate form in complex **1**, while in complex **2**; the ligand coordinates in the keto form.

The molar conductivities of the complexes in DMF (10^{-3} M) solution were measured at 298 K with a Systronic model 303 direct-reading conductivity bridge, which show complex **1** is a non-electrolyte and complex **2** behaves as a 1:1 electrolyte [18].

The magnetic moments of the complexes were calculated from the magnetic susceptibility measurements and the value for complex **1** at room temperature is 1.64 *B.M.* and that for **2** is 1.53 *B.M.* The values are found to be very close to the spin only value 1.73 *B.M.* which indicate the presence of one unpaired electron. Both complexes are EPR active due to the presence of an unpaired electron.

3.3.1. Infrared spectra

The IR spectra were recorded on a Thermo Nicolet AVATAR 370 DTGS model FT-IR spectrophotometer as KBr pellets at SAIF, Kochi, India. The comparison of the main vibrational bands of the ligands with those of the complexes helps to establish their ligating behavior to the metal centre. The selected IR bands of the hydrazones and complexes are represented in Table 3.1.

Table 3.1. Infrared spectral data of the hydrazones and their oxovanadium complexes.

Compound	ν(C=O) cm^{-1}	ν(NH) cm^{-1}	ν(C=N) cm^{-1}	ν(C=N) [a] cm^{-1}	ν(C–O) cm^{-1}	ν(V=O) cm^{-1}
HQb·1.5H$_2$O	1655	3193	1593	----	----	----
Complex **1**	----	----	1582	1593	1384	940
HQn·1.5H$_2$O	1656	3173	1591	----	----	----
Complex **2**	1655	3186	1560	----	----	980

[a] Newly formed C=N.

50

The acylhydrazones contain an amide function, –NH–C(O)–, and consequently they exhibit keto-enol tautomerism. The IR spectrum of the HQb·1.5H$_2$O exhibits two bands at 3193 and 1655 cm^{-1} due to the ν(NH) and ν(C=O), respectively, and these bands are absent in complex **1**. This indicates that the ligand coordinates to the metal in enolate form. A new band appearing at 1384 cm^{-1} is assigned to ν(C–O) band. In the IR spectrum of the HQn·1.5H$_2$O, ν(NH) appears at 3173 cm^{-1} and ν(C=O) at 1656 cm^{-1}. However, in complex **2**, the appearance of ν(NH) and ν(C=O) bands at 3186 and 1655 cm^{-1}, respectively, implies that the ligand coordinates in the keto form. The IR spectrum of complex **1** is shown in Fig. 3.1.
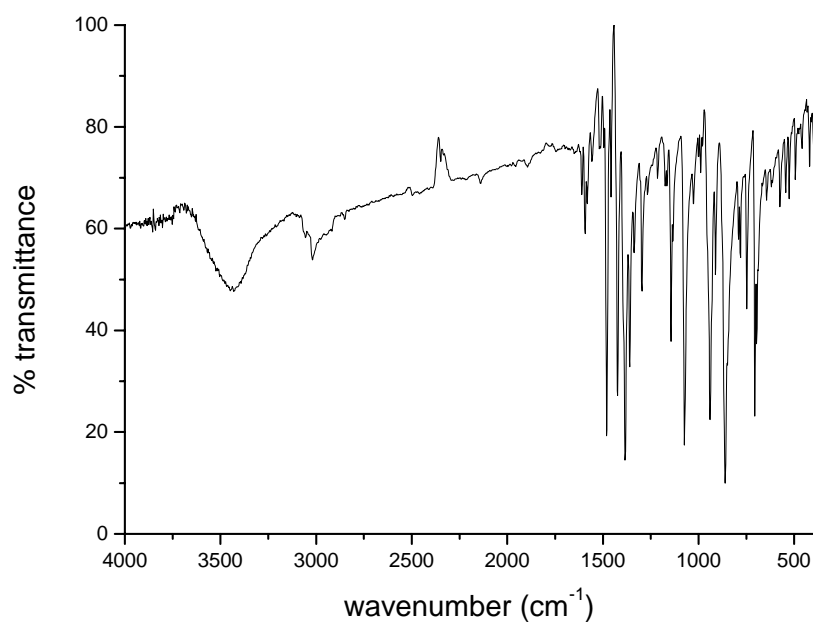
Fig. 3.1. IR spectrum of [VO(Qb)(OMe)]·1.5H$_2$O (**1**).

Each of the acylhydrazones under discussion displays a band in the region ~ 1590 cm^{-1} ascribed to ν(C=N) of the azomethine group [19]. These bands undergo shifts to the lower wavenumbers upon complexation which suggests the coordination of the azomethine-nitrogen to vanadium [20]. In complex **1**, a new band at 1593 cm^{-1} is observed which may be due to the newly formed ν(C=N) band.

The out-of-plane bending modes of vibrations of the free ligands at 625 cm^{-1} are found to be shifted to higher energies in the spectra of complexes indicating the coordination *via* quinoline nitrogen [21].

Further, the intense bands observed at 940 cm^{-1} for complex **1** and 980 cm^{-1} for complex **2** correspond to the terminal V=O stretching band.

The presence of two types of sulfate moieties is evident from the IR spectrum of complex **2**. The strong bands, observed at 1044 and 1170 cm^{-1} and another at 469 cm^{-1} are attributable to a bidentate bridging sulfato group; bands at 1126 and 606 cm^{-1} can be assigned to the presence of an ionic sulfato group [22,23].

3.3.2. Electronic spectra

The spin-orbit coupling for the oxovanadium(IV) complexes is positive and magnetically dilute oxovanadium(IV) complexes should exhibit magnetic moments very close to the spin-only value, 1.73 *B.M.*, as expected for an $S = 1/2$ system. However the value for the complex **2** is 1.53 *B.M.* and the decrease in the value may be due to the antiferromagnetic spin exchange [24].

In phenoxo-, alkoxo- or hydroxo-bridged dimeric oxovanadium(IV) complexes, for which singlet ground states have been reported, direct overlap of the d_{xy} orbital is considered to be the dominant magnetic exchange pathway [25,26]. Recently, some sulfato-bridged oxovanadium(IV) complexes have been reported [24] and it has been mentioned that antiferromagnetic exchanges depend upon the distance between the two metal centers, polarizability of the donor atom, electron density modulating behavior of the auxiliary ligands or bridging groups and geometric distortion of the coordination sphere.

Interpretation of the electronic spectra of oxovanadium(IV) complexes is the subject of continuing investigation and discussion. Usually, three optical bands are observed in the visible region, assigned to ^2E (d_{xz}, d_{yz}) $\leftarrow$ $^2B_2$ (d_{xy}) (v_1), $^2B_1$ ($d_{x^2-y^2}$) $\leftarrow$ $^2B_2$ (d_{xy}) (v_2) and $^2A_1$ (d_{z^2}) $\leftarrow$ $^2B_2$ (d_{xy}) (v_3). The v_3 band is often obscured by intense charge-transfer absorptions.

Electronic spectra of the complexes were recorded in acetonitrile and in DMF, on a UV–vis Double Beam UVD-3500 spectrophotometer in the range 50000–11100 cm^{-1}.

The bands in the range 44000-29000 cm^{-1} are attributed to the n–π^* and π–π^* transitions, which suffered some shift upon complexation, as evidenced by the absorptions observed for the ligand and complexes.

For complex **1**, a band at 23450 cm^{-1} is assigned to the ligand to metal charge transfer (LMCT) transition arising from amide oxygen of the ligand to an empty d orbital of the vanadium centre. This band is found to be blue-shifted to 24450 cm^{-1} for the complex **2**. The presence of strongly coordinating sulfate group in complex **2** shifts the LMCT transition to higher energy.

The two bands at 11680 and 18480 cm^{-1} for **1** are due to the ν_1 and ν_2 transitions, while in **2** d–d bands are observed at 11740 and 18860 cm^{-1} [27,28]. Electronic absorption spectral data of the hydrazones and their V(IV) complexes are summarized in Table 3.2. The electronic spectra, in the range 45000-20000 cm^{-1}, for both the complexes in acetonitrile are given in Figs. 3.2 and 3.3 along with the spectra of the corresponding ligands.

Table 3.2. Electronic spectral data for the hydrazones and their V(IV) complexes.

Compound	Absorbance λ_{max} (cm^{-1})
HQb·1.5H$_2$O	43790, 41640, 35860, 32580, 31690, 30430, 29130
Complex **1**	43810, 42490, 35770, 32810, 31810, 30330, 29050, 27820, 23450, 18480, 11680
HQn·1.5H$_2$O	43920, 41490, 35840, 32580, 31750, 30440, 29150
Complex **2**	41180, 35980, 32150, 30460, 29230, 27950, 24450, 18860, 11740
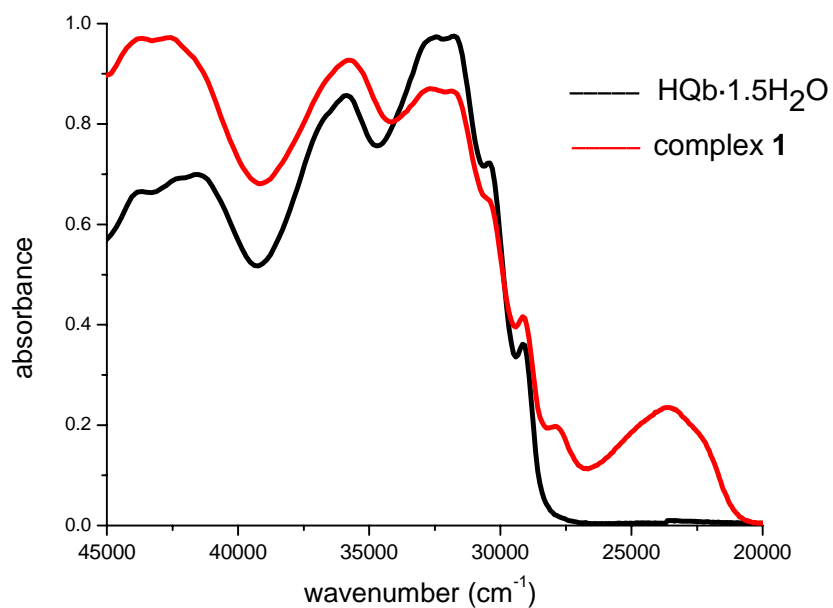
Fig. 3.2. Electronic spectra of HQb·1.5H$_2$O and [VO(Qb)(OMe)]·1.5H$_2$O (**1**) recorded in acetonitrile.
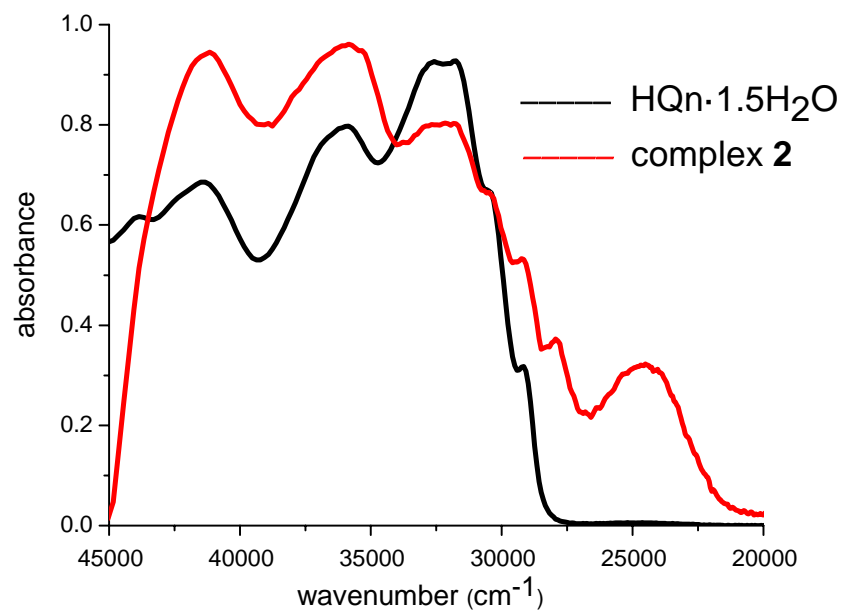
Fig.3.3. Electronic spectra of HQn·1.5H$_2$O and [(VO)$_2$(HQn)$_2$(μ-SO$_4$)] SO$_4$·4H$_2$O (**2**) recorded in acetonitrile.

3.3.3. Electron paramagnetic resonance spectra

Electron paramagnetic resonance (EPR) or electron spin resonance (ESR) spectroscopy is defined as the form of spectroscopy concerned with microwave-induced transitions between magnetic energy levels of electrons having a net spin and orbital angular momentum. EPR spectroscopy is a convenient and effective way to probe the electronic structure of paramagnetic molecules.

In the EPR spectra of oxovanadium(IV) complexes, the g values are typically less than the free electron value. For the case of vanadium(IV), the nuclear spin of ^{51}V is $I = 7/2$, so the states are split into $2I+1 = 8$ different energy states each, separated by the hyperfine coupling constant, A.

The oxidation state of the central vanadium atom in the complexes was confirmed by the measurements of EPR spectroscopy. Complexes **1** and **2** are paramagnetic samples and EPR spectra were recorded in polycrystalline state at 298 K and in frozen DMF at 77 K.

In polycrystalline state at 298 K, EPR spectrum of compound **1** is axial with $g_{\parallel} = 1.941$ and $g_{\perp} = 1.947$ (Fig. 3.4). The spectrum shows two sets of eight-line pattern, characteristic of an unpaired electron being coupled to the vanadium nuclear spin (^{51}V, $I = 7/2$). The anisotropic hyperfine parameters were calculated ($A_{\parallel} = 176.42 \times 10^{-4}$ and $A_{\perp} = 73.51 \times 10^{-4}$ cm^{-1}). The EPR spectrum of complex **1** in DMF at 77 K was not of good quality, probably due to poor glass formation. In frozen DMF, the complex **2** displayed well-resolved axial anisotropy (Fig. 3.5) with two sets of eight lines ($A_{\parallel} = 195.71 \times 10^{-4}$ and $A_{\perp} = 77.14 \times 10^{-4}$ cm^{-1}). The EPR spectrum of the complex **2** in polycrystalline state was difficult to interpret.

The $g_{\parallel} < g_{\perp}$ and $A_{\parallel} > A_{\perp}$ relationships are characteristic of an axially compressed system with unpaired electron in d_{xy} (b_{2g}) orbital [29-32]. The absence of superhyperfine splitting in the spectra also indicates the unpaired

electron to be in d_{xy} orbital localized in metal, thus excluding the possibility of its interaction with ligands [33-37].
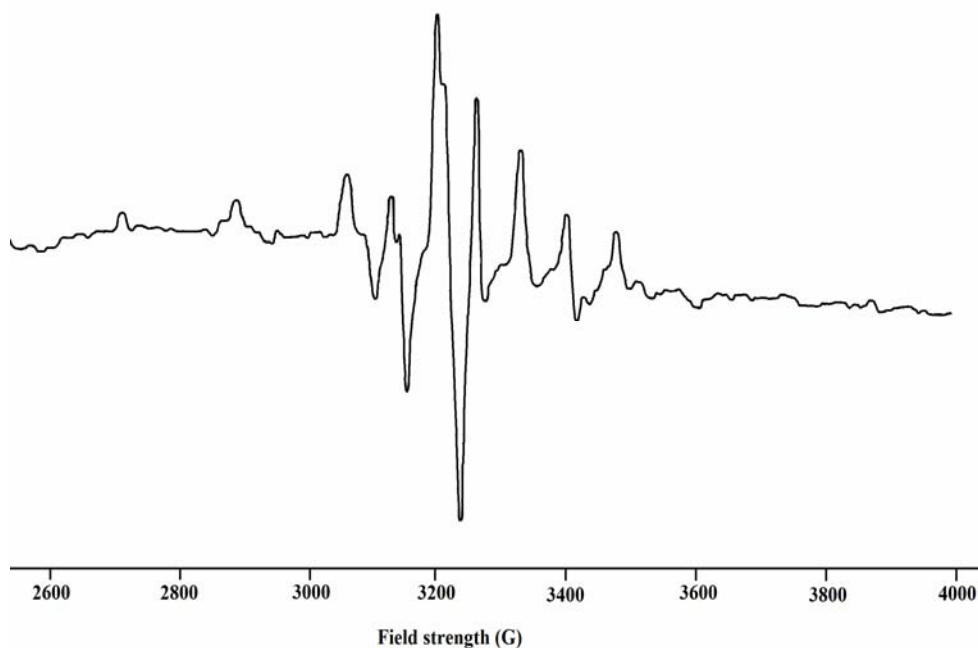
Fig. 3.4. EPR spectrum of [VO(Qb)(OMe)]·1.5H$_2$O (**1**) in polycrystalline state at 298 K.

The molecular orbital coefficients α^2 and β^2 were calculated for the complexes using the following equations [38].

$$\alpha^2 = (2.0023 - g_{\parallel})E/8\lambda\beta^2$$

$$\beta^2 = 7/6 \left[(-A_{\parallel}/P) + (A_{\perp}/P) + (g_{\parallel} - 5\,g_{\perp}/14) - 9g_e/14\right]$$

where $P = 128 \times 10^{-4}$ cm^{-1}, $\lambda = 135$ cm^{-1} and E is the electronic transition energy. The lower values for α^2 compared to β^2 indicate that in-plane σ-bonding is more covalent than in-plane π-bonding. EPR spectral parameters of oxovanadium(IV) complexes are collected in Table 3.3.
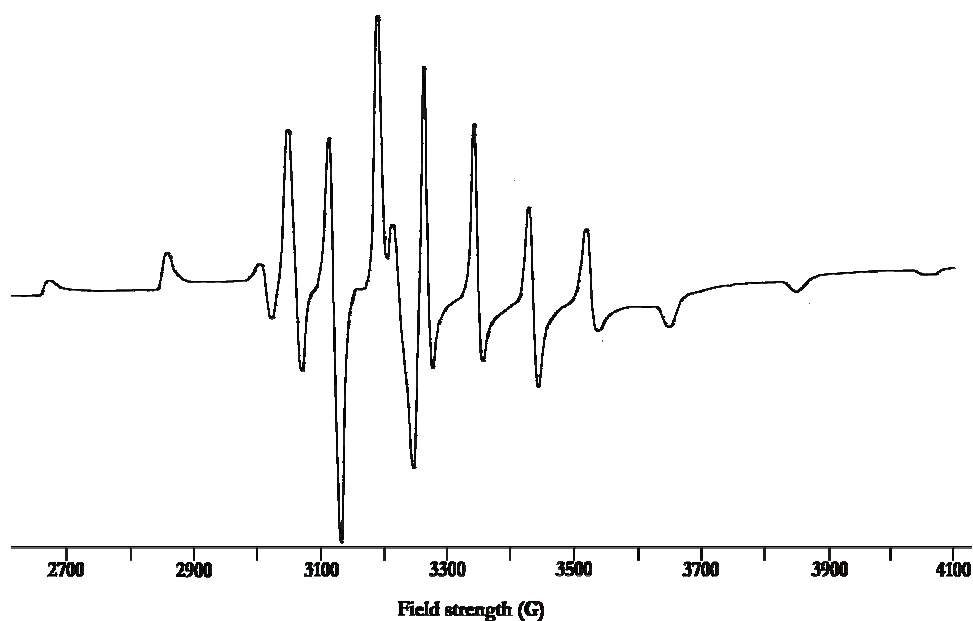
Fig. 3.5. EPR spectrum of $[(VO)_2(HQn)_2(\mu-SO_4)]SO_4 \cdot 4H_2O$ (**2**) in DMF at 77 K.

Table 3.3. EPR spectral parameters of vanadium(IV)complexes in the polycrystalline state at 298 K and in frozen DMF at 77 K.

	Complex **1**	Complex **2**
Polycrystalline state (298 K)	$g_\parallel = 1.941$ $g_\perp = 1.947$ $A_\parallel = 176.42 \times 10^{-4} \text{ cm}^{-1}$ $A_\perp = 73.51 \times 10^{-4} \text{ cm}^{-1}$	---
DMF (77 K)	---	$g_\parallel = 1.928$ $g_\perp = 1.978$ $A_\parallel = 195.71 \times 10^{-4} \text{ cm}^{-1}$ $A_\perp = 77.14 \times 10^{-4} \text{ cm}^{-1}$ $\alpha^2 = 0.756$ $\beta^2 = 1.0335$

References

[1]   A.I. Solomon, R.K. Szilagyi, S.D. George, L. Basumallick, Chem. Rev. 104 (2004) 419.

[2]   S. Bernard, C. Paillat, T. Oddos, Eur. J. Med. Chem. 30 (1995) 471.

[3]   M.M. Heravi, L. Ranjbar, F. Derikvand, H.A. Oskooie, F.F. Bamoharram, J. Mol. Catal. A: Chem. 265 (2007) 186.

[4]   I. Cavaco, J.C. Pessoa, M. Duarte, R.D. Gillard, P. Matias, Chem. Commun. (1996) 1365.

[5]   A. Butler, C.J. Carrano, Coord. Chem. Rev. 109 (1991) 61.

[6]   D. Rehder, Angew. Chem. Int. Ed. Engl. 30 (1991) 148.

[7]   E.C. Constable, F.K. Khan, J. Lewis, M.C. Liptrot, P.R. Raith, J. Chem. Soc., Dalton Trans. (1985) 333.

[8]   J.G. Wu, R.W. Deng, Z.N. Chen, Transit. Met. Chem. 18 (1993) 23.

[9]   D. Kostrewa, H.W. Choe, U. Heinmann, W. Saenger, Biochemistry 28 (1989) 7592.

[10]   N. Nawar, M.A. Khattab, M.M. Bekheit, A.H. El-Kaddah, Synth. React. Inorg. Met.-Org. Chem. 24 (1994) 1281.

[11]   N. Nawar, M.A. Khattab, M.M. Bekheit, A.H. El-Kaddah, Indian J. Chem. 35A (1996) 308.

[12]   C.E. Heyliger, A.G. Tahiliani, J.H. McNeill, Science 227 (1985) 1474.

[13]   A. Butler, J.V. Walker, Chem. Rev. 93 (1993) 1937.

[14]   D. Rehder, Coord. Chem. Rev. 182 (1999) 297.

[15]   C.J. Carrano, C.M. Nunn, R. Quan, J.A. Bonadies, V.L. Pecoraro, Inorg. Chem. 29 (1990) 941.

[16]   P.V. Bernhardt, G.J. Wilson, P.C. Sharpe, D.S. Kalinowski, D.R. Richardson, J. Biol. Inorg. Chem 13 (2008) 107.

[17]   N.A. Mangalam, S. Sivakumar, S.R. Sheeja, M.R.P. Kurup, E.R.T. Tiekink, Inorg. Chim. Acta 362 (2009) 4191.

[18]   W.J. Geary, Coord. Chem. Rev. 7 (1971) 81.

[19]   S. Naskar, D. Mishra, R.J. Butcher, S.K. Chattopadhyay, Polyhedron 26 (2007) 3703.

[20]   S.K. Dutta, S.B. Kumar, S. Bhattacharyya, E.R.T. Tiekink, M. Chaudhury, Inorg. Chem. *36* (1997) 4954.

[21]   P.F. Raphael, E. Manoj, M.R.P. Kurup, Polyhedron 26 (2007) 5088.

[22]   N.A. Mangalam, M.R.P. Kurup, Spectrochim. Acta Part A 71 (2009) 2040.

[23]   K. Nakamoto, Infrared and Raman Spectra of Inorganic and Coordination Compounds, 5th ed., Wiley, New York, 1997.

[24]   R. Das, K.K. Nanda, A.K. Mukherjee, M. Mukherjee, M. Helliwell, K. Nag, J. Chem. Soc., Dalton Trans. (1993) 2241.

[25]   M. Koppen, G. Fresen, K. Wieghardt, R.M. Llusar, B. Nuber, J. Weiss, lnorg. Chem. 27 (1988)721.

[26]   A. Ozarowaski, D. Reinen, Inorg. Chem. 25 (1986) 1704.

[27]   T. Ghosh, S. Bhattacharya, A. Das, G. Mukherjee, M.G.B. Drew, Inorg. Chim. Acta 358 (2005) 989.

[28]   C.W. Hahn, P.G. Rasmussen, J.C. Bayón, Inorg. Chem. 31 (1992) 1963.

[29]   D. Collison, B. Gahan, C.D. Garner, F.E. Mabbs, J. Chem. Soc., Dalton Trans. (1980) 667.

[30]   F.E. Dickson, C.J. Kunesh, E.L. McGinnis, L. Petrakis, Anal.Chem. 44 (1972) 978.

[31]   P.R. Klich, A.T. Daniher, P.R. Challen, D.D. McConville, W.J. Youngs, Inorg. Chem. 35 (1996) 347.

[32]   A. Davidson, N. Edelstein, R.H. Holm, A.H. Maki, J. Am. Chem. Soc. 86 (1964) 2799.

[33]   K.B. Pandeya, O. Prakash, R.P. Singh, J. Ind. Chem. Soc. LX (1983) 531.

[34]   H. Kon, E. Sharpless, J. Chem. Phys. 42 (1965) 906.

[35]   D. Kevelson, S.K. Lee, J. Chem. Phys. 41 (1964) 1896.

[36]   F.A. Walker, R.L. Carlin, P.H. Rieger, J. Chem. Phys. 45 (1966) 4181.

[37]   D. Kivelson, J. Chem. Phys. 33 (1960) 1094.

[38]   N. Raman, Y.P. Raja, A. Kulandaisamy, Proc. Indian Acad. Sci. (Chem. Sci.) 113 (2001) 183.

…..ജ്ഞ…..

SYNTHESES AND SPECTRAL INVESTIGATIONS OF MANGANESE(II) COMPLEXES OF ACYLHYDRAZONES

4.1. Introduction

Manganese is an essential trace nutrient in all forms of life. Manganese and its compounds find very historical importance in medicine and also have some biological importance. The classes of enzymes that have manganese cofactors are very broad and include such classes as oxidoreductases, transferases, hydrolases, lyases, isomerases, ligases, lectins and integrins. The reverse transcriptases of many retroviruses (though not lentiviruses such as HIV) contain manganese. The best known manganese-containing polypeptides may be arginase, the diphtheria toxin, and Mn-containing superoxide dismutase (Mn-SOD). There has been a growing interest in the chemistry and biochemistry of manganese because of its implication in many biological redox processes [1].

The manganese complexes are used as mimics of Mn-SOD and are more suitable than Cu_2Zn_2SOD because manganese has a lower toxicity in mammalian systems [2]. Recently, various mononuclear manganese complexes have been selected for pharmaceutical uses [3] such as manganese complexes with Schiff-base ligands [4].

Complexes of manganese play important roles ranging from bioinorganic chemistry to solid state physics [5,6]. They take part in catalytic reactions and also in many biological redox processes, including photosynthetic oxygen evolution in chloroplasts in plants. The most important and primordial example, yet recognized, of manganese involvement in biological milieu is its unique role in the light-induced oxidation of water to molecular oxygen in photosystem II (PS II) of green plants [7,8].

Manganese(II) complexes are well known for their excellent catalytic activity towards the disproportionation of hydrogen peroxide and a number of them have been shown to catalyze the low temperature peroxide bleaching of fabrics [9,10]. They are also interesting due to their catalytic antioxidant activity. Manganese plays a significant role in enzyme activation. Citrate cyclase catalyzes the cleavage of citrate to oxaloacetate and acetate in the presence of manganese(II) or magnesium(II) [11]. In addition, Mn^{2+} has been often used as a substitute for Mg^{2+}, which does not have a unique spectroscopic signature [12].

Studies of synthetic mono- and oligomeric manganese model complexes provide important insights into the structure and function of the more complex biological systems. It is thus not surprising that, in the past few years, there has been a tremendous surge in research on the synthesis of various manganese complexes [13-16] and the strategy in the synthesis of the manganese complexes has been to incorporate the nitrogen and oxygen ligands to mimic the functional groups characteristic of the biological milieu. In this context, Schiff bases represent suitable and appropriate biomimetic ligands.

The coordination chemistry of manganese has received a great deal of attention because of the variable structures of manganese complexes and the possibility of magnetic coupling interaction [17-21]. The chemistry of manganese, in various oxidation states of the metal and in various combinations of nitrogen and oxygen donor environment, is presently witnessing intense activity. Manganese in biological systems adopts a range of coordination environments and may have oxidation states of +2, +3, +4 and possibly +5.

This chapter focuses on the syntheses and spectral characterization of manganese(II) complexes of the acylhydrazones.

4.2. Experimental

4.2.1. Materials

All the chemicals and solvents used for the syntheses were of analytical grade. Quinoline-2-carbaldehyde (Aldrich), benzhydrazide (Aldrich), nicotinic hydrazide (Aldrich), manganese(II) acetate tetrahydrate (Merck) and manganese(II) chloride tetrahydrate (Merck) were used as received. Solvents were purified by standard procedures before use.

4.2.2. Syntheses of ligands

Preparation of the ligands HQb and HQn were done as described previously in Chapter 2.

4.2.3. Syntheses of manganese(II) complexes

4.2.3a. *Synthesis of [Mn(HQb)Cl$_2$]* (3)

To a solution of HQb·1.5H$_2$O (0.303 g, 1 mmol) in methanol (20 ml), manganese(II) chloride tetrahydrate (0.198 g, 1 mmol) in methanol (20 ml) was added. The resulting solution was refluxed for 4 h. and then kept at room temperature. The pale yellow precipitate of **3** that separated out was filtered, washed with ether and then dried over P$_4$O$_{10}$ *in vacuo*. Yield: 52%. λ_m (DMF): 15 ohm^{-1} cm^2 mol^{-1}. μ (*B.M.*): 6.13. Elemental Anal. Found (Calcd) %: C, 50.24 (50.90); H, 3.41 (3.27); N, 10.53 (10.47) for [Mn(HQb)Cl$_2$].

4.2.3b. *Synthesis of [Mn(Qb)$_2$]* (4)

Manganese (II) acetate tetrahydrate (0.245 g, 1 mmol) in methanol (20 ml) was added to a solution of HQb·1.5H$_2$O (0.606 g, 2 mmol) in methanol (20 ml). The reaction mixture was refluxed for 3 h, cooled and filtered. The dark blue precipitate obtained was washed with methanol followed by ether and then dried over P$_4$O$_{10}$ *in vacuo*. Yield: 58%. λ_m (DMF): 8 ohm^{-1} cm^2 mol^{-1}. μ (*B.M.*): 5.70.

Elemental Anal. Found (Calcd) %: C, 67.60 (67.66); H, 4.41 (4.01); N, 13.78 (13.92) for [Mn(Qb)$_2$].

4.2.3c. *Synthesis of [Mn(HQn)Cl$_2$]·2H$_2$O (5)*

HQn·1.5H$_2$O (0.303 g, 1 mmol) in methanol (20 ml) and manganese(II) chloride tetrahydrate (0.198 g, 1 mmol) in methanol (20 ml) were mixed and refluxed for 4 h. Pale yellow precipitate was obtained. The reaction mixture was cooled and filtered. Then the precipitate was washed with methanol followed by ether and then dried over P$_4$O$_{10}$ *in vacuo*. Yield: 49%. λ_m (DMF): 20 ohm^{-1} cm^2 mol^{-1}. μ (*B.M.*): 5.67. Elemental Anal. Found (Calcd) %: C, 44.27 (43.86); H, 3.59 (3.68); N, 12.93 (12.79) for [Mn(HQn)Cl$_2$]·2H$_2$O.

4.2.3d. *Synthesis of [Mn(Qn)$_2$] (6)*

Manganese acetate tetrahydrate (0.245 g, 1 mmol) in methanol was added to the methanolic solution of HQn·1.5H$_2$O (0.606 g, 2 mmol). The reaction mixture was refluxed for 2 hours, cooled and filtered. The dark blue precipitate obtained was washed with methanol followed by ether and then dried over P$_4$O$_{10}$ *in vacuo*. Yield: 54%. λ_m (DMF): 10 ohm^{-1} cm^2 mol^{-1}. μ (*B.M.*): 5.91. Elemental Anal. Found (Calcd.) (%): C, 63.57 (63.47); H, 3.26 (3.66); N, 18.30 (18.51) for [Mn(Qn)$_2$].

4.3. Results and discussion

The common oxidation states of manganese are +2, +3, +4, +6 and +7, though oxidation states from -3 to +7 are observed. It is reported that manganese (II) is the most common among these different oxidation states, which is the state used in living organisms for essential functions. Mn^{2+} often competes with Mg^{2+} in biological systems. Exchange energy favors the high spin configuration. Due to the absence of LFSE of d^5 configuration, the formation constants of manganese(II) complexes are smaller than those of other first row transition metals.

Here, the reaction of equimolar ratio of the tridentate ligand and the metal salt yielded complexes **3** and **5**, whereas reaction of the ligand and metal salt in

ratio 2:1 resulted in metal complexes **4** and **6**. Based on the elemental analyses, conductivity measurements and spectral investigations, the complexes were formulated.

The manganese(II) complexes were found to be pale yellow or dark blue in color. Here, the acylhydrazones act as NNO - donor ligands and they can coordinate to the metal in neutral keto form or in anionic enolate form. Analytical data show that in complexes **3** and **5**, ligand moiety is in keto form whereas in complexes **4** and **6**, enolization of the ligand has taken place.

The molar conductivities of the complexes in DMF (10^{-3} M) solution were measured at 298 K with a Systronic model 303 direct-reading conductivity bridge, which show the non-electrolytic nature of the complexes in solution [22]. The magnetic moments of the complexes were calculated from the magnetic susceptibility measurements and the values are found to be in the range 5.6 – 6.2 *B.M.*, which are indicative of a high spin d^5 system. The complexes are found to be EPR active.

4.3.1. Infrared spectra

The IR spectra of the manganese complexes were analyzed in comparison with that of their respective free ligands in the region 4000-100 cm^{-1}.

A comparison of the IR spectra of the ligands and the complexes revealed significant variations in the characteristic bands due to coordination with the central metal ion. It was found that the absorption bands attributed to ν(C=O) and ν(N–H) in the free ligands, disappeared in the complexes **4** and **6**, due to coordination through enolate oxygen. But the presence of these bands in the other two complexes revealed the existence of the ligand in keto form in these complexes [23].

In the IR spectrum of complex **3**, the bands due to ν(C=O) and ν(N–H) are observed at 1630 and 3176 cm^{-1}. The azomethine band is shifted to 1546 cm^{-1} due to binding with the metal ion. The shifting of the azomethine (C=N) band to a

lower frequency is attributed to the conjugation of the *p*-orbital on the double bond with the *d*-orbital on the metal ion with reduction of the force constant. The sharp bands at 1492 and 1438 cm^{-1} are due to the aromatic ring vibrations (Fig. 4.1).
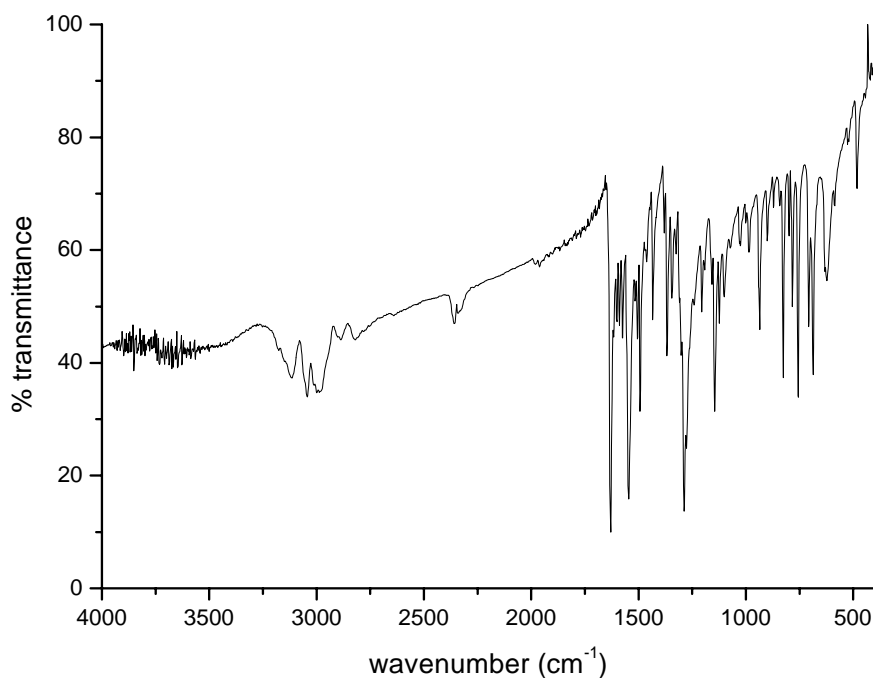
Fig. 4.1. IR spectrum of [Mn(HQb)Cl$_2$] (**3**).

The ligand coordination to the metal centre is substantiated by the bands appearing at 485, 403 and 323 cm^{-1} which are respectively attributed to ν(Mn–N) for azomethine nitrogen, ν(Mn–O) for amide oxygen and ν(Mn–N) for quinoline nitrogen. In the far IR spectrum of the complex [Mn(HQb)Cl$_2$] (**3**), a peak is observed at 303 cm^{-1}, indicating the terminal nature of chlorine atom [24,25].

The band, observed at 1590 cm^{-1} in the IR spectrum of [Mn(Qb)$_2$], is assigned to the new –C=N– moiety, formed as a result of enolization of the ligand on coordination. The azomethine band experienced a negative shift and is observed at 1547 cm^{-1}. The new band at 1368 cm^{-1} is assigned to the ν(C–O) stretch (Fig. 4.2).
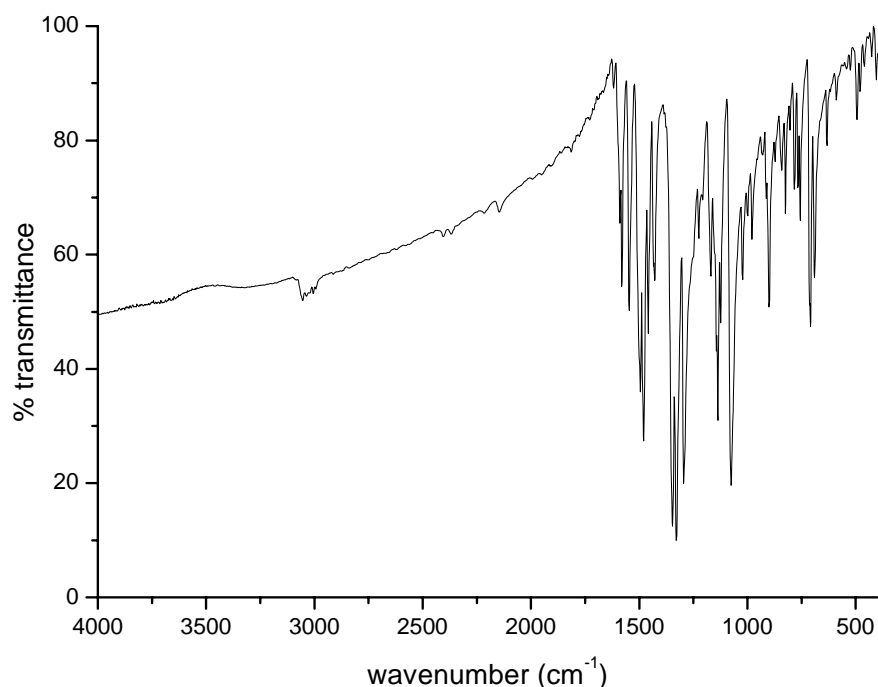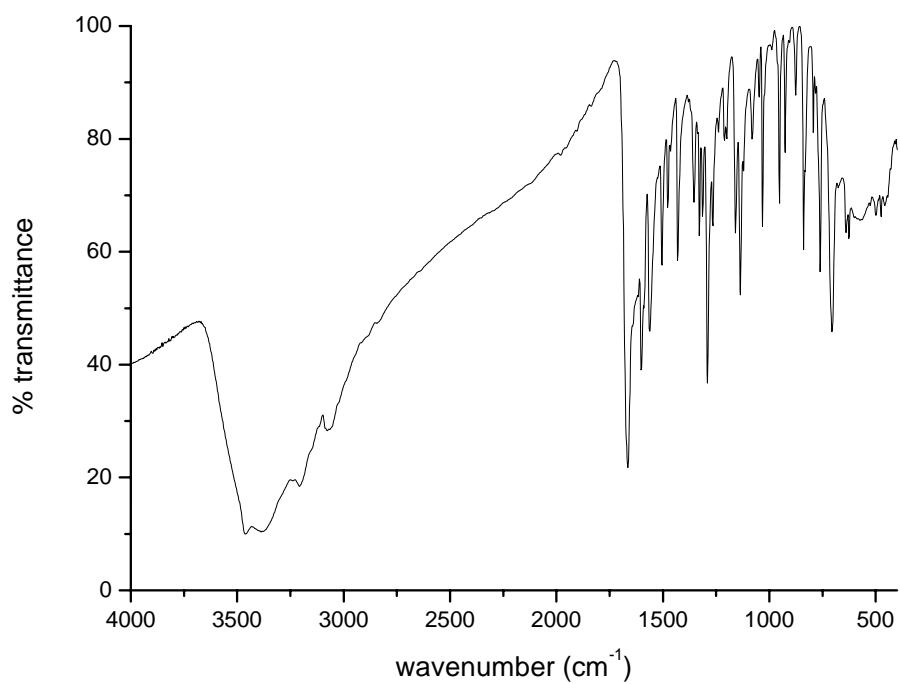
Fig. 4.2. IR spectrum of [Mn(Qb)$_2$] (**4**).

The broad band observed at 3462 cm^{-1} evidences the presence of lattice water in compound [Mn(HQn)Cl$_2$]·2H$_2$O. The bands observed at 1665 and 3203 cm^{-1} are attributed to ν(C=O) and ν(N–H) modes. The ν(C=N) band is observed at 1562 cm^{-1} and the aromatic ring vibrations at 1492 and 1438 cm^{-1} (Fig. 4.3).

In the far IR spectrum of the complex, the bands due to ν(Mn–N) for azomethine nitrogen, ν(Mn–O) for amide oxygen and ν(Mn–N) for quinoline nitrogen appear at 489, 410 and 321 cm^{-1}, respectively. The band observed at 305 cm^{-1} indicates the presence of terminal Mn–Cl stretching frequency.

In the IR spectrum of [Mn(Qn)$_2$], the bands due to ν(C=O) and ν(N–H) are absent and the azomethine band due to coordination with Mn(II) is shifted to 1548 cm^{-1}. The ν(C–O) band is observed at 1352 cm^{-1} and the band due to the newly formed –C=N–group is found at 1585 cm^{-1}. The characteristic ring vibrations were seen in the usual region (Fig. 4.4). The selected IR bands of the hydrazones and complexes are represented in Table 4.1.

67

Fig. 4.3. IR spectrum of [Mn(HQn)Cl$_2$]·2H$_2$O (**5**).
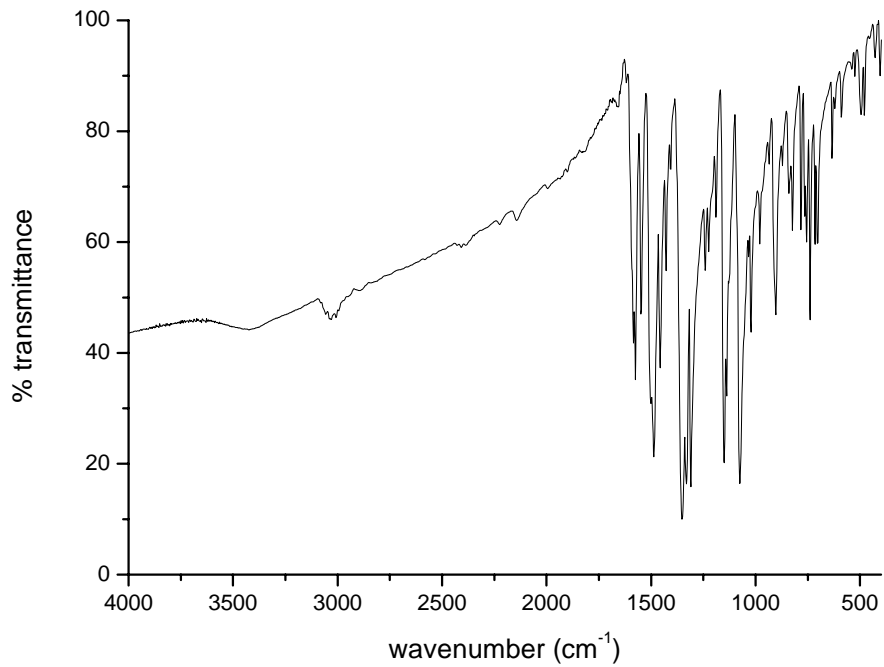
Fig. 4.4. IR spectrum of [Mn(Qn)$_2$] (**6**).

Table 4.1. Infrared spectral data of the hydrazones and their manganese(II) complexes.

Compound	$\nu(C=O)$ cm^{-1}	$\nu(N–H)$ cm^{-1}	$\nu(C=N)$ cm^{-1}	$\nu(C=N)^a$ cm^{-1}	$\nu(C–O)$ cm^{-1}
HQb·1.5H$_2$O	1655	3193	1593	----	----
[Mn(HQb)Cl$_2$] (**3**)	1630	3176	1546	----	----
[Mn(Qb)$_2$] (**4**)	----	----	1547	1590	1347
HQn·1.5H$_2$O	1656	3173	1591	----	----
[Mn(HQn)Cl$_2$]·2H$_2$O (**5**)	1665	3203	1562	----	----
[Mn(Qn)$_2$] (**6**)	----	----	1548	1585	1352

^{a} Newly formed C=N.

4.3.2. Electronic spectra

The Mn(II) complexes belong to the d^5 system. The Tanabe-Sugano diagram shows that the Russell-Saunders term for such a system in high spin state is ^6S and the ground state of high-spin octahedral Mn(II) complex is $^6A_{1g}$. The d^5 configuration gives rise to the ^4G, ^4D and ^4P excited states.

As there are no excited terms of sextet spin multiplicity, spin allowed *d-d* transitions are not expected. Also for octahedral complexes, these transitions are Laporte forbidden. So the *d-d* transitions in a high spin octahedral Mn(II) complexes are doubly forbidden; Laporte forbidden and spin forbidden [26-28]. However, some forbidden transitions occur and consequently, these transitions have an extremely low molar extinction coefficient value.

The electronic spectra of the Mn(II) complexes were recorded both in acetonitrile and DMF, in the region 50000-11000 cm^{-1}. The spectra, within the range 45000-20000 cm^{-1} recorded in acetonitrile, are shown in Figs. 4.5 and 4.6.
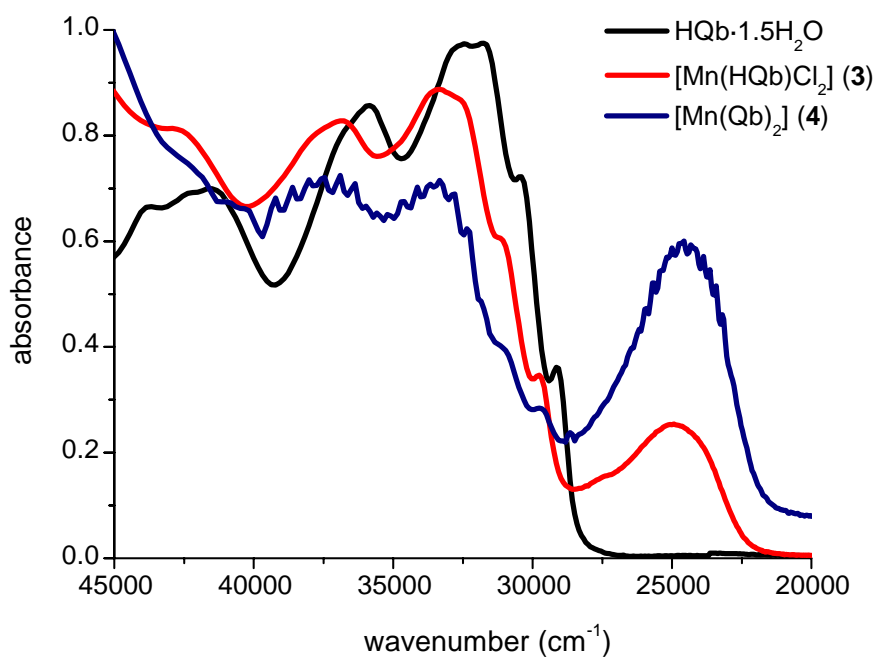
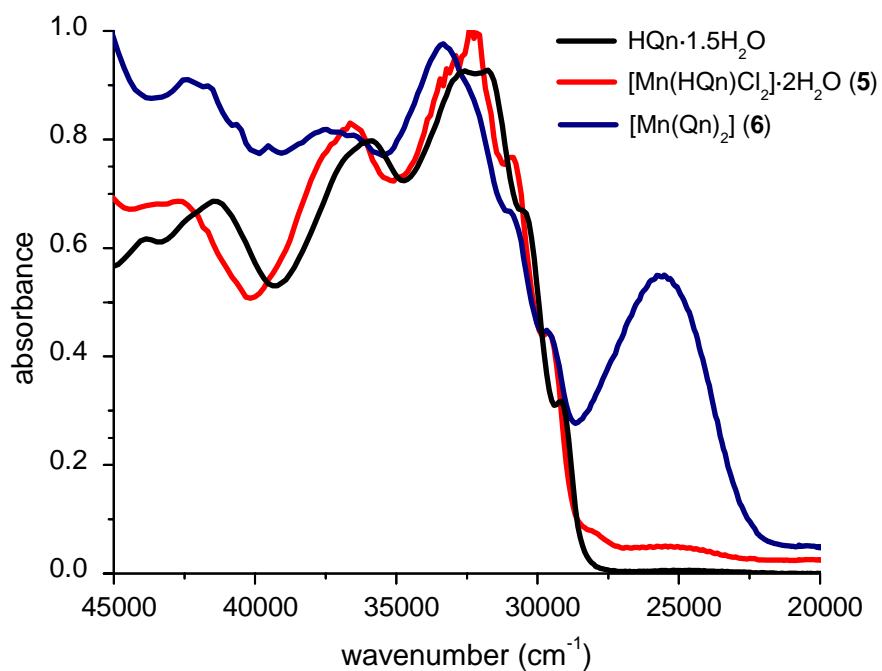**Fig. 4.5.** Electronic spectra of manganese(II) complexes of HQb·1.5H₂O.

Fig. 4.6. Electronic spectra of manganese(II) complexes of HQn·1.5H₂O.

The high intense intraligand transitions and charge transfer transitions, tailing into the visible region, obscure the very weak *d-d* transitions of the manganese(II) complexes. In all the complexes, a high intense transition is observed at *ca*. 24000 cm^{-1} which is assumed to be due to the ligand to metal charge transfer (LMCT) transition.

For octahedral Mn(II) complexes, electronic spectra show two bands at *ca*. 18000 and 20000 cm^{-1}, which are assigned to $^4T_{1g}(G) \leftarrow {}^6A_{1g}$ and $^4T_{2g}(G) \leftarrow {}^6A_{1g}$ respectively. These assignments are obtained by fitting the observed spectrum to the Tanabe Sugano diagram and for d^5 octahedral complex, $\dfrac{Dq}{B} = 1.1$. At this $\dfrac{Dq}{B}$, the ratio of the first transition energy and B (ie, $\dfrac{E}{B}$) is found to be 24.0. The electronic repulsion parameter (Racah parameter), B, is a function of the ligand and the metal ion and is a built in feature of these Tanabe Sugano diagrams [29].

The extent of covalence in metal-ligand bond may be evaluated from the electronic spectrum by estimating the nephelauxetic ratio (β) = $\dfrac{B}{B_o}$. The free ion value of B_o for octahedral Mn^{2+} is 860 cm^{-1}. The value of β decreases with increase in delocalization [26].

The electronic spectra of the manganese(II) complexes [Mn(HQb)Cl$_2$] (**3**) and [Mn(HQn)Cl$_2$]·2H$_2$O (**5**) exhibit weak-intensity absorption bands at *ca*. 18000, 22000 and 27000 cm^{-1}, which may be assigned to the transitions: $^4T_{1g}(G) \leftarrow {}^6A_{1g}$, $^4A_{1g}(G), {}^4E_g(G) \leftarrow {}^6A_{1g}$ (10B+5C), $^4E_g(D) \leftarrow {}^6A_{1g}$ (17B+5C).

The ligand field parameter *B* and *C* values have been calculated by using the second and third transition energies. This is due to the fact that the energies of these two transitions are independent from the crystal field splitting energy and

depends only on the parameters B and C [30,31]. Electronic spectral data for the hydrazones and their manganese(II) complexes are given in Table 4.2.

Table 4.2. Electronic spectral data for the hydrazones and their manganese(II) complexes, recorded in acetonitrile and in DMF.

Compound	Absorbance λ_{max} (cm^{-1})
HQb·1.5H$_2$O	43790, 41640, 35860, 32580, 31690, 30430, 29130
[Mn(HQb)Cl$_2$] (**3**)	35660, 34770, 31540, 30150, 28960, 26750, 24580, 21550, 17360.
[Mn(Qb)$_2$] (**4**)	42250, 40600, 37310, 33510, 31080, 29800, 24530, 20170, 17100,
HQn·1.5H$_2$O	43920, 41490, 35840, 32580, 31750, 30440, 29150
[Mn(HQn)Cl$_2$]·2H$_2$O (**5**)	43860, 42700, 36520, 32900, 32240, 30960, 29680, 27190, 25230, 22410, 18990
[Mn(Qn)$_2$] (**6**)	42410, 41630, 40640, 39530, 37510, 33350, 31000, 29720, 25600, 20500, 19100.

The *Dq* value has been evaluated with the help of curve, transition energies vs. Dq, by Orgel [32] using the energy due to the transition ${}^4T_{1g}(G) \leftarrow {}^6A_{1g}$. Parameters *B* and *C* are linear combination of certain Coulomb and exchange integrals and are generally treated as empirical parameters obtained from the spectra of the free ions. Slater Condon–Shortly parameters F_2 and F_4 are related to the Racah inter-electronic repulsion parameters *B* and *C*, as follows: $B = F_2 - 5F_4$ and $C = 35F_4$ [33]. The ligand field parameters of the complexes are given in Table 4.3.

Table 4.3. Ligand field parameters of manganese(II) complexes.

Compound	*B*	*C*	F_2	F_4	10*Dq* (Δ)	β
[Mn(HQb)Cl$_2$] (**3**)	742.8	2824.4	1146.3	80.7	-----	0.95
[Mn(Qb)$_2$] (**4**)	712.5	-----	-----	-----	7837.5	0.83
[Mn(HQn)Cl$_2$]·2H$_2$O (**5**)	682.9	3116.2	1127.9	89.0	-----	0.87
[Mn(Qn)$_2$] (**6**)	795.8	-----	-----	-----	8754.2	0.92

4.3.3. Electron paramagnetic resonance spectroscopy

The electron spin properties of manganese have long been of interest as a spectroscopic probe of manganese centers in manganese proteins. The Mn(II) system possesses Kramer's ground-state doublets and exhibits characteristic spin transitions in the normal mode X-band regime.

The spin Hamiltonian,

$$\hat{H} = g\beta BS + D\left[S_z^2 - \frac{S(S+1)}{3} \right] + E(S_x^2 - S_y^2) \dots\dots\dots\dots\dots (4.1)$$

may be used to describe the EPR spectra of Mn(II) complexes. In the expression, B is the magnetic field vector, g is the spectroscopic splitting factor, β is the Bohr magneton, D is the axial zero field splitting parameter, E is rhombic zero field splitting parameter and S is the electron spin vector [34].

If D and E are both zero, then the only contributor to the spectrum is the first-order Zeeman term and the result for Mn^{2+} is an isotropic spectrum, with a single six-line signal with g_{eff} near 2.0. In weak ligand fields, Mn(II) centers give a single transition at $g = 2$, which splits into six hyperfine lines by the ^{55}Mn nucleus ($I = 5/2$). However, simple spectra of this type are indicative of a cubic ligand field where the zero-field splitting parameter D is negligible and all of the $\Delta M_s = \pm 1$ transitions are degenerate, as a result. For a small but finite value for D and E, the degeneracy is removed and the spectrum exhibits 5-fold fine structure with a g value of 2.0.

If D is very large, only one transition is expected. However, for the case where D or E is very large, the lowest doublet has effective g values of $g_{\parallel} = 2$ and $g_{\perp} = 6$ for $D \neq 0$ and $E = 0$ but for $D = 0$ and $E \neq 0$, the middle Kramer's doublet has an isotropic g value of 4.29.

In more strongly axial systems where D is comparable to $h\nu$, high-spin d^5 ions such as Mn^{2+} often exhibit tetragonal spectra with $g_{\perp} \approx 6$ and $g_{\parallel} = 2$, a situation observed for many porphyrin, phthalocyanin and related complexes of Mn^{2+}.

73

Depending on the values of D and A, the number of lines observable in the spectra will be 30, 24 or 6. As delocalization increases, A value decreases. When $2D > 5A$, 30 lines will be obtained; when $2D = 5A$, overlapping occurs and we get only 24 lines. When $2D < 5A$, the number of lines still decreases and when $D = 0$, we will see only six lines [35,36].

Ligand fields of lower symmetry are often characterized by a rhombic signal at $g = 4.3$, but this is typically observed for relatively strong field ligands.

The X-band EPR spectra of the manganese complexes were recorded in polycrystalline state at 298 K and in frozen DMF at 77 K. The EPR spectrum of the compound $[Mn(HQb)Cl_2]$ (**3**) at 298 K in polycrystalline state exhibited two g values at $g_1 = 1.984$ and $g_2 = 3.120$, with no hyperfine splitting (Fig. 4.7). The spectrum is very broad due to dipolar interactions and enhanced spin lattice relaxation.
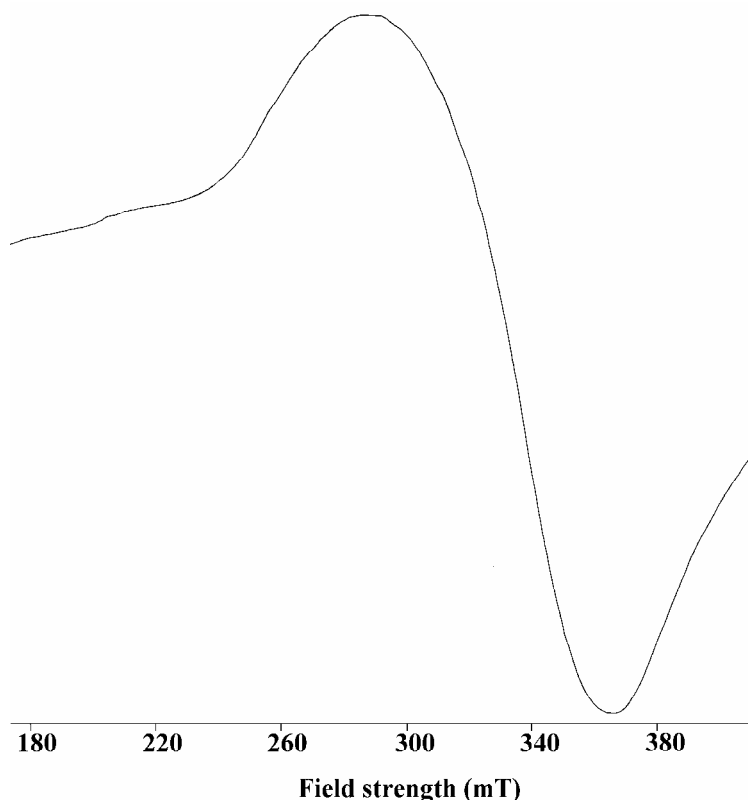
Fig. 4.7. EPR spectrum of $[Mn(HQb)Cl_2]$ (**3**) in polycrystalline state at 298 K.

74

The solution spectrum (Fig. 4.8) of the compound in DMF at 77 K displayed a hyperfine sextet with g = 2.018 and hyperfine coupling constant 69.0 x 10^{-4} cm^{-1}. The hyperfine structure results from a transition from the $|-½, M_I\rangle$ to the $|+½, M_I\rangle$ level, where the $-½$ and $+½$ denote the electron spin magnetic quantum numbers and M_I, the nuclear spin quantum number. The hyperfine spectrum of the compound consists of six allowed lines corresponding to M_s = +5/2, +3/2, +1/2, −1/2, −3/2, −5/2 with ΔM_I = 0 in the transition. The observed g value is very close to the free electron spin value of 2.0023, which is consistent with the typical manganese(II) system and also suggestive of the absence of spin orbit coupling in the ground state $^6A_{1g}$ without another sextet term of higher energy.
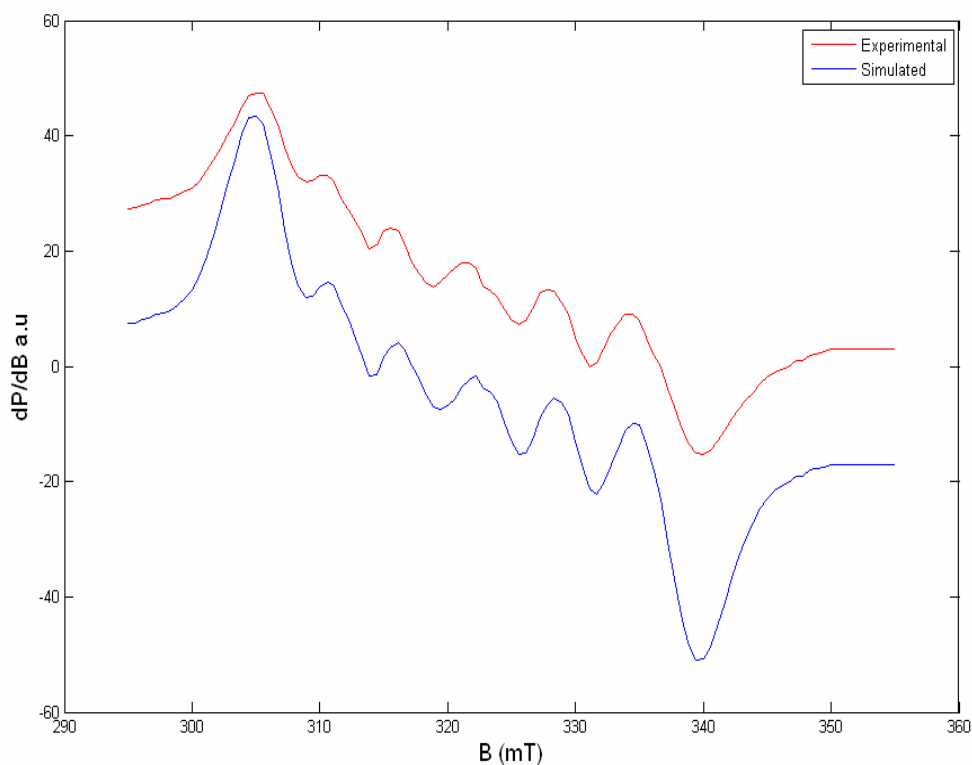

Fig. 4.8. Simulated and experimental best fits of the EPR spectrum of [Mn(HQb)Cl$_2$] (**3**) in DMF at 77 K.

EPR spectrum of [Mn(Qb)$_2$] (**4**) in polycrystalline state at 298 K exhibits three g values; g_1 = 1.802, g_2 = 2.386, g_3 = 3.565 (Fig. 4.9). The three g values imply that the molecule is rhombically distorted. The signals are comparatively broad with no hyperfine splitting. The broadness of the peaks is a characteristic feature of Mn(II) complex in the polycrystalline state, which arises due to dipolar interactions and enhanced spin lattice relaxation [36].

The compound [Mn(Qb)$_2$] in DMF at 77 K displays three g values at g_1 = 1.803, g_2 = 2.368 and g_3 = 3.310.

A broad isotropic signal with g_{iso} = 2.053 was found for the compound [Mn(HQn)Cl$_2$]·2H$_2$O (**5**) in polycrystalline state at 298 K and the hyperfine structure is not observed in the spectrum (Fig. 4.10).
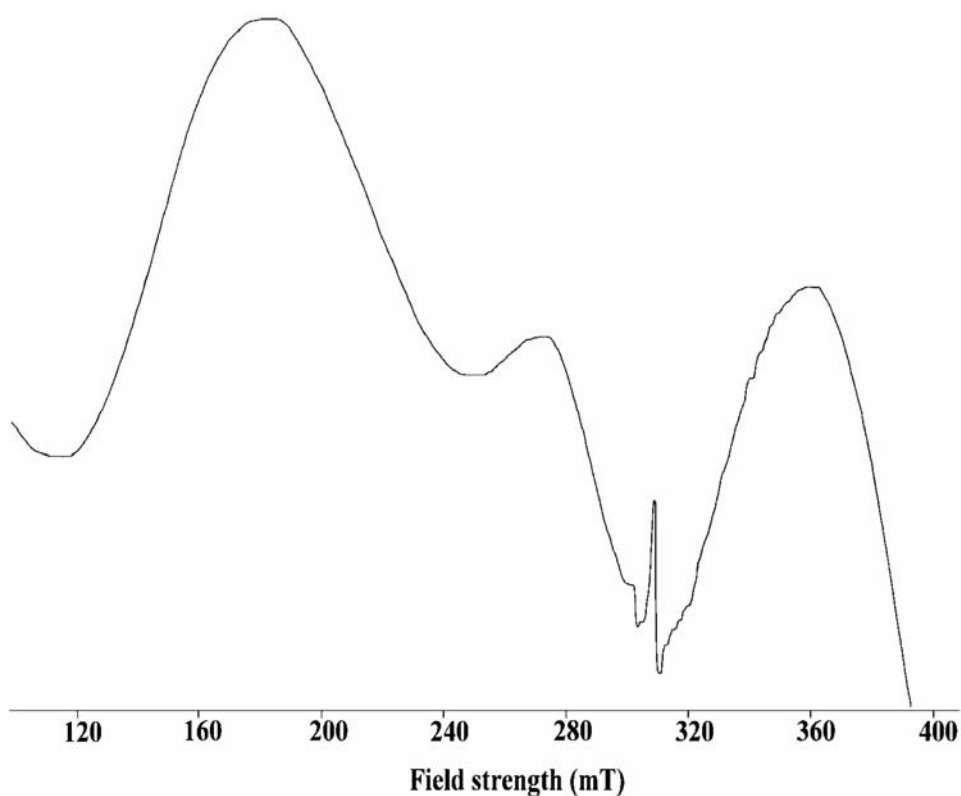
Fig. 4.9. EPR spectrum of [Mn(Qb)$_2$] (**4**) in polycrystalline state at 298 K.
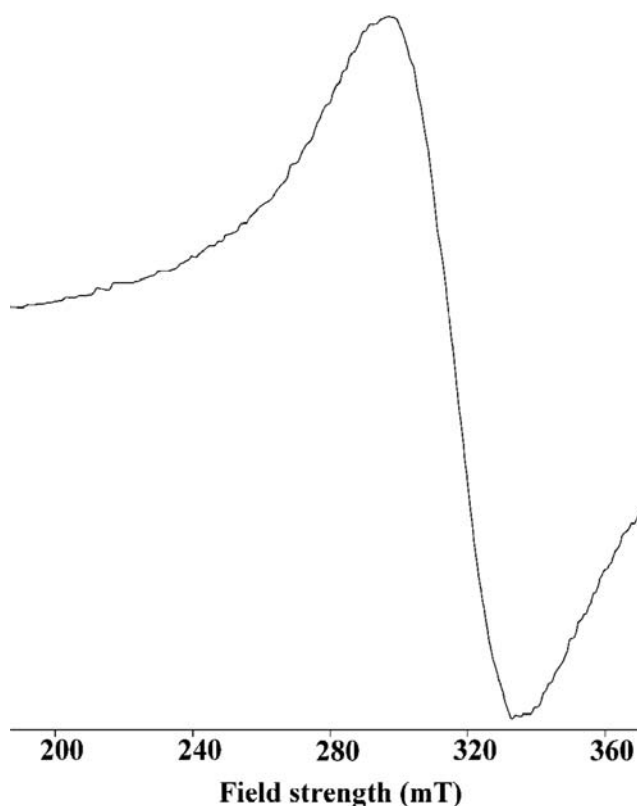
Fig. 4.10. EPR spectrum of [Mn(HQn)Cl$_2$]·2H$_2$O (**5**) in polycrystalline state at 298 K.

In DMF at 77 K, the EPR spectrum of [Mn(HQn)Cl$_2$]·2H$_2$O (**5**) is isotropic with g_{iso} = 1.996. The spectrum exhibits sixfold well-resolved hyperfine splitting pattern with the coupling constant A_{iso} = 96 x 10^{-4} cm^{-1} (Fig. 4.11).

Due to the interaction of the unpaired electron with the Mn(II) nucleus (I = 5/2), a hyperfine sextet (2nI+1 lines) observed corresponds to ΔM_s = ±1 and ΔM_I = 0. But due to the nuclear quadrupole effect, the forbidden lines corresponding to ΔM_I = ±1 transitions may arise. This is observed in the EPR spectrum of [Mn(HQn)Cl$_2$]·2H$_2$O (**5**) in DMF at 77 K as a pair of low intensity lines in between each of the two main hyperfine lines. According to Bleaney and Low, such forbidden transitions are brought about by the mixing of the nuclear hyperfine levels by the zero field splitting parameter D [37-40].

77
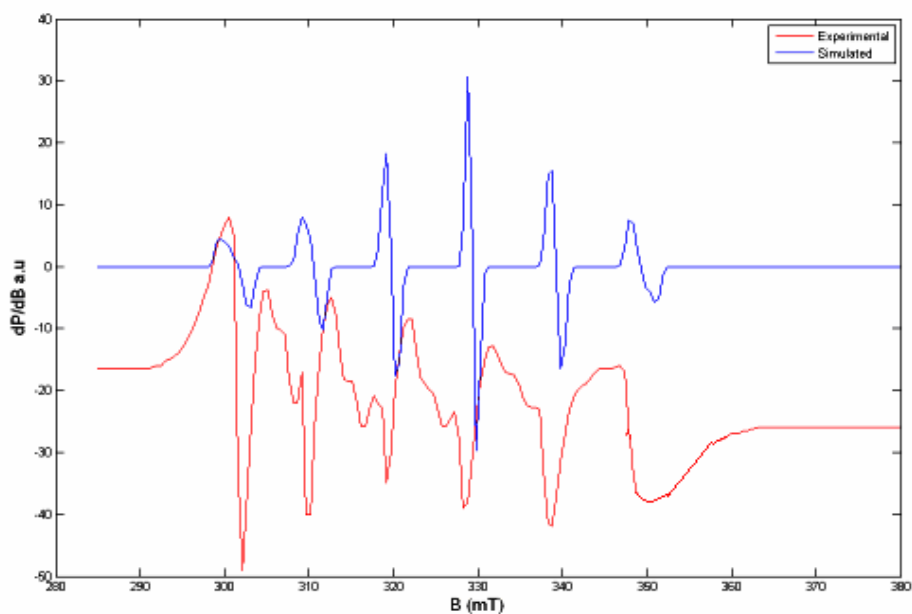
Fig. 4.11. Simulated and experimental best fits of the EPR spectrum of [Mn(HQn)Cl$_2$]·2H$_2$O (**5**) in DMF at 77 K.

The EPR spectrum of [Mn(Qn)$_2$] (**6**) in polycrystalline state at 298 K gave two *g* values; g_1 = 1.991 and g_2 = 2.773. The spectrum is broad with no hyperfine splitting (Fig. 4.12).
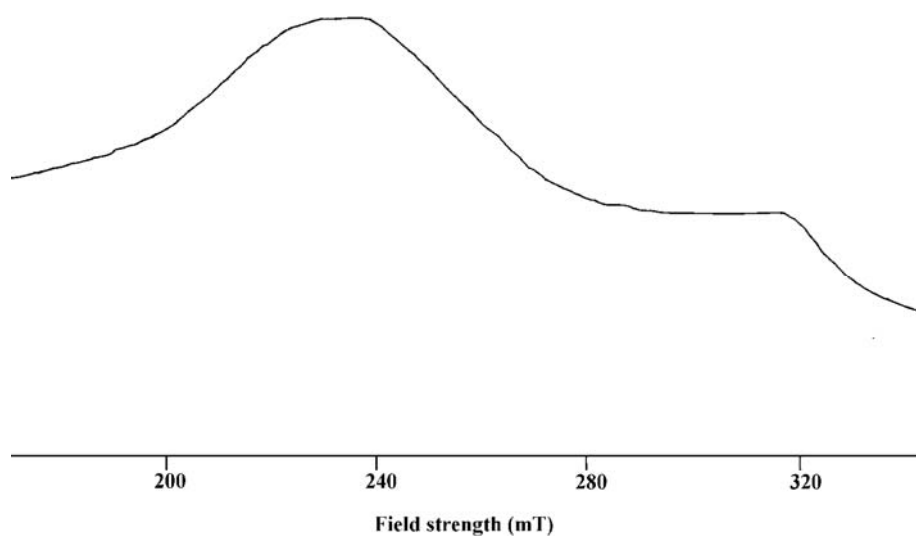
Fig. 4.12. EPR spectrum of [Mn(Qn)$_2$] (**6**) in polycrystalline state at 298 K.

The compound $[Mn(Qn)_2]$ (**6**) displayed four *g* values viz. 2.034, 2.421, 3.181 and 4.920 for the frozen solution spectrum in DMF at 77 K. The hyperfine splitting constant, *A*, calculated for the hyperfine sextet in the high field region is 117.7×10^{-4} cm^{-1}.

4.3.4. Cyclic voltammetry

Cyclic voltammograms were recorded on a CHI II20A electrochemical analyzer with a three electrode compartment consisting of a platinum disc working electrode, platinum wire counter electrode and Ag/Ag$^+$ reference electrode. The solutions of complexes in DMF have been used to study the electrochemical properties using TBAP (tetrabutylammonium phosphate) as the supporting electrolyte. The voltammogram is run between the potentials of +2000 and –2000 mV at a scan speed of 100 mV/s. Cyclic voltammetric data for the hydrazones and their Mn(II) complexes are tabulated in Table 4.4.

Table 4.4. Cyclic voltammetric data for the hydrazones and their Mn(II) complexes.

Compound	E_{pc} / mV (I_{pc} / μA)	E_{pa} / mV (I_{pa} / μA)
HQb·1.5H$_2$O	-220 (0.91)	520 (3.48)
[Mn(HQb)Cl$_2$] (**3**)	147 (3.32), -499 (5.60)	539 (4.46)
[Mn(Qb)$_2$] (**4**)	-----	-----
HQn·1.5H$_2$O	-280 (1.83)	830 (13.8)
[Mn(HQn)Cl$_2$]·2H$_2$O (**5**)	-134 (0.75), -761 (0.94)	-----
[Mn(Qn)$_2$] (**6**)	-98 (0.47)	790 (1.71), -60 (1.20)

The complex $[Mn(HQb)Cl_2]\cdot2H_2O$ (**3**) displays two reductive responses, *viz* 147 mV (3.32 μA), -499 mV (5.60 μA). The oxidative peak at 539 mV (4.46 μA), which is very close to the oxidative response of the corresponding ligand, is attributed to the ligand based oxidation reaction. The absence of the metal centered oxidative peak in the complex may be due to the presence of more

electronegative chlorine atoms attached to the metal ion. Generally, the presence of an electron withdrawing group stabilizes the lower oxidation state and electron donating group favors the higher oxidation state of the metal centre. Electronegative chlorine lowers the electron density on the manganese ion and oxidation of the Mn(II)-Mn(III) becomes more difficult [41].

The cyclic voltammogram of complex [Mn(Qn)$_2$] (**4**) was of poor quality and cannot be interpreted.

In the cyclic voltammogram of complex [Mn(HQn)Cl$_2$]·2H$_2$O (**5**), two reductive responses were observed at -134 mV (0.75 µA) and -761 mV (0.94 µA) and oxidative response was absent.

In the cyclic voltammogram of complex [Mn(Qn)$_2$] (**6**), one reductive response was observed at -98 mV (0.47 µA) and two oxidative responses at 790 mV (1.71 µA) and -60 mV (1.20 µA). The oxidative peak at 790 mV may be due to the ligand based reaction.

Figs. 4.13 - 4.15 illustrate cyclic voltammograms of manganese complexes, [Mn(HQb)Cl$_2$], [Mn(HQn)Cl$_2$]·2H$_2$O (**5**) and [Mn(Qn)$_2$] (**6**).
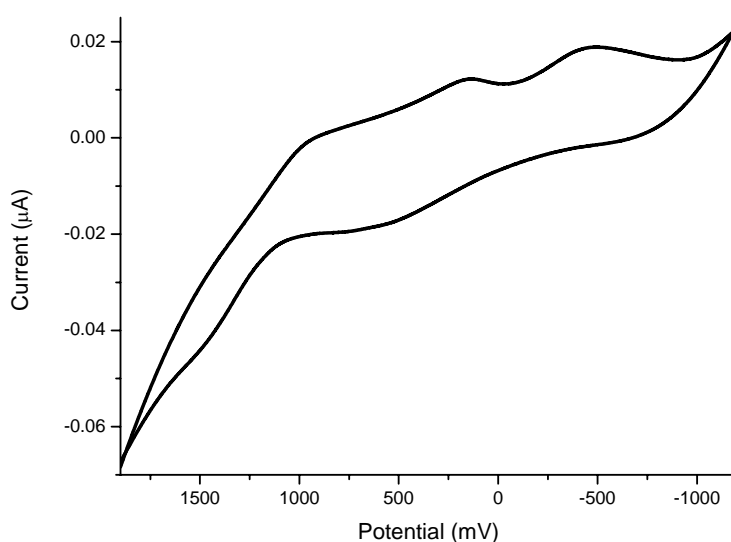
Fig. 4.13. Cyclic voltammogram of [Mn(HQb)Cl$_2$] (**3**) in DMF at 100 mV s^{-1}.
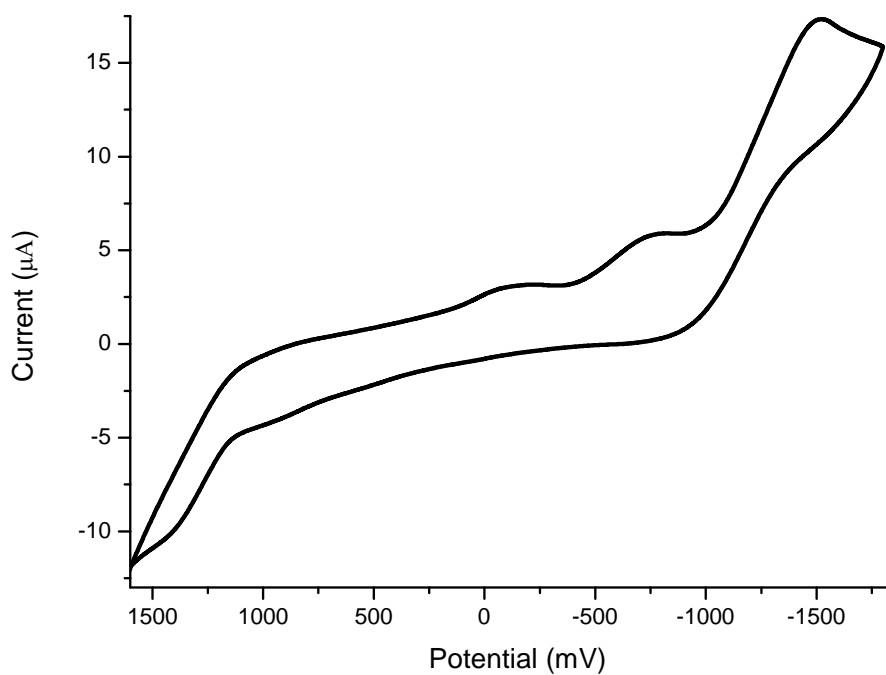
Fig. 4.14. Cyclic voltammogram of [Mn(HQn)Cl$_2$]·2H$_2$O (**5**) in DMF at 100 mV s^{-1}.
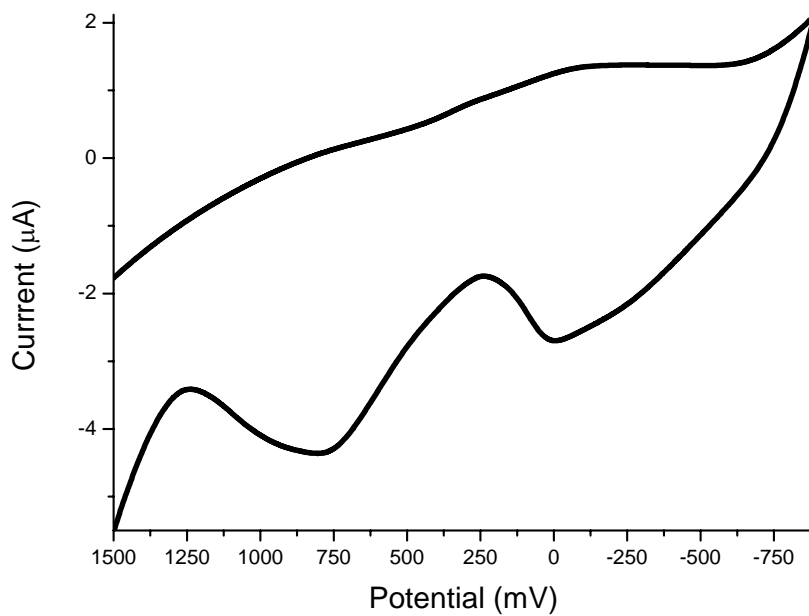
Fig. 4.15. Cyclic voltammogram of [Mn(Qn)$_2$] (**6**) in DMF at 100 mV s^{-1}.

81

References

[1]   V.L. Pecoraro, M.J. Baldwin, A. Gelasco, Chem. Rev. 94 (1994) 807.

[2]   D.P. Riley, Chem. Rev. 99 (1999) 2573.

[3]   G.C. Dismukes, Chem. Rev. 96 (1996) 2909.

[4]   R.F. Pasternack, A. Banth, J.M. Pasternack, C.S. Johnson, J. Inorg. Biochem. 15 (1981) 261.

[5]   W.C. Stallings, K.A. Pattridge, R.A. Strong, M.L. Ludwig, J. Biol. Chem. (1985) 1624.

[6]   K. Wieghardt, Angew. Chem. Int. Ed. Engl. 28 (1989) 1153.

[7]   R.J. Debus, Biochim. Biophys. Acta 269 (1992) 1102.

[8]   G. Christou, J.B. Vincent, Biochim. Biophys. Acta 259 (1987) 897.

[9]   M. Pick, I. Roboni, J. Fridovich, J. Am. Chem. Soc. 96 (1974) 7329.

[10]   R. Hage, Recl. Trav. Chim. Pays-Bas. 115 (1996) 385.

[11]   M. Yagi, M. Kaneko, Chem. Rev. 101 (2001) 21.

[12]   G.H. Reed, R.R. Poyner, Metal ions in Biological Systems, M. Dekker: New York, 37 (2000) 183.

[13]   T. Matsushita, L. Spencer, D.T. Sawyer, Inorg. Chem. 27 (1988) 1167.

[14]   K. Yamaguchi, D.T. Sawyer, Inorg. Chem. 24 (1985) 971.

[15]   M.K. Chan, W.H. Armstrong, J. Am. Chem. Soc. 112 (1990) 4985.

[16]   E.V. Caemdbecke, W. Kutner, K.M. Kadish, Inorg. Chem. 32 (1992) 438.

[17]   N. Tamura, M. Ikeuchi, Y. Inoue, Biochim. Biophys. Acta 973 (1989) 281.

[18]   O. Kahn, Molecular Magnetism, VCH, New York (1993).

[19]   J.S. Miller, M. Drillon (Eds.), Magnetism: Molecules to Materials, Wiley-VCH, Weinheim (2002).

[20]   Y. Kono, I. Fridovrich, J. Biol. Chem. 250 (1983) 6015.

[21]   R.C. Valeutine, B.M. Shapire, E.R. Stadtman, Biochem. 7 (1968) 2143.

[22] W.J. Geary, Coord. Chem. Rev. 7 (1971) 81.

[23] Nakamoto, Infrared and Raman Spectra of Inorganic and Coordination Compounds, 5th Ed., Wiley, New York (1997).

[24] V. Philip, V. Suni, M.R.P. Kurup, M. Nethaji, Polyhedron 25 (2006) 1931.

[25] B.S. Garg, M.R.P. Kurup, S.K. Jain, Y.K. Bhoon, Transit. Met. Chem. 13 (1988) 309.

[26] J.E. Huheey, E.A. Keiter, R.L. Keiter, Inorganic Chemistry, Principles of Structure and Reactivity, 4th Ed., Harper Collins College Publishers, New York (1993).

[27] W. Linert, F. Renz, R. Boca, J. Coord. Chem. 40 (1996) 293.

[28] S. Purohit, A.P. Koley, L.S. Prasad, P.T. Manoharan, S. Ghosh, Inorg. Chem. 28 (1989) 375.

[29] R.L. Dutta, A. Syamal, Elements of Magnetochemistry, 2nd Ed., (1993).

[30] N.K. Singh, S.K. Kushwaha, Ind. J. Chem. 39A (2000) 1070.

[31] C. Preti, G. Tosi, Aust. J. Chem. 20 (1976) 543.

[32] A.A. Razik, A.K.A. Hadi, Transit. Met. Chem. 19 (1994) 84.

[33] D. Shukla, L.K. Gupta, S. Chandra, Spectrochim. Acta Part 71A (2008) 746.

[34] D.J.E. Ingram, Spectroscopy at Radio and Microwave Frequencies, 2nd Ed., Butterworth, London (1967).

[35] K.B. Pandeya, R. Singh, P. Mathur, R.P. Singh, Transit. Met. Chem. 11 (1986) 347.

[36] B.S. Garg, M.R.P. Kurup, S.K. Jain, Y.K. Bhoon, Transit. Met. Chem. 13 (1988) 92.

[37] B.T. Allen, J. Chem. Phys. 43 (1965) 3820.

[38] B.T. Allen, D.W. Nebert, J. Chem. Phys. 41 (1964) 1983.

[39] B. Bleaney, R.S. Rubins, Proc. Phys. Soc. A77 (1961) 103.

[40] E. Friedman, W. Low, Phys. Rev. 120 (1960) 408.

[41] M. Koikawa, H. Okawa, J. Chem. Soc., Dalton Trans. (1988) 641.

…..৪৩৩…..

SYNTHESES AND CHARACTERIZATION OF COBALT(II) COMPLEXES OF ACYLHYDRAZONES

Contents	**5.1 Introduction**
	5.2 Experimental
	5.3 Results and Discussion
	References

5.1. Introduction

Cobalt exhibits two important oxidation states as +2 and +3 and salts of Co(II) are more stable, as they are not easily oxidised to Co(III) state. However, in basic solutions, oxidation of Co^{2+} to Co^{3+} takes place relatively easily. It is usually found that when both oxidation states of an element are subjected to complex formation, the overall formation constant is greater for the higher oxidation state and thus complexation makes it difficult to be reduced. Thus, Co(III) is stabilised by complexation and Co(II) forms relatively few complexes, which are not as stable as the corresponding complexes of Co(III). However, high spin six coordinate, high/low spin five coordinate and four coordinate complexes of Co(II) are widely reported [1-3].

Schiff base metal complexes have been widely studied because they have industrial, antifungal, antibacterial, anticancer and herbicidal applications [4-7]. They serve as models for biologically important species and find applications in biomimetic catalytic reactions. It is known that the existence of metal ions bonded to biologically active compounds may enhance their activities. There has been a

growing interest in the chemistry and biochemistry of cobalt because of its implication in many biological redox processes [8,9].

We now report the synthesis and characterization of Co(II) complexes of tridentate acylhydrazones.

5.2. Experimental

5.2.1. Materials

All the chemicals and solvents used for the syntheses were of analytical grade. Quinoline-2-carbaldehyde (Aldrich), benzhydrazide (Aldrich), nicotinic hydrazide (Aldrich), cobalt(II) acetate tetrahydrate (BDH), cobalt(II) bromide, potassium thiocyanate (Merck) and sodium azide (Reidel-De Haen) were used as received.

5.2.2. Syntheses of ligands

Preparation of the ligands was done as described previously in Chapter 2.

5.2.3. Syntheses of cobalt(II) complexes

5.2.3a. *Synthesis of [Co(Qb)₂] (7)*

HQb·1.5H$_2$O (0.606 g, 2 mmol) was dissolved in methanol (20 ml) by stirring and to this solution, cobalt(II) acetate tetrahydrate (0.249 g, 1 mmol) in methanol (20 ml) was added and refluxed the solution for 2 hours. Then the solution was cooled at room temperature. The dark brown crystalline precipitate of **7** obtained was washed with methanol followed by ether and then dried over P$_4$O$_{10}$ *in vacuo*. Yield: 78.9%. λ_m (DMF): 7 ohm^{-1} cm^2 mol^{-1}. μ (*B.M.*): 4.84. Elemental Anal. Found (calcd.) (%): C, 67.14 (67.22); H, 4.08 (3.98); N, 13.50 (13.83) for [Co(Qb)$_2$].

5.2.3b. *Synthesis of [Co(Qn)₂] (8)*

HQn·1.5H$_2$O (0.606 g, 2 mmol) was dissolved in methanol (20 ml) by stirring and to this solution, cobalt(II) acetate tetrahydrate (0.249 g, 1 mmol) in methanol (20 ml) was added and refluxed the solution for 4 hours. The dark brown precipitate of **8** obtained was washed with methanol followed by ether and

then dried over P_4O_{10} *in vacuo*. Yield: 74.5%. λ_m (DMF): 9 ohm^{-1} cm^2 mol^{-1}. μ (*B.M.*): 4.89. Elemental Anal. Found (calcd.) (%): C, 63.49 (63.06); H, 3.99 (3.64); N, 18.36 (18.38) for [Co(Qn)$_2$].

5.2.3c. *Synthesis of [Co(Qn)Br]·H$_2$O* (**9**)

HQn·1.5H$_2$O (0.303 g, 1 mmol) was dissolved in methanol (20 ml) by stirring and to this solution, cobalt(II) bromide (0.218 g, 1 mmol) in methanol (20 ml) was added and refluxed the solution for 4 hours. The brown precipitate of **9** obtained was washed with methanol followed by ether and then dried over P_4O_{10} *in vacuo*. Yield: 34.9%. λ_m (DMF): 13 ohm^{-1} cm^2 mol^{-1}. μ (*B.M.*): 4.92. Elemental Anal. Found (calcd.) (%): C, 44.59 (44.47); H, 2.85 (3.03); N, 12.50 (12.97) for [Co(Qn)Br]·H$_2$O.

5.2.3d. *Synthesis of [Co(Qn)SCN]* (**10**)

HQn·1.5H$_2$O (0.303 g, 1 mmol) was dissolved in methanol (20 ml) by stirring. To this solution, KSCN (0.097 g, 1 mmol) in methanol (10 ml) was added followed by cobalt(II) acetate tetrahydrate (0.249 g, 1 mmol) in methanol (20 ml) and refluxed the mixture for 4 hours. The compound **10** was obtained as brown precipitate. It was then washed with methanol followed by ether and then dried over P_4O_{10} *in vacuo*. Yield: 68.2%. λ_m (DMF): 25 ohm^{-1} cm^2 mol^{-1}. μ (*B.M.*): 4.76. Elemental Anal. Found (Calcd) %: C, 52.18 (52.05); H, 3.11 (2.83); N, 17.68 (17.85) for [Cu(Qn)SCN].

5.2.3e. *Synthesis of [Co(Qn)N$_3$]* (**11**)

HQn·1.5H$_2$O (0.303 g, 1 mmol) was dissolved in methanol (20 ml) by stirring. To this solution, NaN$_3$ (0.065 g, 1 mmol) in methanol (10 ml) and cobalt(II) acetate tetrahydrate (0.249 g, 1 mmol) in methanol (20 ml) were added and stirred the mixture for 2 hours. The brown precipitate of **11** was washed with methanol followed by ether and then dried over P_4O_{10} *in vacuo*. Yield: 58.4%. λ_m (DMF): 13 ohm^{-1} cm^2 mol^{-1}. μ (*B.M.*): 4.85 Elemental Anal. Found (Calcd) %: C, 51.01 (51.08); H, 3.04 (2.95); N, 26.41 (26.06) for [Co(Qn)N$_3$].

Caution: Although not encountered in our experiments, azido complexes of metal ions with organic ligands are potentially explosive. Only a small amount of the material should be prepared and it should be handled with care.

5.3. Results and discussion

The reaction of quinoline-2-carbaldehyde with hydrazide in 1:1 ratio in methanol gives the corresponding hydrazone. The complexes were prepared by the reaction of the ligand with the metal salts in methanol. Based on the elemental analyses, conductivity measurements and spectral investigations, the complexes were formulated.

Five cobalt(II) complexes of hydrazones were prepared and they are found to be brown in color. The molar conductivities of the complexes in DMF (10^{-3} M) solutions were measured at 298 K with a Systronic model 303 direct-reading conductivity bridge, which show that all the complexes are non-conducting in nature [10]. The magnetic moments of the complexes were calculated from the magnetic susceptibility measurements at room temperature. The effective magnetic moments for the complexes are found to be in the range 4.70-5.00 *B.M.*, which are typical for a high spin cobalt(II) system [11].

5.3.1. Infrared spectra

The IR spectra of the hydrazones and their Co(II) complexes were recorded in the solid state as KBr discs. The bands of diagnostic importance are listed in Table 5.1.

The spectra of hydrazones exhibit a peak at 3193 and 3173 cm^{-1} for HQb·1.5H$_2$O and HQn·1.5H$_2$O, respectively and this band is assigned to the stretching frequency of the N–H group. Also, they exhibit a sharp band at *ca.* 1655 cm^{-1}, which is attributable to the stretching mode of the C=O group. It is worthy mentioning that both of these bands are absent in the spectra of the complexes. This is due to the ability of hydrazones to exhibit keto-enol tautomerism. From the IR spectra of complexes, it is confirmed that the

hydrazones coordinate to the metal centre in the enolate form. In the complexes, a new band is observed at *ca*. 1330 cm^{-1} which is due to the ν(C–O) band formed due to the enolization of the hydrazone moiety [12,13].

**Table 5.1.** IR spectral data of hydrazones and their Co(II) complexes.

Compound	ν(C=O) cm^{-1}	ν(NH) cm^{-1}	ν(C=N) cm^{-1}	ν(C=N)[a] cm^{-1}	ν(C–O) cm^{-1}	ν(N–N) cm^{-1}
HQb·1.5H$_2$O	1655	3193	1593	----	----	1184
[Co(Qb)$_2$] (**7**)	----	----	1544	1580	1330	1209
HQn·1.5H$_2$O	1656	3173	1591	----	----	1195
[Co(Qn)$_2$] (**8**)	----	----	1546	1583	1331	1201
[Co(Qn)Br]·H$_2$O (**9**)	----	----	1554	1590	1339	1199
[Co(Qn)SCN] (**10**)	----	----	1551	1589	1337	1198
[Co(Qn)N$_3$] (**11**)	----	----	1552	1589	1330	1199

[a] Newly formed C=N bond.

The azomethine band, ν(C=N), is observed at around 1590 cm^{-1} in the spectra of the hydrazones, but this band is shifted to lower wavenumber in the case of the complexes. This red shift indicates the participation of azomethine nitrogen in coordination. The ν(N–N) band is observed at 1184 cm^{-1} for HQb·1.5H$_2$O and 1195 cm^{-1} for HQn·1.5H$_2$O. The increase in frequency of this band in the spectra of the complexes again confirms the coordination of hydrazone through azomethine nitrogen. The increase in ν(N–N) value in the spectra of complexes is due to the increase in its double bond character, off-setting the loss of electron density *via* donation to the metal.

In the spectra of complexes, a new band is observed at *ca.* 1580 cm^{-1} which is due to the stretching frequency of the newly formed C=N group on enolization. The sharp medium intensity band at 985-954 cm^{-1} is assigned to the pyridine ring breath mode of vibration [13,14]. The sharp medium bands within the 920-620

cm^{-1} range can be assigned to the various out-of-plane deformations of the aromatic C–H groups. IR spectrum of [Co(Qb)$_2$] (**7**) is shown in Fig. 5.1.
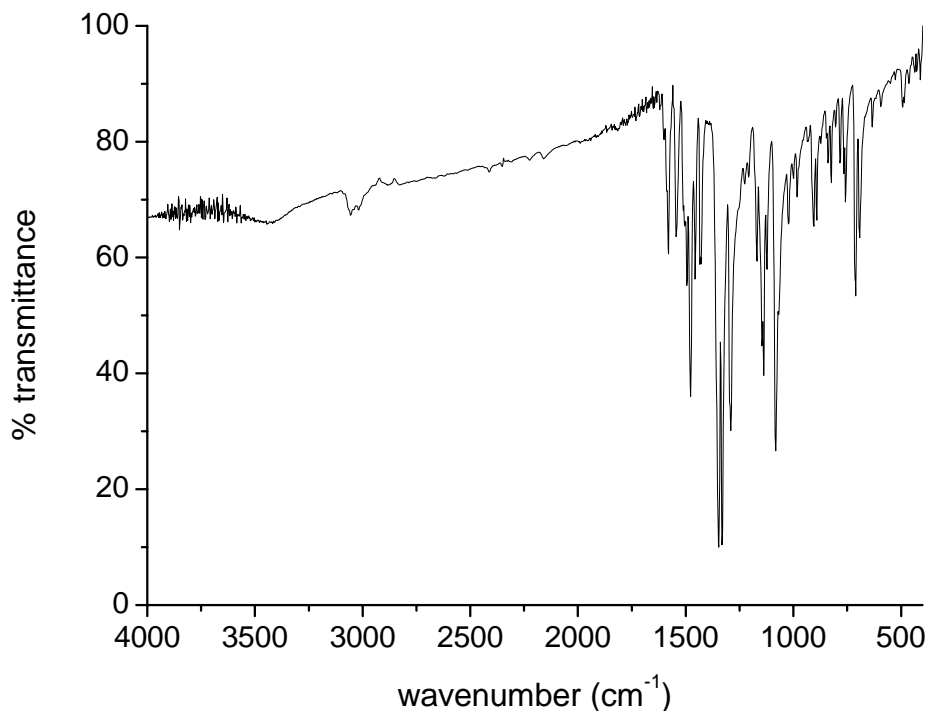
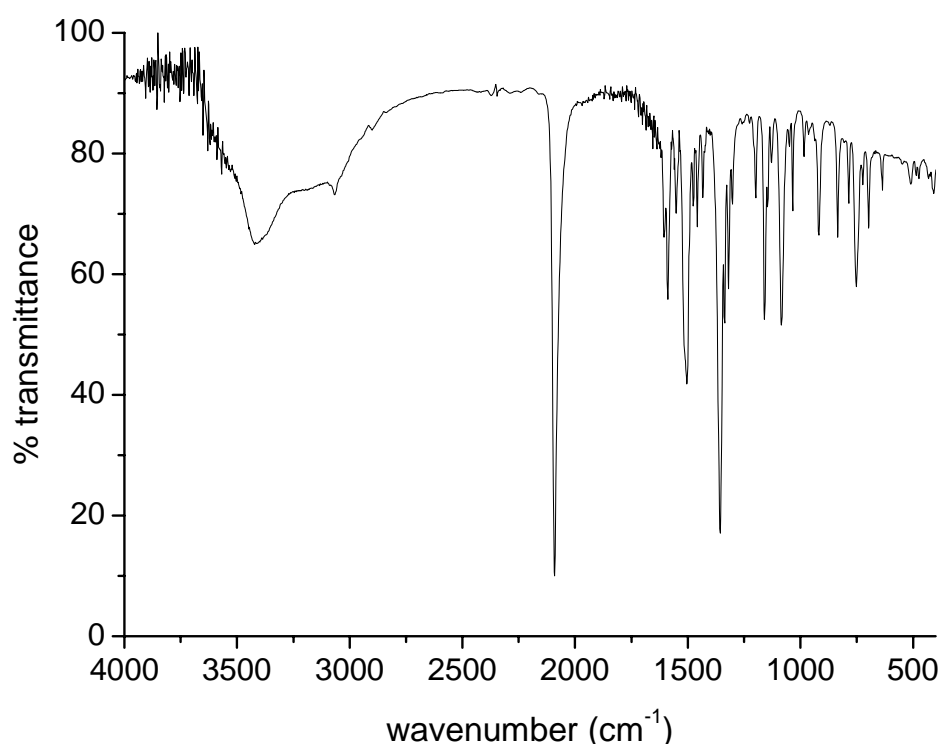**Fig. 5.1.** IR spectrum of [Co(Qb)$_2$] (**7**).

A thiocyanate ion is a typical ambidentate ligand involving two different terminal donor atoms; the sulfur atom and the nitrogen atom. The SCN group may coordinate to a metal through the nitrogen or sulfur or both sulfur and nitrogen. Thiocyanate coordination is known to occur in thiocyanate M-SCN, isothiocyanate M-NCS and binuclear M-SCN-M (bridging) forms. The mode of coordination can be determined from the vibrational modes. The CN stretching frequencies are generally lower in N–bonded complexes (near and below 2050 cm^{-1}) than in S-bonded complexes (near 2100 cm^{-1}) and the bridging [M-NCS-M'] complexes exhibits v(CN) well above 2100 cm^{1}. The v(CS) band for S-bonded complexes are found in the 720-690 cm^{-1} region. The N-bonded complexes exhibit a

single sharp δ(NCS) band near 480 cm^1, where as the S-bonded complexes show several weak bands near 421 cm^{-1} [15].

The complex [Co(Qn)SCN] (**10**) (Fig. 5.2) exhibits strong and sharp bands at 2091, 723 cm^{-1} and several bands of low intensity near 421 cm^{-1} which can be attributed to ν(CN), ν(CS) and δ(NCS) respectively. These values are typical for S-bonded thiocyanato complexes.

Fig. 5.2. IR spectrum of [Co(Qn)SCN] (**10**).

The azido compound, [Co(Qn)N$_3$] (**11**), exhibited the antisymmetric ν(NNN) vibration as a sharp band observed at 2058 cm^{-1}. Another band at 1319 cm^{-1} is assigned to ν_s(NNN) of the coordinated azido group [16]. The broad bands observed at 636 and 432 cm^{-1} in the spectrum of the complex are assigned to δ(NNN) and ν(Co–N$_{azido}$) bands (Fig. 5.3).
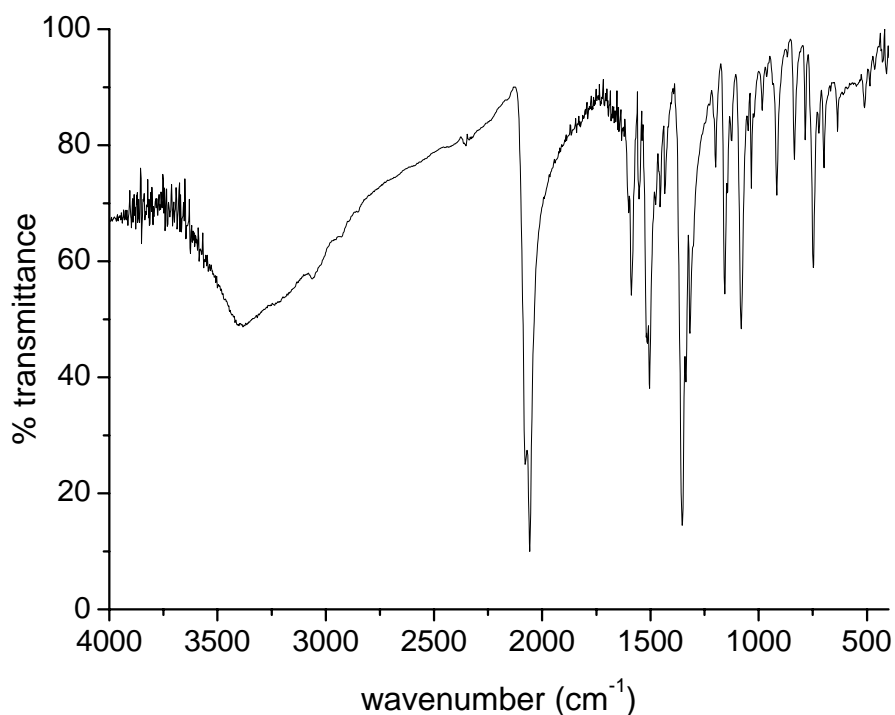
91

Fig. 5.3. IR spectrum of [Co(Qn)N$_3$] (**11**).

5.3.2. Electronic spectra

The observed values of magnetic moments for cobalt(II) complexes are generally diagnostic of the coordination geometry about the metal ion. The low-spin square-planar cobalt(II) complexes may be 2.9 *B.M.*, arising from one unpaired electron plus an apparently large orbital contribution [17].

Both tetrahedral and high-spin octahedral cobalt(II) complexes possess three unpaired electrons but may be distinguished by the magnitude of the deviation of μ_{eff} from the spin-only value. The magnetic moment of tetrahedral cobalt(II) complexes with an orbitally non-degenerate ground term is increased above the spin only value *via* contribution from higher orbitally degenerate terms and occurs in the range 4.2–4.7 *B.M.*; octahedral cobalt(II) complexes, however, maintain a large contribution due to ^4T_g ground term and exhibit μ_{eff} in the range 4.8–5.6 *B.M.* [18].

The magnetic moments of the complexes reported herein are in the range 4.70-5.00 *B.M.* showing the presence of three unpaired electrons with a high-spin octahedral configuration. These values are larger than the spin only value of high-spin cobalt(II) (3.87 *B.M.*; $\mu_{SO} = [4S(S+/1)]^{1/2}$; $S = 3/2$). The values are close to the value expected when the spin and orbital angular momenta exist independently [5.20 *B.M.*; $\mu_{LS} = [L(L+/1) + 4S(S+1)]^{1/2}$; $L = 3$, $S = 3/2$]. This indicates a contribution of the orbital angular momentum [1,11].

The d^7 system, with the ground state term ^4F, is split into three states in an octahedral crystal field. So, in an octahedral geometry, Co^{2+} complexes usually show three bands corresponding to the spin allowed transitions $^4T_{2g}(F) \leftarrow {}^4T_{1g}(F)$ (v_1), $^4A_{2g}(F) \leftarrow {}^4T_{1g}(F)$ (v_2) and $^4T_{1g}(P) \leftarrow {}^4T_{1g}(F)$ (v_3) transitions. Electronic spectra of all the cobalt(II) complexes in DMF showed three bands in the region 11510-12730, 14940-16230 and 17820-18970 cm^{-1}, which may be assigned to the v_1, v_2 and v_3 of octahedral Co(II) system [19-21].

The electronic absorption spectra of the hydrazones and their cobalt(II) complexes were recorded both in acetonitrile and DMF within the region 45000-11000 cm^{-1}.

The intense broad band observed for the complexes in the region 24530-26100 cm^{-1} is assigned to the intramolecular charge transfer transitions involving the whole molecule [19-23]. Electronic spectra of the hydrazones and their metal complexes, within the region 45000-20000 cm^{-1}, are shown in Figs. 5.4 and 5.5. The *d-d* bands observed for [Co(Qn)$_2$] (**8**) and [Co(Qb)SCN] (**10**) are shown in Fig. 5.6.

The bands in the region 32000-44000 cm^{-1} are assigned to π-π* transitions within the ligand moiety. The spectra show bands in the range 27000-32000 cm^{-1}, assignable to n-π* transitions of the azomethine and amide functions. These intraligand bands are slightly shifted on complexation. Electronic spectral data of the hydrazones and their cobalt(II) complexes are given in Table 5.2.
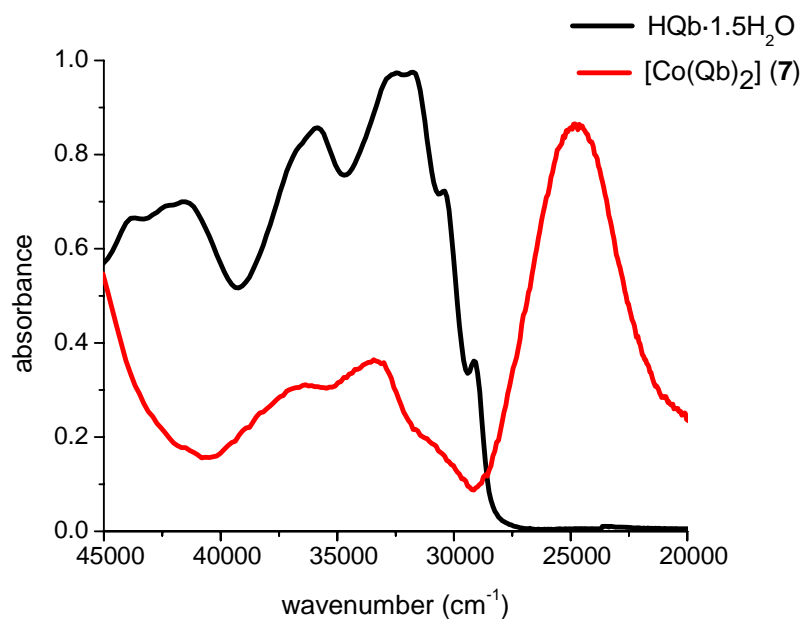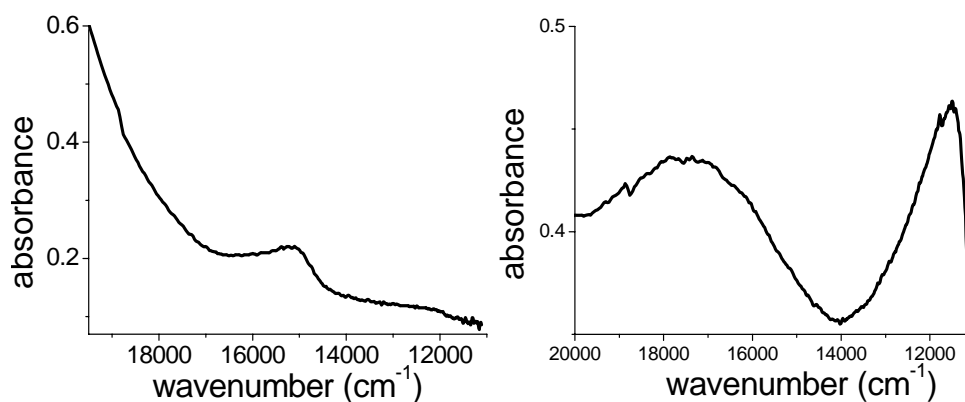
Fig. 5.4. Electronic spectra of HQb·1.5H$_2$O and [Co(Qb)$_2$] (**7**), recorded in acetonitrile.
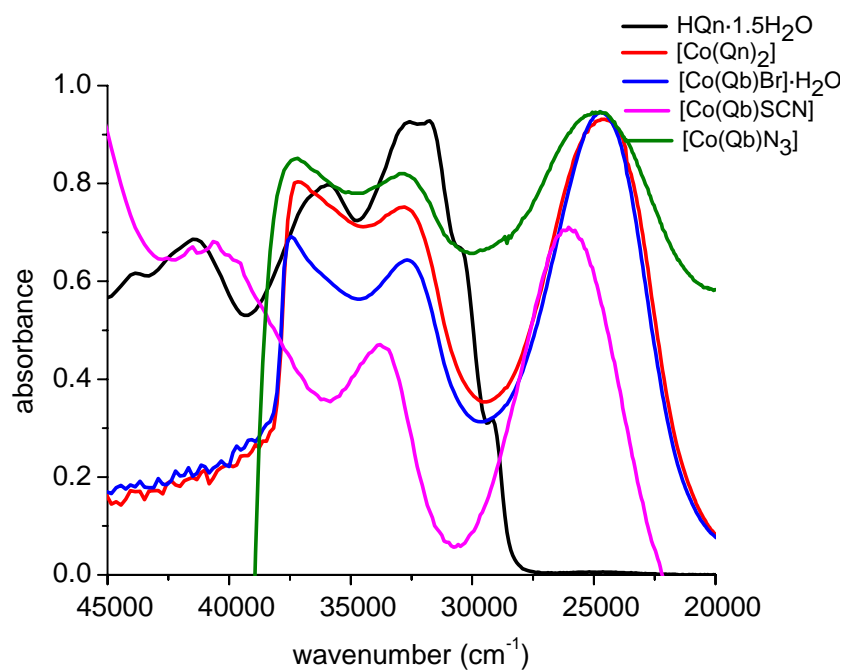
Fig. 5.5. Electronic spectra of HQn·1.5H$_2$O and its Co(II) complexes, recorded in acetonitrile.

Fig. 5.6. *d-d* bands observed for (a) [Co(Qn)$_2$] (**8**) and (b) [Co(Qb)SCN] (**10**), recorded in DMF

Table 5.2. Electronic spectral data of the hydrazones and their cobalt(II) complexes.

Compound	Absorbance λ$_{max}$ (cm^{-1})
HQb·1.5H$_2$O	43790, 41640, 35860, 32580, 31690, 30430, 29130
[Co(Qb)$_2$] (**7**)	36530, 33360, 31050, 24760, 17890, 15650, 12730
HQn·1.5H$_2$O	43920, 41490, 35840, 32580, 31750, 30440, 29150
[Co(Qn)$_2$] (**8**)	37060, 32900, 24530, 17860, 15170, 12130
[Co(Qb)Br]·H$_2$O (**9**)	37430, 32640, 24740, 18840, 16170, 11630
[Co(Qb)SCN] (**10**)	37390, 32850, 24880, 17820, 16230, 11510
[Co(Qb)N$_3$] (**11**)	40560, 33800, 26030, 18970, 14940, 11790

5.3.3. Cyclic voltammetry

Cyclic voltammograms of the hydrazones and their Co(II) complexes were recorded on a CHI 608D electrochemical analyzer with a three electrode compartment consisting of a platinum disc working electrode, platinum wire counter electrode and Ag/Ag$^+$ reference electrode. The solutions of complexes in DMF have been used to study the electrochemical properties using TBAP (tetrabutylammonium phosphate) as the supporting electrolyte. The voltammogram is run between the potentials of +2000 and –2000 mV at a scan speed of 100 mV/s.

The electrochemical behavior of metal complexes with N, O - donor ligands has been studied in order to monitor spectral and structural changes accompanying electron transfer [24].

95

A comparative study of the cyclic voltammetric behavior of the hydrazones with their metal complexes could provide information on whether the redox reaction of the metal complexes is metal centered or ligand centered. The potentials of both the metal centered oxidation and reduction reflect the influence of the electronic nature of the ligand.

The cobalt(II)/cobalt(I) redox process is influenced by coordination number, stereochemistry and the hard/soft character of the ligand donor atoms [25,26]. The cyclic voltammetric data for the hydrazones and their Co(II) complexes are listed in Table 5.3. Representative cyclic voltammograms are shown in Figs. 5.7 and 5.8.

Patterson and Holm have shown that softer ligands tend to produce more positive E^0 values, while hard acids give rise to negative E^0 value. The observed values for the complexes of hydrazone indicate considerable "hard acid" character comparable to ligand like ethylene diamine, (E^0, - 350 mV) which is likely to be due to the pyridyl and azomethine nitrogen donors and solvent coordination [27].

Table 5.3. Cyclic voltammetric data for the hydrazones and their Co(II) complexes

Compound	E_{pc} / mV (I_{pc} / μA)	E_{pa} / mV (I_{pa} / μA)
HQb·1.5H$_2$O	-220 (0.91)	520 (3.48)
[Co(Qb)$_2$] (**7**)	-430 (0.41)	800 (0.84)
	280 (0.22)	-70(0.12)
		-380 (0.34)
HQn·1.5H$_2$O	-280 (1.83)	830 (13.8)
[Co(Qn)$_2$] (**8**)	-330 (0.55)	810 (0.66)
	260 (0.43)	-100 (0.05)
		-530 (0.26)
[Co(Qb)Br]·H$_2$O (**9**)	-280 (1.48)	
	300 (1.31)	-----
[Co(Qb)SCN] (**10**)	-790 (0.42)	490 (0.11)
	240 (0.31)	-670 (0.65)
	690 (0.21)	
[Co(Qb)N$_3$] (**11**)	-300 (1.72)	940 (5.66)
	380 (1.06)	670 (0.73)
	970 (5.07)	-60 (1.23)

Absence of peaks for some complexes may result from kinetic complications during electron transfer, uncompensated solution resistance etc.

The drop of the voltammetric currents in the case of complexes compared to the corresponding ligand can be attributed to diffusion of the metal complex bound to the large ligand moiety. Additional peaks are observed for the complexes **9**, **10** and **11**, which may be due to the presence of coligands, which are also susceptible to redox processes.

(a)	(b)
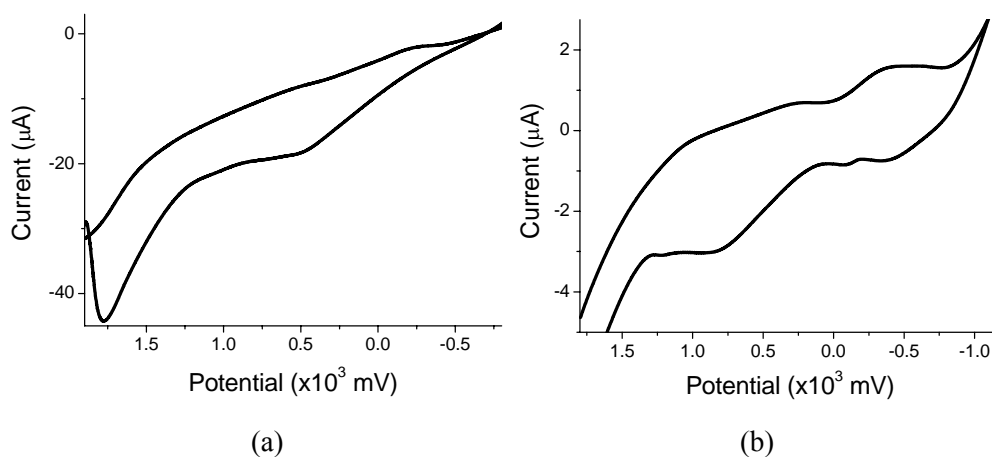
Fig. 5.7. Cyclic voltammograms of (a) HQb·1.5 H₂O and (b) [Co(Qb)₂] (**7**).

(c)	(d)
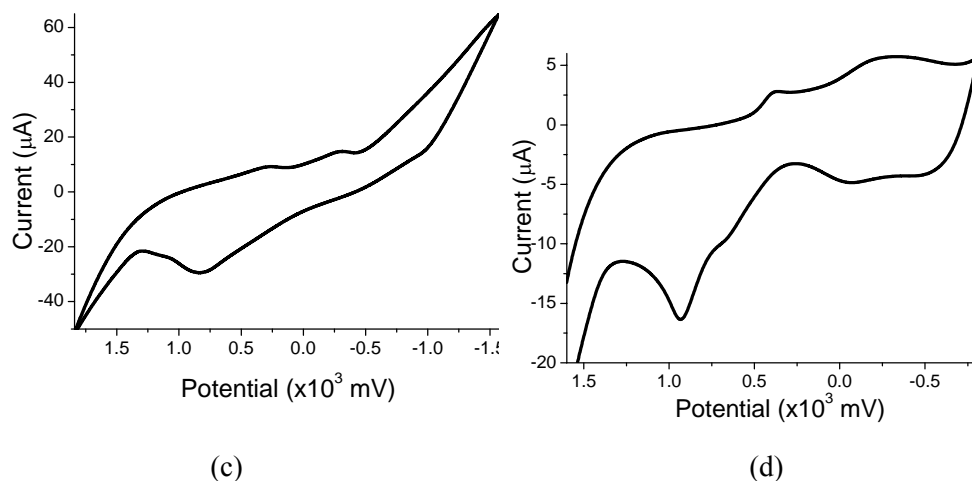
Fig. 5.8. Cyclic voltammograms of (c) HQn·1.5 H₂O and (d) [Co(Qb)N₃] (**11**).

97

References

[1]   M.J. Hossain, H. Sakiyama, Inorg. Chim. Acta 338 (2002) 255.

[2]   B.N. Figgis, M.A. Hitchman, Ligand Field Theory and its Applications, Wiley/VCH, New York (2000).

[3]   J.S. Wood, Inorg. Chem. 7 (1968) 852.

[4]   D.F. Averill, R.F. Borman, Inorg. Chem. 17 (1978) 3389.

[5]   L. Salmon, C.B. Charreton, A. Gaudemer, P. Moisy, F. Bedioui, J. Devynck, Inorg. Chem. 29 (1990) 2734.

[6]   K.A. Lance, K.A. Goldshy, D.H. Busch, Inorg. Chem. 29 (1990) 4537.

[7]   P.G. Cozzi, Chem. Soc. Rev. 33 (2004) 410.

[8]   E. Canpolat, M. Kaya, J. Coord. Chem. 57 (2004) 1217.

[9]   M. Yildiz, B. Dulger, S.Y. Koyuncu, B.M.Yapici, J. Indian Chem. Soc 81(2004) 7.

[10] W.J. Geary, Coord. Chem. Rev. 7 (1971) 81.

[11] M. Yamami, M. Tanaka, H. Sakiyama, T. Koga, K. Kobayashi, H. Miyasaka, M. Ohba, H. Okawa, J. Chem. Soc., Dalton Trans. (1997) 4595.

[12] S. Naskar, D. Mishra, R.J. Butcher, S.K. Chattopadhyay, Polyhedron 26 (2007) 3703.

[13] K. Nakamoto, Infrared and Raman Spectra of Inorganic and Coordination Compounds, 5th Ed., Wiley, New York (1997).

[14] P.F. Raphael, E. Manoj, M.R.P. Kurup, Polyhedron 26 (2007) 5088.

[15] K.B. Yatsimirskii, Pure and Appl. Chem. 49 (1977) 115.

[16] M. Joseph, V. Suni, M.R.P. Kurup, M. Nethaji, A. Kishore, S.G. Bhat, Polyhedron 23 (2004) 3069.

[17] B.N. Figgis, R.S. Nyholm, J. Chem. Soc. (1958) 4190.

[18] S. Yamada, Coord. Chem. Rev. 1 (1966) 415.

[19] S. Chandra, Sangeetika, V.P. Tyagi, S. Raizada, Synth. React. Inorg. Met Org. Chem. 33 (2003) 147.

[20] A.B.P. Lever, Inorganic Electronic Spectroscopy, 1st Ed., Elsevier, Amsterdam (1968).

[21] A.B.P. Lever, J. Lewis, J. Chem. Soc. (1963) 2552.

[22] S. Chandra, S.D. Sharma, K. Gupta, Sangeetika, J. Saudi Chem. Soc. 6 (2002) 451.

[23] S. Chandra, Sangeetika, S.D. Sharma, Spectrochim. Acta 59A (2003) 755.

[24] A.M. Bond, R.L. Martin, Coord. Chem. Rev. 54 (1984) 23.

[25] M.C. Granger, G.M. Swain, J. Electrochem. Soc. 146 (1999) 4551.

[26] C.M. Pharr, P.R. Griffiths, Anal. Chem. 69 (1997) 4673.

[27] V. Eisner, A.J. Bard, H. Lund, Encyclopedia of Electrochemistry of the elements, M. Dekker, New York, 13 (1979) 338.

…..✍ℭℜ…..

SYNTHESES OF COPPER(II) COMPLEXES OF ACYLHYDRAZONES AND THEIR CHARACTERIZATION

6.1. Introduction

Copper (II) is a biologically active essential ion and it forms the active centers in several metalloenzymes and proteins. Its chelating ability and positive redox potential allow participation in biological transport reactions. The copper atom transforms between the Cu(I) and Cu(II) oxidation states in redox reactions involving copper containing enzymes. This is an essential factor for many of the properties of these enzymes [1-9].

Like all transition metal ions, the copper(II) ion is characterized by its ability to form coordination complexes with a wide range of ligands and illustrating a variety of stereochemistries. Further, copper(II) complexes possess a wide range of biological activity and are among the most potent antiviral, antitumor and anti-inflammatory agents. Copper(II) complex of salicylaldehyde benzoyl hydrazone was shown to be a potent inhibitor of DNA synthesis and cell growth. This hydrazone also has mild bacteriostatic activity and a range of analogues has been investigated as potential oral iron chelating drugs for genetic disorders such as thalassemia [10-13].

Common oxidation states of copper include the less stable copper(I) state (d^{10}) and the more stable copper(II) state (d^9). Under unusual conditions, a +3 state (d^8) and even an extremely rare +4 state (d^7) also can be obtained. The most common oxidation state of copper is +2 and Cu(II) complexes have been extensively studied.

Cu(II) cations may be stabilized by complex formation with various ligands and the ligand field splits the *d*-orbitals. They readily form coordination complexes involving coordination numbers 4, 5 & 6 with tetrahedral, square planar, trigonal bipyramidal, square pyramidal, octahedral and distorted octahedral geometries [1].

It is less typical that these stereochemistries are dominated by the formation of nonregular structures, involving significant bond length and bond angle distortions from the regular geometries. The major responsibility for this unusual behavior must arise from the d^9 electron configuration. As a consequence of the non-spherical symmetry of the copper(II) ion with d^9 configuration, its complexes exhibit distorted forms of the basic stereochemistries and Jahn-Teller effect plays a major role in deciding the distortion effect of stereochemistries of Cu(II) complexes.

Hydrazones and their copper(II) complexes have been studied in recent years owing to their pharmacological interest. This chapter deals with the synthesis and characterization of Cu(II) complexes with acylhydrazones, derived from quinoline-2-carbaldehyde. The hydrazones coordinate to the metal as chelating ligands and the expected coordination is most often *via* the quinoline nitrogen, azomethine nitrogen and amide oxygen. We used different spectral techniques such as IR, electronic and EPR to explore the geometry and stereochemistry of the complexes.

6.2. Experimental

6.2.1. Materials

All the chemicals and solvents used for the syntheses were of analytical grade. Quinoline-2-carbaldehyde (Sigma Aldrich), benzhydrazide (Sigma Aldrich),

nicotinic hydrazide (Sigma Aldrich), copper(II) chloride dihydrate (Merck), copper(II) acetate monohydrate (Qualigens), copper(II) nitrate trihydrate (S.D.fine-chemicals Ltd), copper(II) perchlorate hexahydrate (Sigma Aldrich), copper(II) bromide (Sigma Aldrich), potassium thiocyanate (Merck) and sodium azide (Reidel-De Haen) were used without further purification.

6.2.2. Syntheses of ligands

Preparation of the ligands was done as described previously in Chapter 2.

6.2.3. Syntheses of copper (II) complexes of quinoline-2-carbaldehyde benzoyl hydrazone

6.2.3a. *Synthesis of [Cu(HQb)Cl$_2$]* (12)

CuCl$_2$·2H$_2$O (0.170 g, 1 mmol) in methanol (20 ml) was added to HQb·1.5H$_2$O (0.303 g, 1 mmol), dissolved in methanol (20 ml) by stirring. The mixture was refluxed for 2 hours. Then, it was cooled and filtered. The dark green precipitate of **12** was washed with methanol followed by ether and then dried over P$_4$O$_{10}$ *in vacuo*. Yield: 48.9%. λ_m (DMF): 15 ohm^{-1} cm^2 mol^{-1}. μ (*B.M.*): 1.96. m.p.: 230-232 °C. Elemental Anal. Found (Calcd) %: C, 49.41 (49.83); H, 3.18 (3.20); N, 10.34 (10.25) for [Cu(HQb)Cl$_2$].

6.2.3b. *Synthesis of [Cu(Qb)$_2$]* (13)

HQb·1.5H$_2$O (0.606 g, 2 mmol) was dissolved in methanol (20 ml) by stirring and to this solution, Cu(OAc)$_2$·H$_2$O (0.199 g, 1 mmol) in hot methanol (20 ml) was added and refluxed the solution for 3 hours. The brown crystalline precipitate of **13** obtained was washed with methanol followed by ether and then dried over P$_4$O$_{10}$ *in vacuo*. Yield: 54.5%. λ_m (DMF): 6 ohm^{-1} cm^2 mol^{-1}. μ (*B.M.*): 1.83. m.p.: 265-267 °C. Elemental Anal. Found (calcd.) (%): C, 66.74 (66.71); H, 3.62 (3.95); N, 13.57 (13.73) for [Cu(Qb)$_2$].

6.2.3c. *Synthesis of [Cu(Qb)NCS]·H$_2$O* (14)

HQb·1.5H$_2$O (0.303 g, 1 mmol) was dissolved in methanol (20 ml) by stirring. To this solution, KSCN (0.097 g, 1 mmol) in methanol (10 ml) was added

followed by $Cu(OAc)_2 \cdot H_2O$ (0.199 g, 1 mmol) in hot methanol (20 ml) and refluxed the mixture for 4 hours. The compound **14** was obtained as dark green precipitate. It was then washed with methanol followed by ether and then dried over P_4O_{10} *in vacuo*. Yield: 75.2%. λ_m (DMF): 25 ohm^{-1} cm^2 mol^{-1}. μ (*B.M.*): 1.62. m.p.: 220-222 °C. Elemental Anal. Found (Calcd) %: C, 52.47 (52.23); H, 3.11 (3.41); N, 13.35 (13.53); S, 7.63 (7.75) for $[Cu(Qb)NCS] \cdot H_2O$.

6.2.3d. *Synthesis of [Cu(Qb)N₃]₂·H₂O* (**15**)

HQb·1.5H₂O (0.303 g, 1 mmol) was dissolved in methanol (20 ml) by stirring. To this solution, NaN₃ (0.065 g, 1 mmol) in methanol (10 ml) and $Cu(OAc)_2 \cdot H_2O$ (0.199 g, 1 mmol) in hot methanol (20 ml) were added and stirred the mixture for 2 hours. The dark green precipitate of **15** was washed with methanol followed by ether and then dried over P_4O_{10} *in vacuo*. Yield: 68.5%. λ_m (DMF): 7 ohm^{-1} cm^2 mol^{-1}. μ (*B.M.*): 1.15. Elemental Anal. Found (Calcd) %: C, 52.96 (52.51); H, 3.33 (3.37); N, 21.54 (21.61) for $[Cu(Qb)N_3]_2 \cdot H_2O$.

6.2.3e. *Synthesis of [Cu(HQb)Br]₂Br₂* (**16**)

CuBr₂ (0.223 g, 1 mmol) in methanol (20 ml) was added to HQb·1.5H₂O (0.303 g, 1 mmol), dissolved in methanol (20 ml) by stirring. The mixture was then refluxed for half an hour. Then, it was cooled and filtered. The dark green precipitate was washed with methanol followed by ether and then dried over P_4O_{10} *in vacuo*. Yield: 43.1%. λ_m (DMF): 124 ohm^{-1} cm^2 mol^{-1}. μ (*B.M.*): 1.18. m.p.: 218-220 °C. Elemental Anal. Found (Calcd) %: C, 40.94 (40.95); H, 2.84 (2.63); N, 7.93 (8.43) for $[Cu(HQb)Br]_2Br_2$.

6.2.4. Syntheses of copper(II) complexes of quinoline-2-carbaldehyde nicotinic hydrazone

6.2.4a. *Synthesis of [Cu(HQn)Cl₂]* (**17**)

CuCl₂·2H₂O (0.170 g, 1 mmol) in methanol (20 ml) was added to HQn·1.5H₂O (0.303 g, 1 mmol), dissolved in methanol (20 ml) by stirring. The mixture was refluxed for 2 hours. Then, it was cooled and filtered. The dark green precipitate of **17** was washed with methanol followed by ether and then dried over

P_4O_{10} *in vacuo*. Yield: 52.8%. λ_m (DMF): 32 ohm^{-1} cm^2 mol^{-1}. μ (*B.M.*): 1.79. m.p.: 238-240 °C. Elemental Anal. Found (Calcd) %: C, 46.85 (46.79); H, 3.34 (2.94); N, 13.73 (13.64) for [Cu(HQn)Cl$_2$].

6.2.4b. *Synthesis of [Cu(Qn)$_2$]* (**18**)

HQn·1.5H$_2$O (0.606 g, 2 mmol) was dissolved in methanol (20 ml) by stirring. To this solution, Cu(OAc)$_2$·H$_2$O (0.199 g, 1 mmol) in hot methanol (20 ml) was added and refluxed the mixture for 3 hours. The brown crystalline precipitate of **18** obtained was washed with methanol followed by ether and then dried over P_4O_{10} *in vacuo*. Yield: 63.5%. λ_m (DMF): 20 ohm^{-1} cm^2 mol^{-1}. μ (*B.M.*): 1.79. m.p.: 257-258 °C. Elemental Anal. Found (calcd.) (%) : C, 61.56 (61.68); H, 3.77 (3.72); N, 18.15 (17.98) for [Cu(Qn)$_2$].

6.2.4c. *Synthesis of [Cu(Qn)NO$_3$]·H$_2$O* (**19**)

HQn·1.5H$_2$O (0.303 g, 1 mmol) was dissolved in methanol (20 ml) by stirring. To this solution, Cu(NO$_3$)$_2$·3H$_2$O (0.241 g, 1 mmol) in methanol (20 ml) was added and refluxed the solution for 4 hours. Dark green crystalline precipitate was formed. The mixture was cooled and filtered. The dark green crystalline precipitate of **19** was then washed with methanol followed by ether and then dried over P_4O_{10} *in vacuo*. Yield: 53.2%. λ_m (DMF): 14 ohm^{-1} cm^2 mol^{-1}. μ (*B.M.*): 1.93. m.p.: 250-252 °C. Elemental Anal. Found (calcd.) (%) : C, 45.54 (45.88); H, 2.79 (3.13); N, 16.76 (16.72) for [Cu(Qn)NO$_3$]·H$_2$O.

6.2.4d. *Synthesis of [Cu(Qn)ClO$_4$]·H$_2$O* (**20**)

Copper perchlorate hexahydrate (0.370 g, 1 mmol) in methanol (20 ml) was added to HQn·1.5H$_2$O (0.303 g, 1 mmol), dissolved in methanol (20 ml) by stirring. The mixture was refluxed for 4 hours. Then, it was cooled and filtered. The dark green crystalline precipitate of **20** was washed with methanol followed by ether and then dried over P_4O_{10} *in vacuo*. Yield: 83.9%. λ_m (DMF): 34 ohm^{-1} cm^2 mol^{-1}. μ (*B.M.*): 1.69. Elemental Anal. Found (calcd.) (%) : C, 42.23 (42.12); H, 2.53 (2.87); N, 12.23 (12.28) for [Cu(Qn)ClO$_4$]·H$_2$O.

105

6.2.4e. *Synthesis of [Cu(Qn)NCS]·H₂O* (21)

HQn·1.5H$_2$O (0.303 g, 1 mmol) was dissolved in methanol (20 ml) by stirring. To this solution, Cu (CH$_3$COO)$_2$·H$_2$O (0.199 g, 1 mmol) and KSCN (0.097 g, 1 mmol) in methanol (20 ml) were added and refluxed the solution for 4 hours. The dark green precipitate of **21** was washed with methanol followed by ether and then dried over P$_4$O$_{10}$ *in vacuo*. Yield: 84.5%. λ_m (DMF): 30 ohm^{-1} cm^2 mol^{-1}. μ (*B.M.*): 1.97. m.p.: 180-182 °C. Elemental Anal. Found (calcd.) (%) : C, 49.45 (49.21); H, 2.70 (3.16); N, 16.99 (16.88); S, 7.85 (7.73) for [Cu(Qn)NCS]·H$_2$O.

6.2.4f. *Synthesis of [Cu(Qn)N₃]·H₂O* (22)

HQn·1.5H$_2$O (0.303 g, 1 mmol) was dissolved in methanol (20 ml) by stirring. To this solution, Cu(CH$_3$COO)$_2$·H$_2$O (0.199 g, 1 mmol) and NaN$_3$ (0.065 g, 1 mmol) in methanol (20 ml) were added and stirred the mixture for 2 hours. The dark green precipitate of **22** was washed with methanol followed by ether and then dried over P$_4$O$_{10}$ *in vacuo*. Yield: 89.5%. λ_m (DMF): 5 ohm^{-1} cm^2 mol^{-1}. μ (*B.M.*): 1.85. Elemental Anal. Found (calcd.) (%): C, 48.54 (48.18); H, 2.87 (3.29); N, 24.15 (24.58) for [Cu(Qn)N$_3$]·H$_2$O.

6.2.4g. *Synthesis of [Cu(HQn)Br₂]* (23)

CuBr$_2$ (0.223 g, 1 mmol) in methanol (20 ml) was added to HQn·1.5H$_2$O (0.303 g, 1 mmol), dissolved in methanol (20 ml) by stirring. The mixture was then refluxed for half an hour. Then, it was cooled and filtered. The dark green precipitate of **23** was washed with methanol followed by ether and then dried over P$_4$O$_{10}$ *in vacuo*. Yield: 62.8%. λ_m (DMF): 34 ohm^{-1} cm^2 mol^{-1}. μ (*B.M.*): 1.63. m.p.: 214-216 °C. Elemental Anal. Found (Calcd) %: C, 38.84 (38.46); H, 2.87 (2.42); N, 10.95 (11.21) for [Cu(HQn)Br$_2$].

Caution: Although not encountered in our experiments, azido and perchlorate complexes of metal ions with organic ligands are potentially explosive. Only a small amount of the material should be prepared and it should be handled with care.

6.3. Results and discussion

The reaction of quinoline-2-carbaldehyde with hydrazide in 1:1 ratio in methanol gives the corresponding hydrazone. The complexes were prepared by the reaction of the ligand with the copper(II) salts in methanol. Based on the elemental analyses, conductivity measurements and spectral investigations, the complexes were formulated.

Twelve copper (II) complexes of acylhydrazones were prepared and they are found to be dark green or brown in color. The molar conductivities of the complexes in DMF (10^{-3} M) solution were measured at 298 K with a Systronic model 303 direct-reading conductivity bridge, which showed that compound **16** is a 2:1 electrolyte while all other complexes are non-conducting in nature [14].

The magnetic moments of the complexes were calculated from the magnetic susceptibility measurements at room temperature. The effective magnetic moments for the complexes **15** and **16** are found to be 1.15 and 1.18 *B.M.* respectively, which suggest some interaction between metal centers. However, for all other complexes, the values are found to be in the range 1.62-2.00 *B.M.*, which are very close to the spin-only value of 1.73 *B.M.* for a typical copper(II) system.

6.3.1. Infrared spectra

IR spectra in the range 4000-50 cm^{-1} were recorded for complexes and assignments were done in comparison with that of their respective free ligands. The selected IR bands of the hydrazones and complexes are represented in Table 6.1.

A comparison of the IR spectra of ligands and the metal complexes showed that significant variations have occurred in the characteristic frequencies upon complexation. The IR spectra of compounds [Cu(HQb)Cl$_2$] (**12**), [Cu(HQb)Br]$_2$Br$_2$ (**16**), [Cu(HQn)Cl$_2$] (**17**) and [Cu(HQn)Br$_2$] (**23**) showed a sharp band around 1680 and a medium band at 3180 cm^{-1}, which correspond to

ν(C=O) and ν(N–H) respectively. This explains that the ligand is not deprotonated for coordination and the Cu(II) valency is satisfied by the two halide anions [15].

Table 6.1. Infrared spectral data of the hydrazones and their copper(II) complexes.

Compound	ν(C=O) cm^{-1}	ν(N–H) cm^{-1}	ν(C=N) cm^{-1}	ν(C=N)^a cm^{-1}	ν(C–O) cm^{-1}	ν(N–N) cm^{-1}
HQb·1.5H$_2$O	1655	3193	1593	----	----	1184
[Cu(HQb)Cl$_2$] (**12**)	1663	3176	1548	----	----	1205
[Cu(Qb)$_2$] (**13**)	----	----	1546	1581	1328	1202
[Cu(Qb)NCS]·H$_2$O (**14**)	----	----	1556	1585	1332	1208
[Cu(Qb)N$_3$]$_2$·H$_2$O (**15**)	----	----	1552	1582	1332	1208
[Cu(HQb)Br]$_2$Br$_2$ (**16**)	1681	3179	1536	----	----	1202
HQn·1.5H$_2$O	1656	3173	1591	----	----	1195
[Cu(HQn)Cl$_2$] (**17**)	1698	3182	1560	----	----	1199
[Cu(Qn)$_2$] (**18**)	----	----	1547	1576	1331	1206
[Cu(Qn)NO$_3$]·H$_2$O (**19**)	----	----	1558	1581	1334	1201
[Cu(Qn)ClO$_4$]·H$_2$O (**20**)	----	----	1556	1591	1340	1213
[Cu(Qn)NCS]·H$_2$O (**21**)	----	----	1588	1554	1335	1208
[Cu(Qn)N$_3$]·H$_2$O (**22**)	----	----	1586	1552	1337	1210
[Cu(HQn)Br$_2$] (**23**)	1666	3180	1539	----	----	1210

^{a} Newly formed C=N bond

IR spectrum of the complex [Cu(HQb)Cl$_2$] (**12**) is shown in Fig. 6.1. The chloro complexes **12** and **17** showed peaks at 306 and 303 cm^{-1} respectively, which are assigned to terminal ν(Cu–Cl) band. The medium band at 256 cm^{-1}, together with a band at 153 cm^{-1} in the far IR spectrum of the complex **16** has been assigned to the ν(Cu–Br) in a bridging mode. The complex **23** shows ν(Cu–Br) band at 250 cm^{-1} which indicates the presence of coordinated bromine and the absence of bands near 150 cm^{-1} is consistent with the terminal (Cu–Br) bond [16].
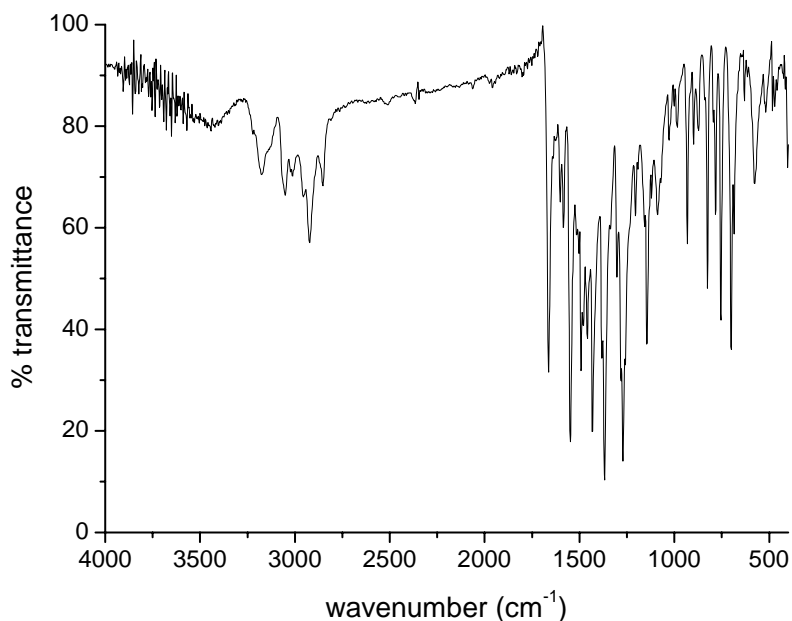
**Fig. 6.1.** IR spectrum of [Cu(HQb)Cl$_2$] (**12**).

For all other complexes, ν(C=O) and ν(N–H) are absent which indicate that the ligand is coordinated to the metal in the deprotonated form and due to the enolization, a new band appears at *ca.* 1330 cm^{-1} due to ν(C–O) band. The azomethine band (ν(C=N)) showed a shift to lower wavenumbers by 30-60 cm^{-1} in the spectra of the complexes indicating the coordination via the azomethine nitrogen. The occurrence of ν(N–N) at higher wavenumbers in the spectra of the complexes compared to that of the ligand confirms the participation of azomethine nitrogen in coordination. The increase in the frequency of this band in the spectra of complexes is due to the increase in the bond strength.

The sharp bands observed at 1500-1450 cm^{-1} are assigned to the ring vibrations. The Cu–N$_{quin.}$ vibrational frequency was observed at 280 cm^{-1}. Some new bands with medium to weak intensities appear in the region 450-550 cm^{-1} in the complexes under study which are tentatively assigned to ν(Cu–N) and ν(Cu–O) modes. Weak bands observed at around 2000 cm^{-1} are assigned to C–H mode vibrations. Also, an intense band located at 750 cm^{-1} is typical of aromatic rings vibrations. As expected, these bands are not affected by chelation [17,18].

The bands observed in 3400–3460 cm^{-1} region in the spectra of complexes **14**, **15**, **19**, **20**, **21** and **22** are assigned to lattice water molecules. The IR spectra of complexes [Cu(Qb)$_2$] (**13**) and [Cu(Qn)$_2$] (**18**) are shown in Figs. 6.2 and 6.3 respectively.
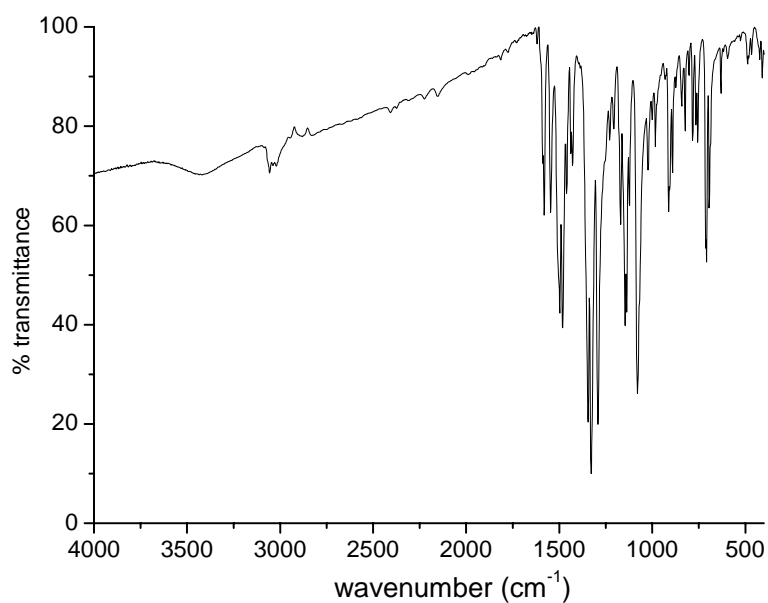
Fig. 6.2. IR spectrum of [Cu(Qb)$_2$] (**13**).
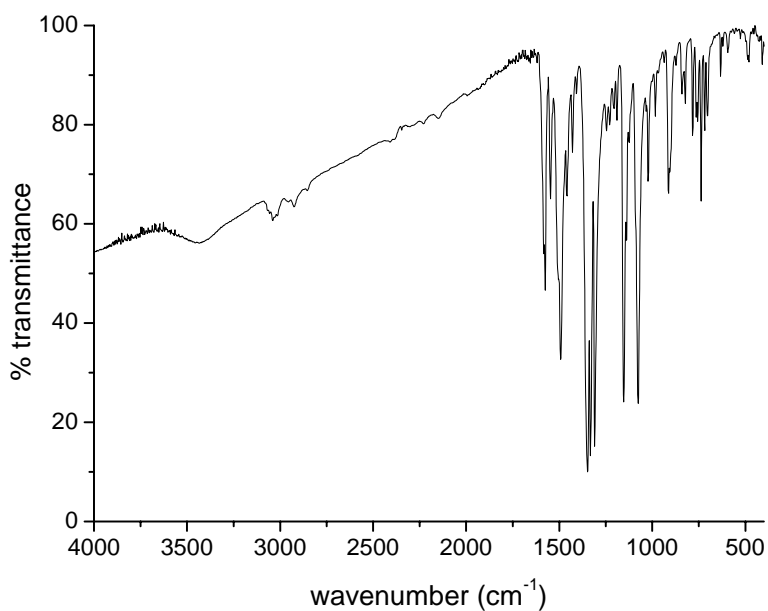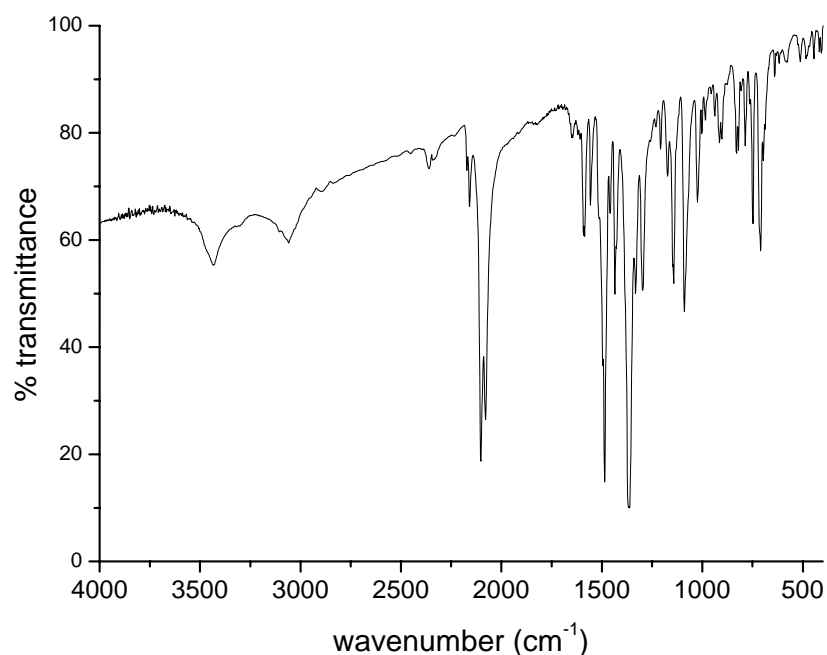

Fig. 6.3. IR spectrum of [Cu(Qn)$_2$] (**18**).

The SCN group may coordinate to a metal through the nitrogen or sulfur or both sulfur and nitrogen. The CN stretching frequencies are generally lower in N–bonded complexes (near and below 2050 cm^{-1}) than in S-bonded complexes (near 2100 cm^{-1}) and the bridging [M-NCS-M'] complexes exhibits v(CN) well above 2100 cm[1]. The v(CS) band for S-bonded complexes are found in the 720-690 cm^{-1} region. The N-bonded complexes exhibit a single sharp δ(NCS) band near 480 cm[1], where as the S-bonded complexes show several weak bands near 421 cm^{-1} [19,20].

Compound [Cu(Qb)NCS]·H$_2$O (**14**) has a very strong band at 2079 cm^{-1}, a medium band at 914 cm^{-1} and a weak band at 513 cm^{-1} corresponding to v(CN), v(CS) and δ(NCS) modes of the NCS group, respectively (Fig. 6.4).

Fig. 6.4. IR spectrum of [Cu(Qb)NCS]·H$_2$O (**14**).

In the IR spectrum of the compound [Cu(Qn)NCS]·H$_2$O (**21**), v(CN), v(CS) and δ(NCS) modes, respectively, appear at 2076, 914 and 503 cm^{-1} [21]. The

intensity and position of these bands indicate the unidentate coordination of the thiocyanate group through the nitrogen (Fig. 6.5).
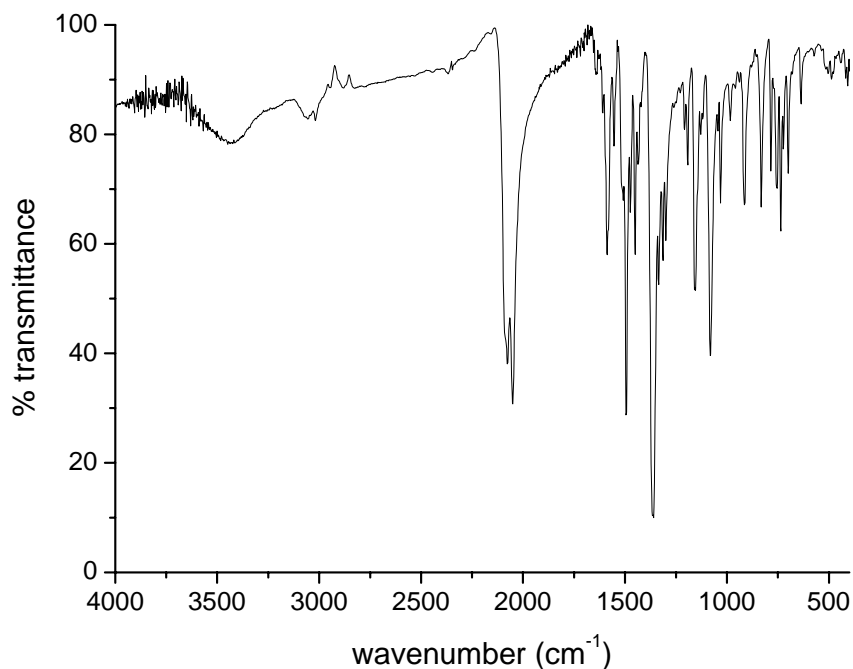
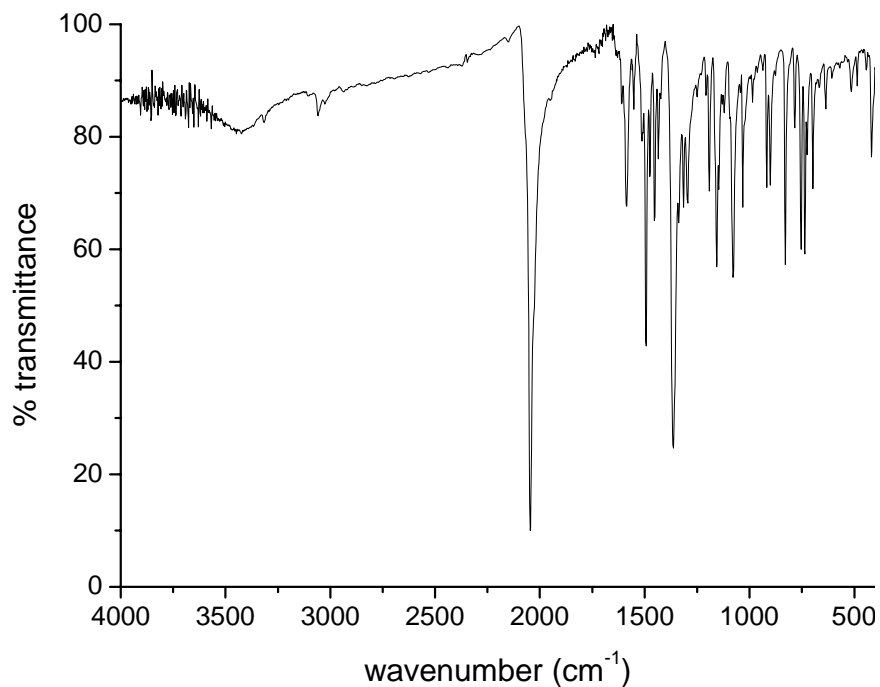**Fig. 6.5.** IR spectrum of [Cu(Qn)NCS]·H$_2$O (**21**).

The azido complex [Cu(Qb)N$_3$]$_2$·H$_2$O (**15**) shows a sharp band at 2054 cm^{-1} and another one at 1291 cm^{-1} (Fig. 6.6). These are assigned to ν_a and ν_s of the coordinated azido group. The broad bands observed at 637 and 449 cm^{-1} for the complex are assigned to δ(N–N–N) and ν(Cu–N$_{azido}$) bands.

Similarly compound [Cu(Qn)N$_3$]·H$_2$O (**22**) exhibits two bands at 2045 and 1295 cm^{-1} corresponding to ν_a and ν_s of the coordinated azido group and also two broad bands at 633 and 490 cm^{-1} which are attributable to δ(N–N–N) and ν(Cu–N$_{azido}$) bands (Fig. 6.7).
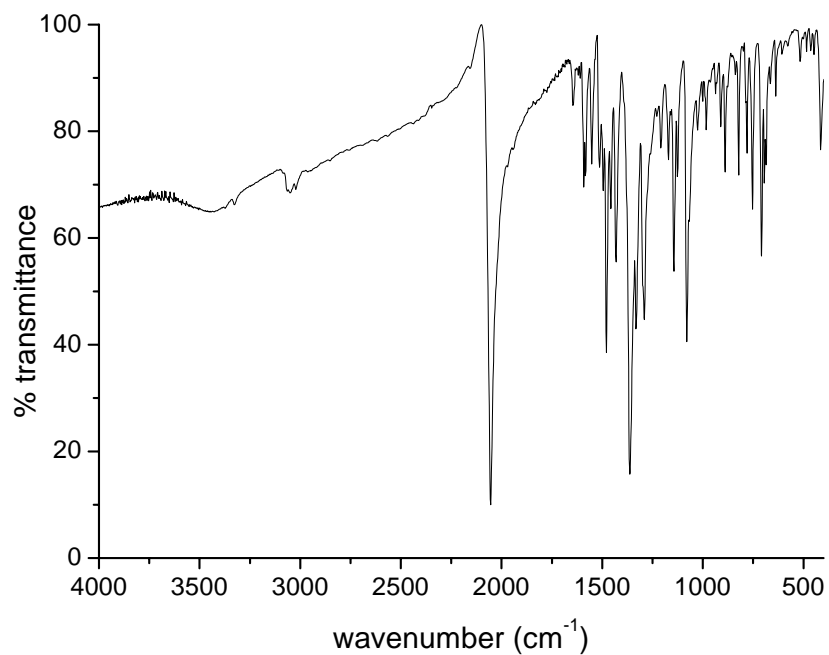
Fig. 6.6. IR spectrum of $[Cu(Qb)N_3]_2 \cdot H_2O$ (**15**).

Fig. 6.7. IR spectrum of $[Cu(Qn)N_3] \cdot H_2O$ (**22**).

According to Gatehouse *et al.*, for nitrato complexes, the unidentate and bidentate NO_3 groups exhibit three NO stretching bands. The separation of the two highest-frequency bands is 115 cm^{-1} for the unidentate complex, whereas it is 186 cm^{-1} for the bidentate complex. We found that the compound **19** exhibits three strong bands at 1500, 1370 and 1094 cm^{-1} corresponding to stretching bands of the nitrato group indicating the presence of a terminal monodentate coordination of the nitrato group [17]. The fact that the nitrato group is terminally bonded is understood from the separation of 130 cm^{-1} between two highest-frequency bands just mentioned above.

The IR spectrum of the compound $[Cu(Qn)ClO_4]·H_2O$ (**20**) displays two bands at 1169 and 1100 cm^{-1} and a strong band at 621 cm^{-1} and a weak band at 916 cm^{-1} indicating the presence of coordinated perchlorate (Fig. 6.8). The band at 1169 cm^{-1} is assignable to $v_3(ClO_4)$ and the band at 621 cm^{-1} assignable to $v_4(ClO_4)$ [17,22].
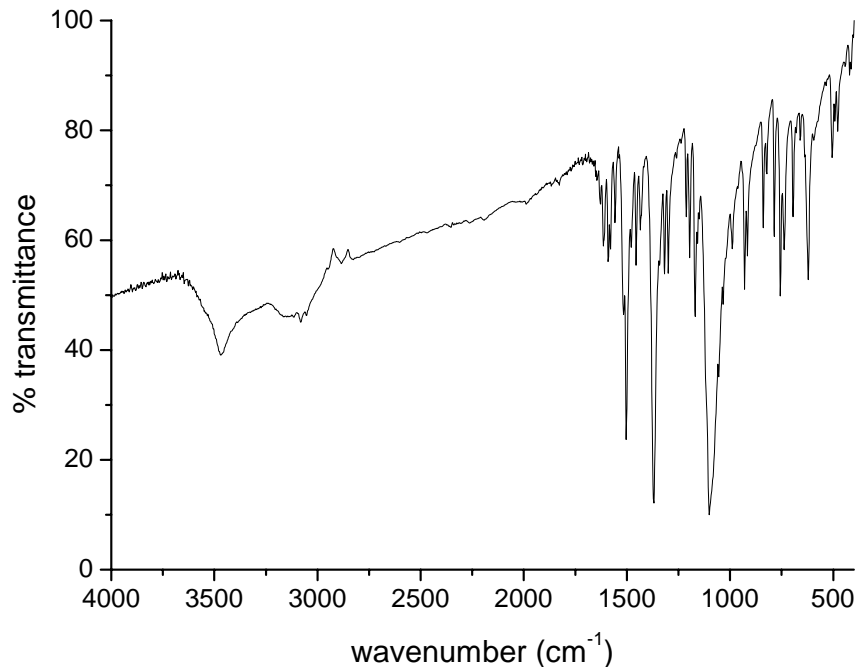
Fig. 6.8. IR spectrum of $[Cu(Qn)ClO_4]·H_2O$ (**20**).

6.3.2. Electronic spectra

The electronic absorption spectra are often very helpful in the evaluation of results furnished by other methods of structural investigation. The electronic spectra of copper(II) complexes is the most difficult from which to obtain useful structural information, due to flexible stereochemistry of the copper(II) ions.

The Cu(II) ion, with $3d^9$ outer electronic configuration, is typical due to its stereochemical flexiblity. While strong field ligands generally yield square planar or six coordinate tetragonal complexes, weak fields give rise to almost any stereochemistry. The presence of nine electrons ensures that some electrons are σ-antibonding and it is perhaps this feature together with the Jahn-Teller effect in appropriate cases which give rise to a range of distorted structures to copper(II) complexes. So the electronic spectra of the species will be uncertain.

Copper(II) has the spectroscopic ground state term ^2D which will be split by an octahedral field into two levels, $^2T_{2g}$ and ^2E_g. However, if the geometry around copper(II) complex is of lower symmetry, the energy levels again split resulting in more transitions and its electronic spectrum is somewhat more complicated. In a tetragonal field, with $d_{x^2-y^2}$ (b_{1g}) ground state, three spin allowed transitions are possible *viz.* $^2A_{1g} \leftarrow {}^2B_{1g}$, $^2B_{2g} \leftarrow {}^2B_{1g}$ and $^2E_g \leftarrow {}^2B_{1g}$ and they occur in the ranges 12000 - 17000, 15500 - 18000 and 17000 - 20000 cm^{-1}, respectively [23].

The low energy region in the absorption spectrum is dominated by transitions from the filled *d*-orbitals to the half-occupied higher energy orbital. Since these *d*-orbitals are split in energy by ligand field at the metal centre, the associated *d-d* transitions are sensitive probes of the ligand geometry.

The high intense ligand-to-metal charge transfer (LMCT) transitions are observed at the higher energy region. The intensity of these transitions reflects the overlap of the ligand and metal orbitals involved in the charge transfer. Their energy splitting reflects differences in π and σ ligand-metal bonding interactions.

115

UVD-3500, UV-vis Double Beam Spectrophotometer was used to record the electronic spectra of the hydrazones and their complexes. The spectra of all the compounds were recorded in acetonitrile solutions in the range 45000-20000 cm^{-1} and in DMF in the range 20000-10000 cm^{-1} (Figs. 6.9 and 6.10).

(a)

(b)
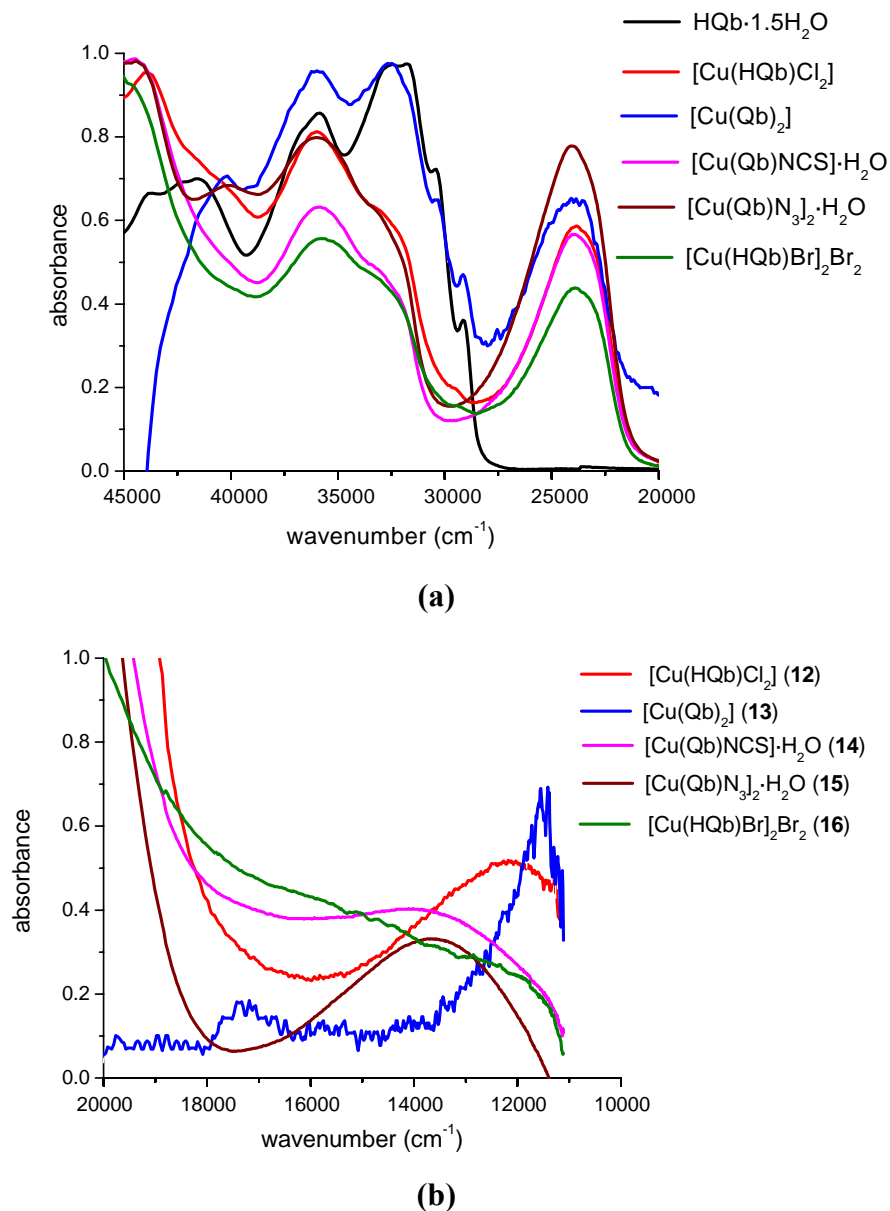
Fig. 6.9. Electronic spectra of $HQb \cdot 1.5H_2O$ and its copper(II) complexes (a) in acetonitrile and (b) in DMF.
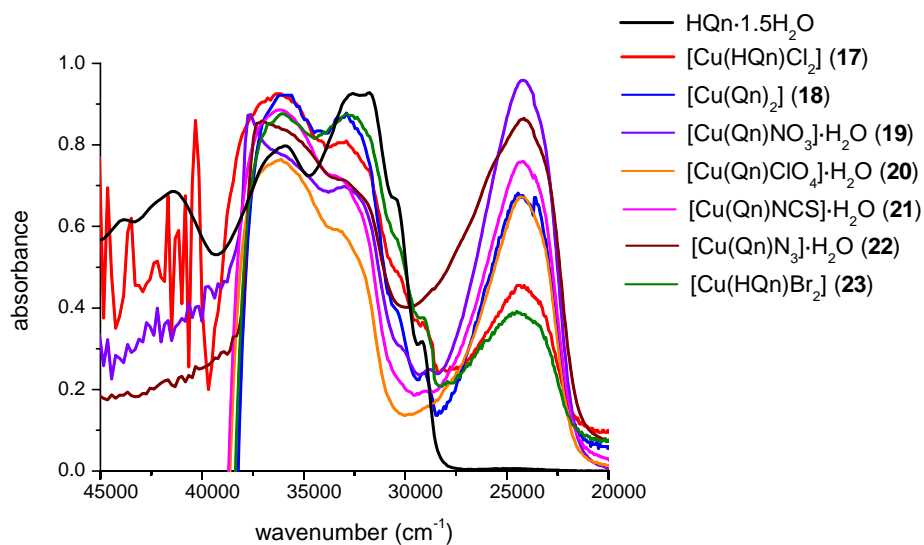
(a)
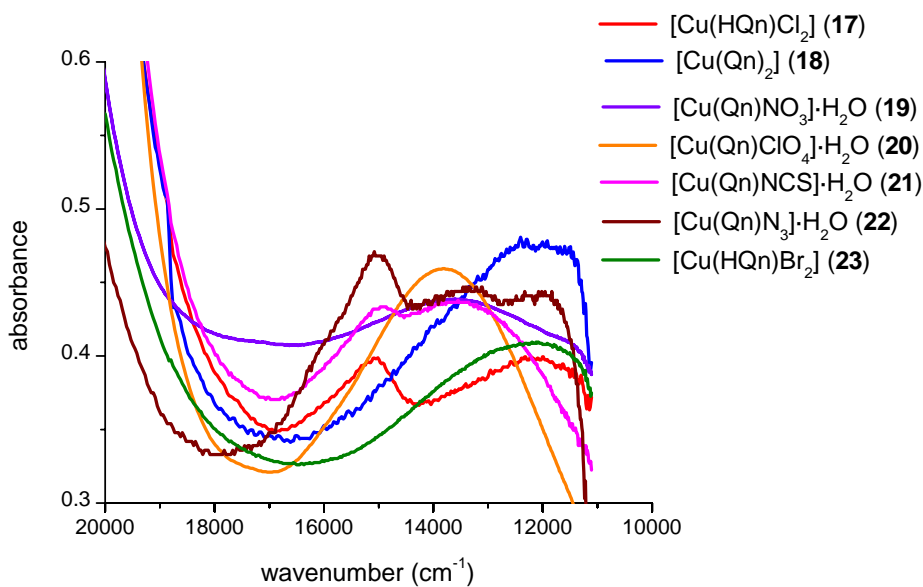
(b)

Fig. 6.10. Electronic spectra of HQn·1.5H$_2$O and its copper(II) complexes (a) in acetonitrile and (b) in DMF.

In the electronic spectra of the hydrazones and their copper(II) complexes, the bands centered in the 45000-27000 cm^{-1} region are assigned to the intraligand transitions. In all the complexes, an intense band was observed near 24000 cm^{-1} which is absent in the ligand and is attributed to the ligand-to-metal charge transfer (LMCT) transition.

The low intensity bands in the visible region are due to the *d-d* transitions. Due to the broadness of the bands, all the expected bands cannot be distinguished. This is because of the fact that the low-lying four *d* orbitals lie very close together and so each transition cannot be distinguished by their energy. Hence it is very difficult to resolve the bands into separate components. The electronic spectral data obtained are tabulated in Table 6.2.

Table 6.2. Electronic spectral data of the hydrazones and their copper(II) complexes.

Compound	Absorbance λ_{max} (cm^{-1})
HQb·1.5H$_2$O	43790, 41640, 35860, 32580, 31690, 30430, 29130
[Cu(HQb)Cl$_2$] (**12**)	43940, 41760, 35990, 32940 (sh), 29470, 23790, 12140
[Cu(Qb)$_2$] (**13**)	40310, 35980, 32600, 30380 (sh), 29180, 23910, 17370, 11550
[Cu(Qb)NCS]·H$_2$O (**14**)	44520, 35860, 32890 (sh), 23920, 13840,
[Cu(Qb)N$_3$]$_2$·H$_2$O (**15**)	44470, 40150, 35980, 33140 (sh), 24080, 13620
[Cu(HQb)Br]$_2$Br$_2$ (**16**)	44470, 35700, 33100, 29310, 23870, 11940
HQn·1.5H$_2$O	43920, 41490, 35840, 32580, 31750, 30440, 29150
[Cu(HQn)Cl$_2$] (**17**)	36270, 33060, 31860 (sh), 30380 (sh), 29140 (sh), 24280, 15060, 12130
[Cu(Qn)$_2$] (**18**)	35950, 33020, 30480 (sh), 29100, 24480, 23560, 12010
[Cu(Qn)NO$_3$]·H$_2$O (**19**)	42500, 37510, 35860 (sh), 32980, 30180 (sh), 28770, 24200, 13640, 11550 (sh)
[Cu(Qn)ClO$_4$]·H$_2$O (**20**)	36380, 33250, 24280, 13840
[Cu(Qn)NCS]·H$_2$O (**21**)	36250, 33350, 29030, 24280, 14930, 13560
[Cu(Qn)N$_3$]·H$_2$O (**22**)	36970, 33020, 24160, 15060, 11760
[Cu(HQn)Br$_2$] (**23**)	36100, 32790, 30410 (sh), 29160 (sh), 27910, 24450, 12120

6.3.3. Electron paramagnetic resonance spectroscopy

EPR spectroscopy has been widely used in the study of paramagnetic complexes. The copper(II) ion, with a d^9 configuration, has an effective spin of $S = \frac{1}{2}$ and is associated with a spin angular momentum, $M_s = \pm\frac{1}{2}$, leading to a doubly degenerate spin state in the absence of a magnetic field. In a magnetic field, the degeneracy is lifted between these states and the energy difference between them is given by

$$\Delta E = h\nu = g\beta B$$

where h is Planck's constant, ν is the microwave frequency for transition from $M_s = +\frac{1}{2}$ to $M_s = -\frac{1}{2}$, g is the Lande splitting factor (equal to 2.0023 for a free electron), β is the Bohr magneton and B is the magnetic field.

For the case of a $3d^9$ copper(II) ion, the appropriate spin Hamiltonian assuming a B_{1g} ground state is given by:

$$\hat{H} = \beta[g_{\parallel}H_aS + g_{\perp}(H_xS_x + H_yS_y)] + A_{\parallel}I_zS_z + A_{\perp}(I_xS_x + I_yS_y)$$

where all the symbols have their usual meaning.

The factors that determine the type of EPR spectrum observed are the nature of the electronic ground state, the symmetry of the effective ligand field about the Cu(II) ion and the mutual orientations of the local molecular axes of the separate Cu(II) chromophores in the unit cell [24,25].

The EPR spectra of the copper(II) complexes were recorded in polycrystalline state at 298 K and in DMF at 77 K in the X-band, using 100-kHz modulation; g factors were quoted relative to the standard marker TCNE ($g = 2.00277$), at the SAIF, IIT, Bombay, India.
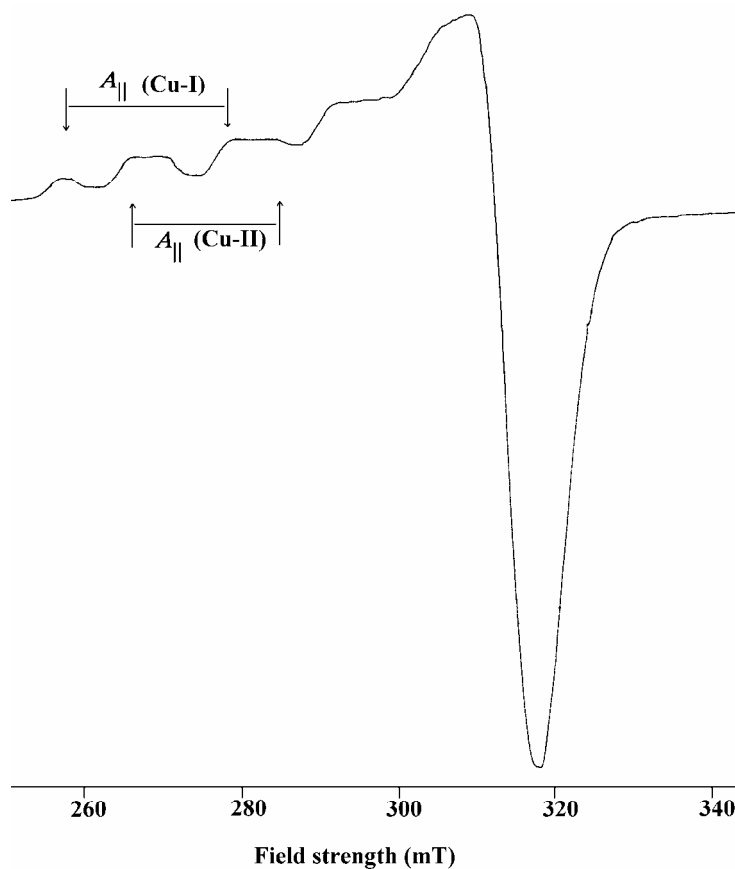
The EPR spectrum of the complex [Cu(HQb)Cl$_2$] (**12**) is isotropic in the polycrystalline state at 298 K and is shown in Fig. 6.11.
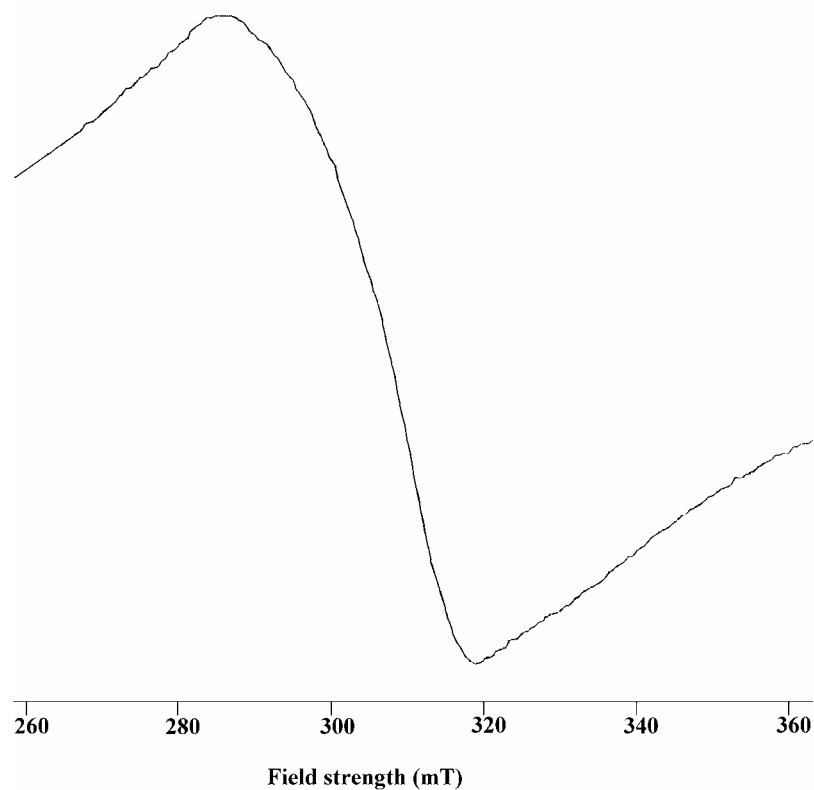
Fig. 6.11. The EPR spectrum of [Cu(HQb)Cl$_2$] (**12**) in the polycrystalline state at 298 K.

Such isotropic spectra, consisting of a broad signal and hence only one *g* value, arise from extensive exchange coupling through misalignment of the local molecular axes between different molecules (dipolar broadening) and enhanced spin lattice relaxation. These types of spectra unfortunately give no information on the electronic ground state of the metal ion present in the complexes.

In DMF at 77 K, the complex [Cu(HQb)Cl$_2$] (**12**) displays an anisotropic spectrum with an axial *g* tensor and well-resolved parallel hyperfine splitting due to the interaction of the unpaired electron with ^{63,65}Cu ($I = 3/2$). The spectrum (Fig. 6.12) shows eight lines in the parallel region, which may be due to the presence of two copper sites (indicated as Cu-I and Cu-II) due to the coordination of solvent, DMF, to the metal centre.

Fig. 6.12. The EPR spectrum of [Cu(HQb)Cl$_2$] (**12**) in DMF at 77 K.

The complex [Cu(Qb)$_2$] (**13**) shows an isotropic spectrum in the polycrystalline state at 298 K with g_{iso} = 2.177. The spectrum is presented in Fig. 6.13.

The frozen solution EPR spectrum of **13** in DMF (Fig. 6.14) is reverse axial in nature with $g_{\parallel}$ = 2.163 and $g_{\perp}$ = 2.220. The hyperfine structure is not observed in the spectrum. The anisotropy of the *g*-tensor indicates that tetragonal distortion is present in the compound due to Jahn Teller effect. As the coordinated groups are not equivalent, only static distortion can occur. As the *g* values are less than 2.3, considerable covalent character is expected to the metal-ligand bonds. The absence of hyperfine structure restricts the calculation of the bonding parameters [23,24].

121
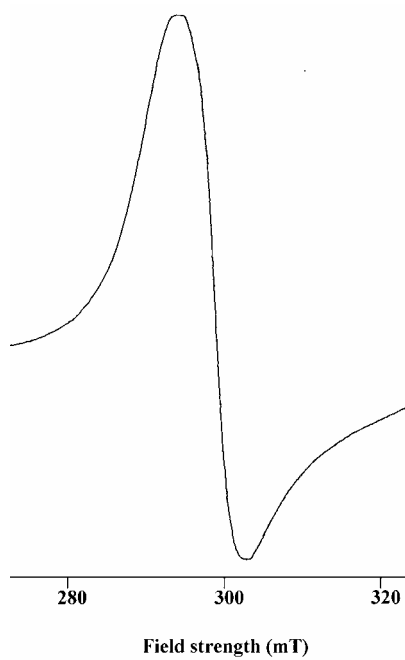
Fig. 6.13. The EPR spectrum of [Cu(Qb)$_2$] (**13**) in the polycrystalline state at 298 K.
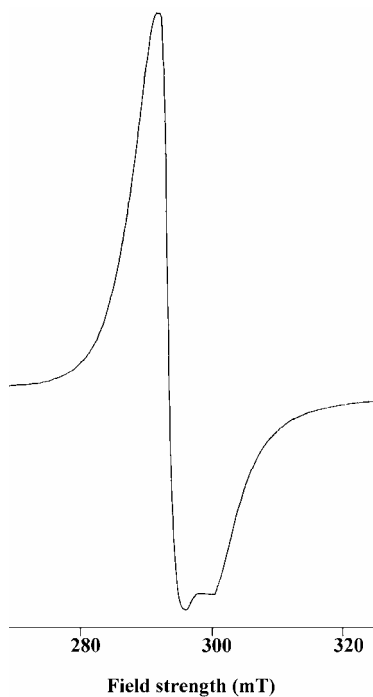
Fig. 6.14. The EPR spectrum of [Cu(Qb)$_2$] (**13**) in DMF at 77 K.

The thiocyanato complex $[Cu(Qb)NCS] \cdot H_2O$ (**14**) gives an isotropic spectrum in the polycrystalline state at 298 K (Fig. 6.15).
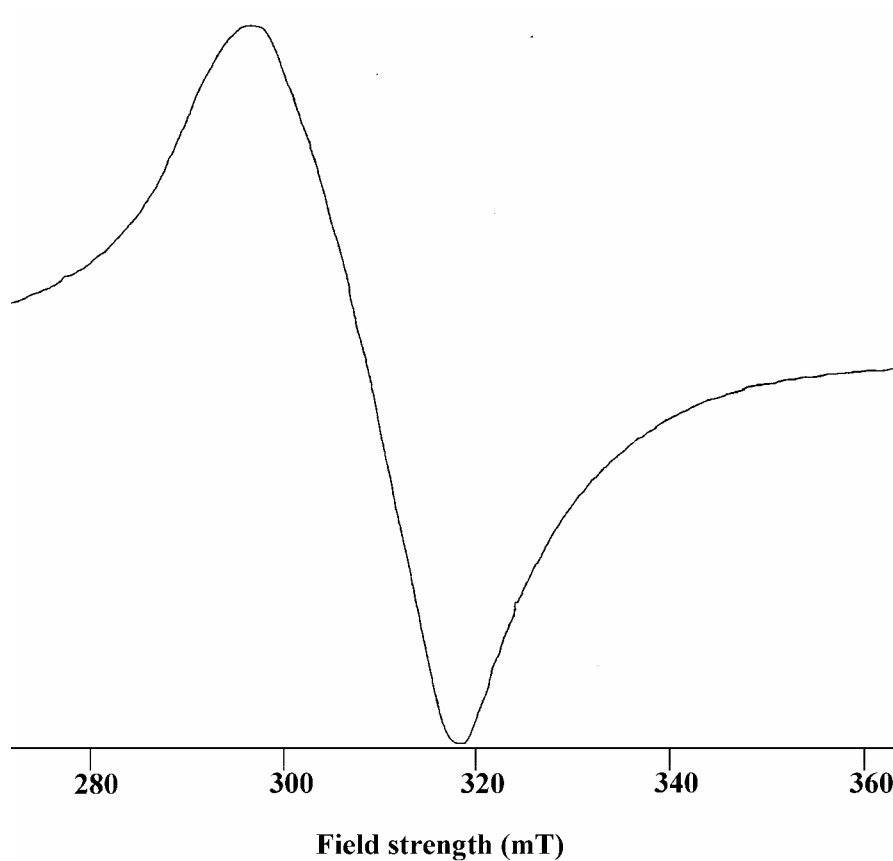
Fig. 6.15. The EPR spectrum of $[Cu(Qb)NCS] \cdot H_2O$ (**14**) in polycrystalline state at 298 K.

In DMF at 77 K, the complex **14** gives axial spectrum with four well-resolved hyperfine lines in the parallel region (Fig.6.16) with the hyperfine splitting constant $A_{\parallel} = 182.44 \times 10^{-4}$ cm^{-1}.

123

Field strength (mT)
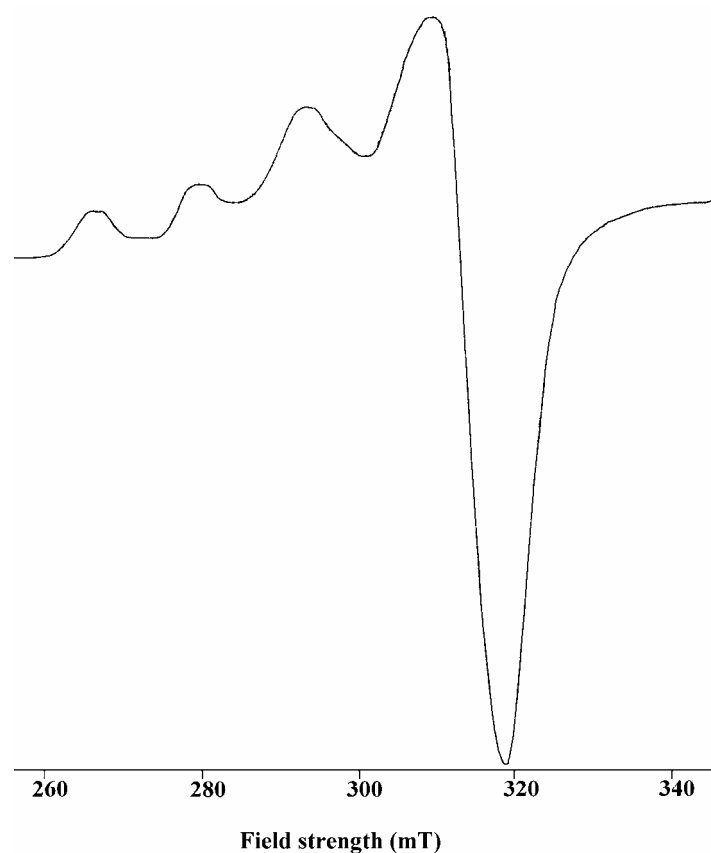
Fig. 6.16. The EPR spectrum of $[Cu(Qb)NCS] \cdot H_2O$ (**14**) in DMF at 77 K.

An axial spectrum was obtained for the complex $[Cu(Qb)N_3]_2 \cdot H_2O$ (**15**) in the solid state at room temperature with $g_\parallel = 2.214$ and $g_\perp = 2.071$ (Fig. 6.17). Proctor and co-workers have postulated that the geometric parameter $G = (g_\parallel\text{-}2.0023)/(g_\perp\text{-}2.0023)$ indicates the possibility of exchange interaction in the copper(II) complexes. If $G > 4.4$, exchange interaction is negligible and if it is less than 4.4, considerable exchange interaction is present in the solid complex [25-27].

In the present case, the value is 3.082, which indicates considerable exchange interaction exists in the complex in the solid state. The spectra are often broad because of the fast spin-lattice relaxation and exchange coupling
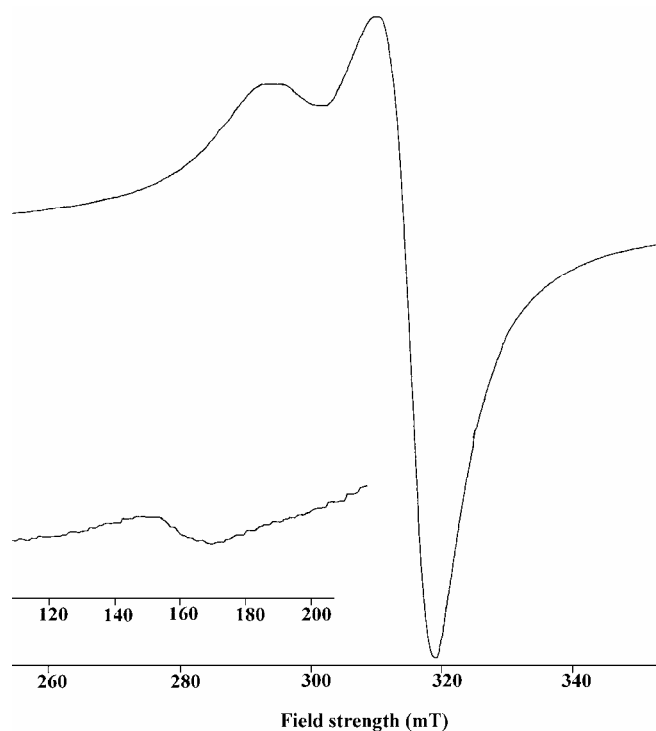
Fig. 6.17. The EPR spectrum of $[Cu(Qb)N_3]_2 \cdot H_2O$ (**15**) in polycrystalline state at 298 K.

In addition to the allowed ($\Delta M_s = \pm 1$) transitions, forbidden ($\Delta M_s = \pm 2$) transitions are also present in the spectrum of **15** in polycrystalline state at 298 K. In polynuclear copper(II) complexes, due to Cu–Cu dipolar interaction, the zero field splitting parameter, D gives rise to transitions corresponding to $\Delta M_s = \pm 2$. In the X-band spectra, $\Delta M_s = \pm 1$ transitions are associated with fields of *ca.* 3000 Gauss, while the $\Delta M_s = \pm 2$ transitions generate an absorption at the half field value of *ca.* 1500 Gauss and the presence of this half field band is a useful criterion for dipolar interaction from the presence of some dinuclear (or polynuclear) complex formation.

The solid state EPR spectrum of the complex **15** at 298 K exhibited a half field signal at $g = 4.120$. The half-field transition is a fingerprint for the dimers and appears at a magnetic field position where the isolated cations are not expected to contribute.

125

The EPR spectrum of compound **15** in the frozen state exhibits an axial spectrum (Fig. 6.18) with four well-resolved hyperfine lines in the parallel region. We got a half field signal at $g = 4.186$.
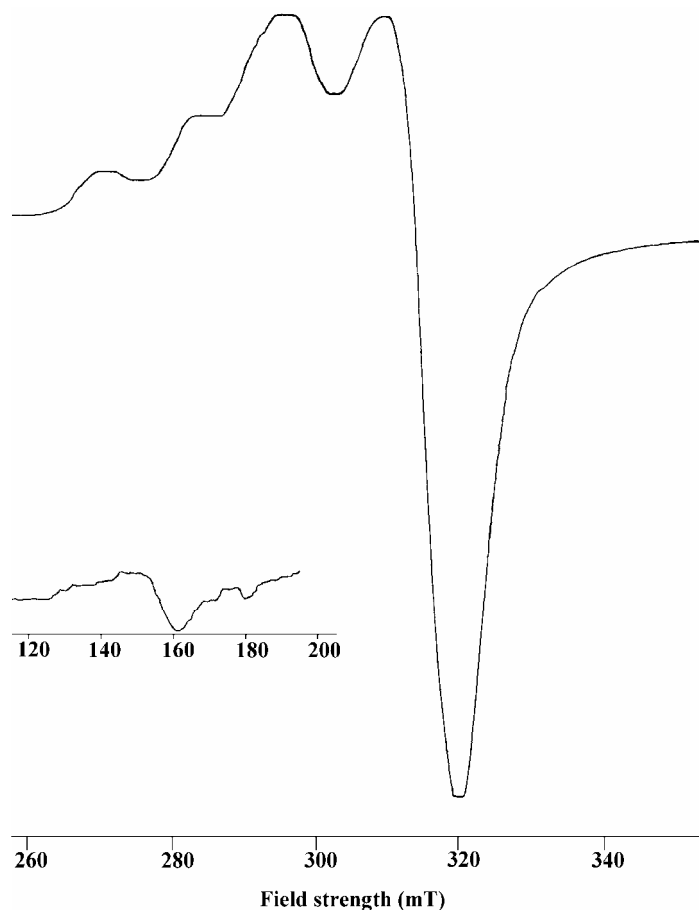
Fig. 6.18. The EPR spectrum of $[Cu(Qb)N_3]_2 \cdot H_2O$ (**15**) in DMF at 77 K.

In polycrystalline state at 298 K, the EPR spectrum of $[Cu(HQb)Br]_2Br_2$ (**16**) is isotropic (Fig. 6.19). The solution EPR spectrum of the compound **16** in DMF at 77 K (Fig. 6.20) displayed rhombic features with three g values ($g_1 = 2.056$, $g_2 = 2.108$ and $g_3 = 2.265$). Only the signal in the low field region (g_3) exhibited hyperfine splittings due to Cu(II) nucleus. However, the spectrum has the general appearance of one derived from monomeric species and we observed no $\Delta M_s = \pm 2$ transition, characteristic of exchange-coupled dimers.

Field strength (mT)
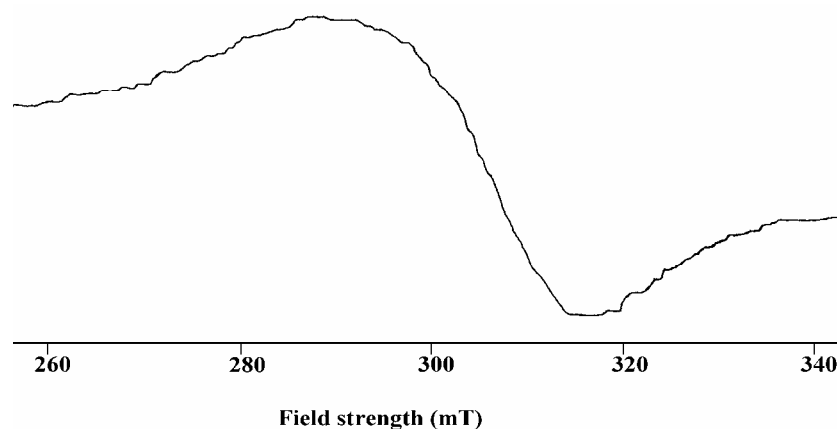
Fig. 6.19. The EPR spectrum of [Cu(HQb)Br]$_2$Br$_2$ (**16**) in polycrystalline state at 298 K.

Absence of half field signals for the compound reinforces the assumption of very weak super exchange interactions. It may be due to the fact that the Cu^{2+} ions may be far enough removed from one another (> 6 Å), since the bridging units are large bromide ions. So direct dipolar interactions are very small and therefore, there is no substantial change in the spectrum from one characteristic of essentially isolated Cu^{2+} units.

Field strength (mT)
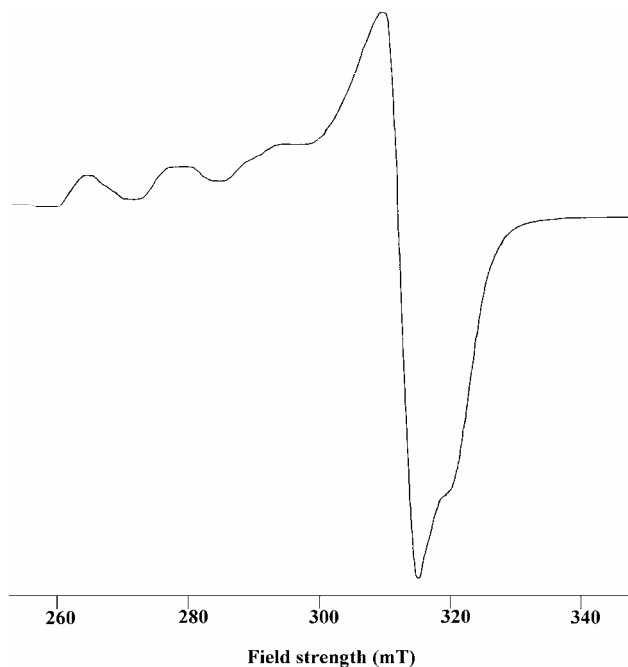
Fig. 6.20. The EPR spectrum of [Cu(HQb)Br]$_2$Br$_2$ (**16**) in DMF at 77 K.

127

The g_3 value of the complex **16** is less than 2.3 and they assign considerable covalent character to the metal–ligand bonds. Also the lowest g value (g_1) is less than 2.04 indicating a compressed rhombic symmetry with all axes aligned parallel and is consistent with distorted trigonal bipyramidal stereochemistry or a compressed axial symmetry or rhombic symmetry with slight misalignment of the axes.

In the spectra with $g_3 > g_2 > g_1$, rhombic spectral parameter $R = (g_2–g_1)/(g_3–g_2)$ may be significant. If $R > 1$, a predominant d_z^2 ground state is present. If $R < 1$, a predominant $d_{x^2-y^2}$ ground state is present and when $R = 1$, then the ground state is approximately an equal mixture of d_z^2 and $d_{x^2-y^2}$, the structure is intermediate between square planar and trigonal bipyramidal geometries. Here, $R = 0.33$, which suggests a $d_{x^2-y^2}$ ground state is present in the compound **16**.

The spectrum of [Cu(HQn)Cl$_2$] (**17**) in polycrystalline state at 298 K gives three g values *viz.* g_1, g_2 and g_3, indicating rhombic distortion in their geometry (Fig. 6.21).
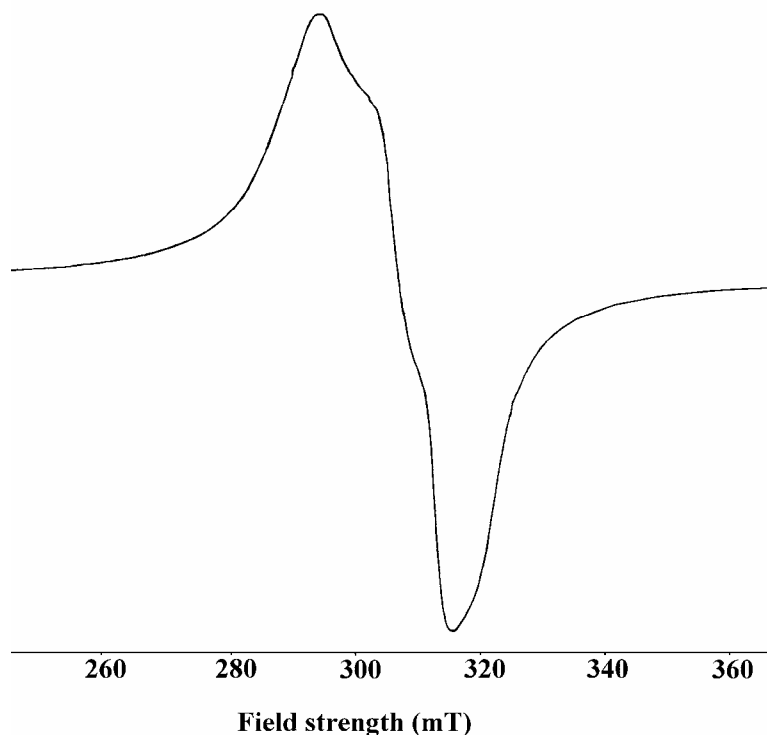
Fig. 6.21. The EPR spectrum of [Cu(HQn)Cl$_2$] (**17**) in polycrystalline state at 298 K.

The lowest g value (g_1) is > 2.04 indicating a rhombic, distorted square based pyramidal geometry. For rhombic spectra,

$G = g_3 – 2.0023/g_\perp – 2.0023$; where $g_\perp = (g_1 + g_2)/2$.

The parameter R for rhombic systems can be calculated as

$R = (g_2 – g_1)/(g_3 – g_2)$

The value obtained for the compound **17** is 0.86 and since $R < 1$, $d_{x^2-y^2}$ ground state of the copper(II) ion is expected [28,29].

In DMF at 77 K, the compound **17** displays an axial spectrum with $g_\parallel = 2.219$ and $g_\perp = 2.093$ with a partial resolution of hyperfine structure (Fig.6.22).
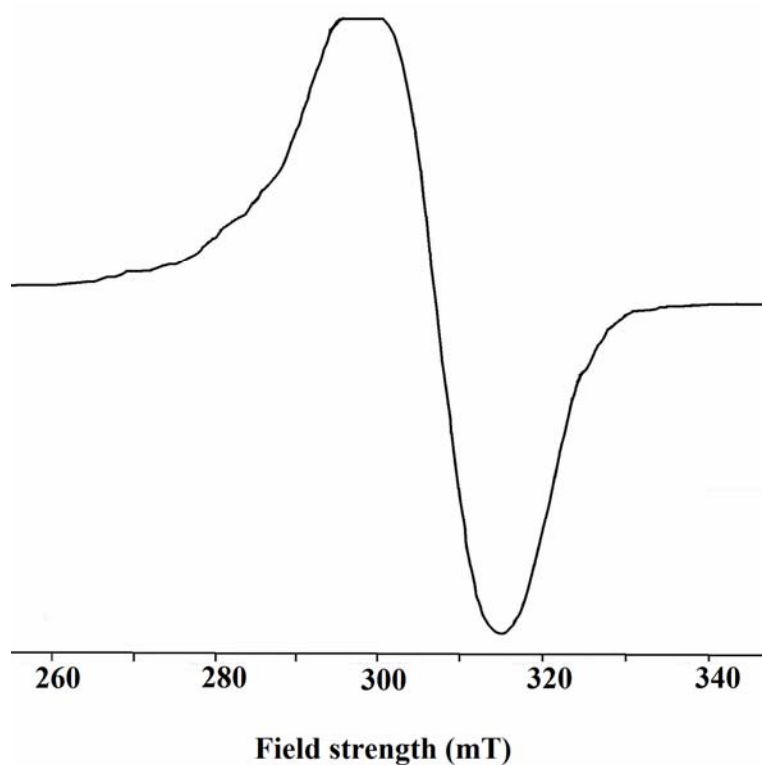
Fig. 6.22. The EPR spectrum of $[Cu(HQn)Cl_2]$ (**17**) in DMF at 77 K.

The solution spectrum of complex **17** was recorded in DMF at 298 K (Fig. 6.23). The spectrum is isotropic in nature with four hyperfine lines.
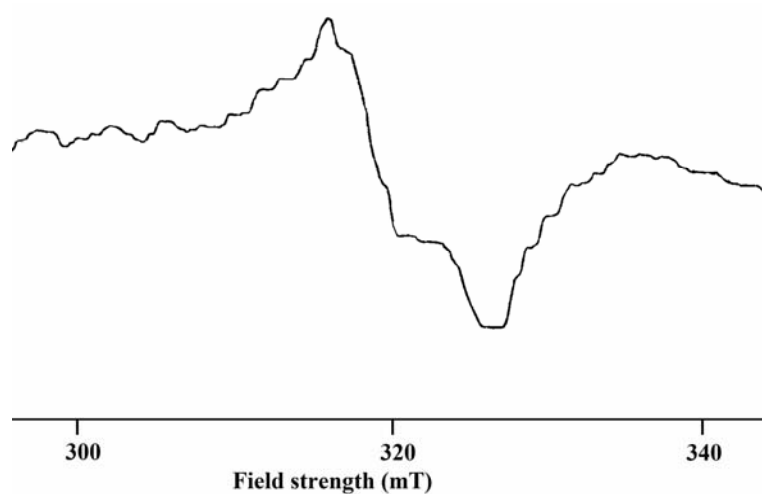
Fig. 6.23. The EPR spectrum of $[Cu(HQn)Cl_2]$ (**17**) in DMF at 298 K.

The hyperfine splitting is due to the interaction of the electron spin with the copper nuclear spin (^{65}Cu, $I = 3/2$). The isotropic nature of the spectra is due to the tumbling motion of the molecules in DMF.

The EPR spectrum of $[Cu(Qn)_2]$ (**18**) is isotropic both in polycrystalline state at 298 K (Fig. 6.24) and in DMF at 77 K (Fig. 6.25).
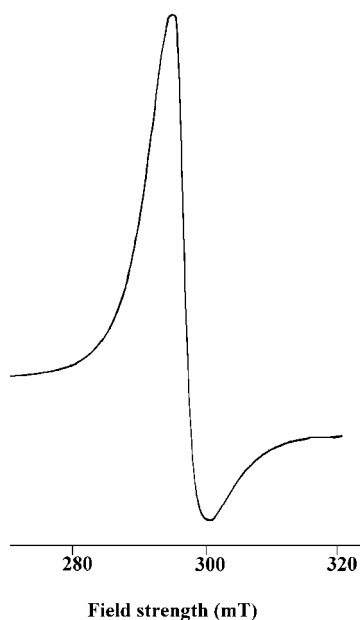
Fig. 6.24. The EPR spectrum of $[Cu(Qn)_2]$ (**18**) in polycrystalline state at 298 K.

Field strength (mT)
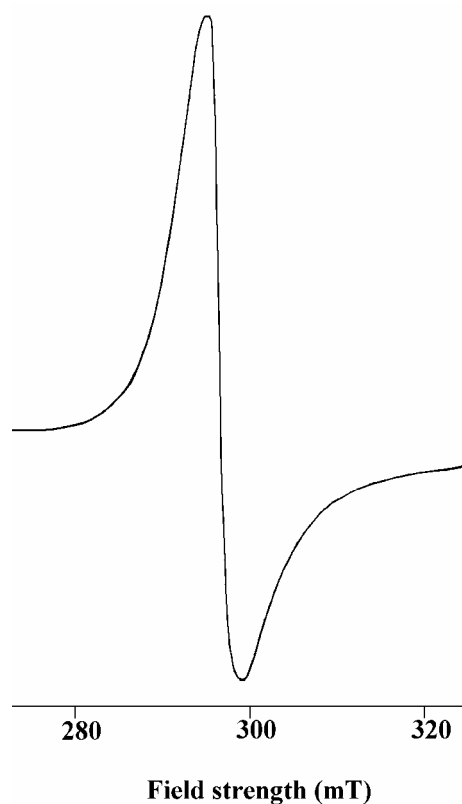
Fig. 6.25. The EPR spectrum of [Cu(Qn)$_2$] (**18**) in DMF at 77 K.

EPR spectrum of **18** was also recorded in DMF at 298 K and we got an isotropic one and the hyperfine structure of the spectrum is of poor resolution.

The solid state EPR spectrum of compound [Cu(Qn)NO$_3$]·H$_2$O (**19**) at 298 K shows rhombic features with $g_1 = 2.057$, $g_2 = 2.114$ and $g_3 = 2.207$ (Fig. 6.26). As mentioned earlier, since the lowest g value (g_1) is >2.04 a rhombic, distorted square based pyramidal geometry is expected for this compound. The parameters G and R were calculated and found to be 2.460 and 0.61, respectively. In view of the fact that the geometric parameter $G < 4.4$ and $R < 1$, $d_{x^2-y^2}$ ground state of the copper(II) ion is assigned to the compound **19**.

131
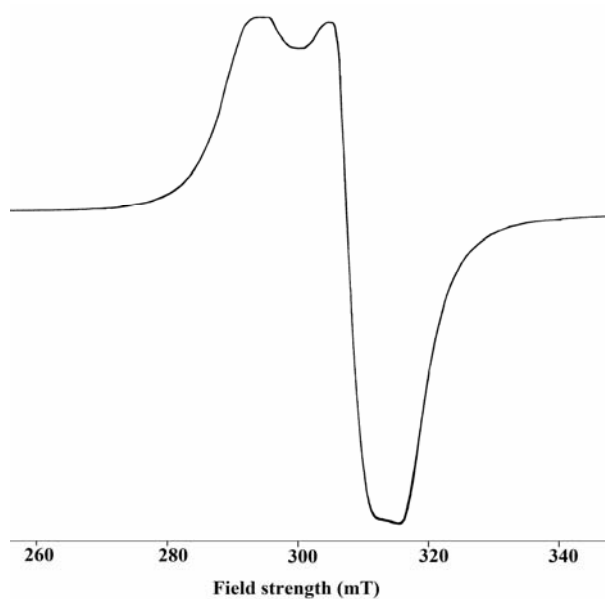
Fig. 6.26. The EPR spectrum of $[Cu(Qn)NO_3]\cdot H_2O$ (**19**) in polycrystalline state at 298 K.

An axial spectrum is observed for the compound **19** in DMF at 77 K (Fig. 6.27). But the hyperfine structure is not well-resolved and this may be due to the poor glass formation. The spectrum gives $g_\parallel = 2.241$, $g_\perp = 2.121$ and $A_\parallel = 177.86 \times 10^{-4}$ cm^{-1}.
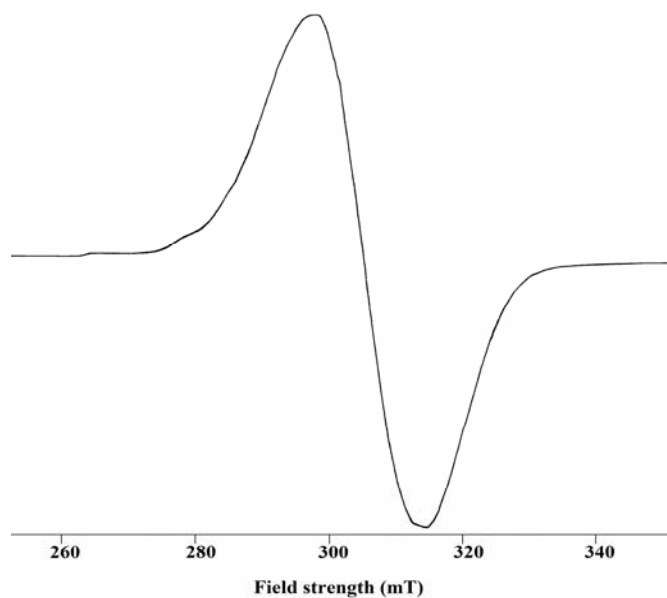
Fig. 6.27. The EPR spectrum of $[Cu(Qn)NO_3]\cdot H_2O$ (**19**) in DMF at 77 K.

The EPR spectrum of $[Cu(Qn)NO_3] \cdot H_2O$ (**19**) in DMF at 298 K was recorded and is shown in Fig. 6.28. As in the previous case, we got an isotropic spectrum. The well resolved four hyperfine lines was obtained with $A_{iso} = 130.32 \times 10^{-4}$ cm^{-1}.
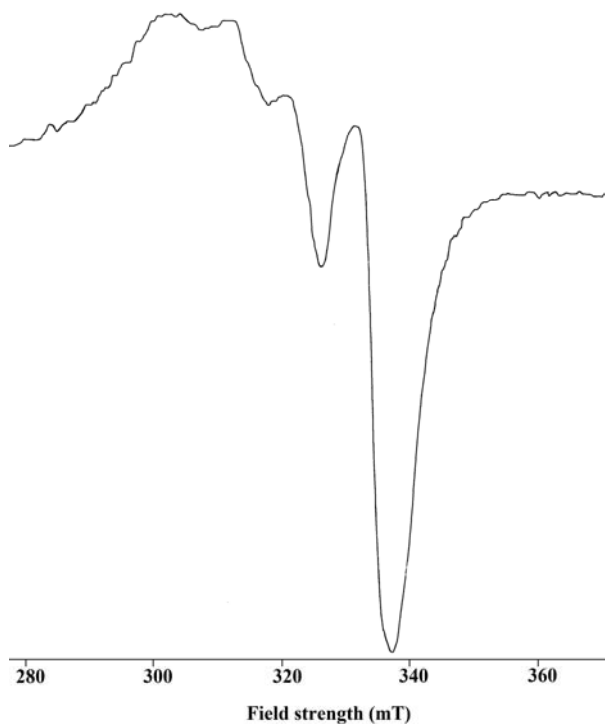
Fig. 6.28. The EPR spectrum of $[Cu(Qn)NO_3] \cdot H_2O$ (**19**) in DMF at 298 K.

In polycrystalline state at 298 K, the compound $[Cu(Qn)ClO_4] \cdot H_2O$ (**20**) gives rhombic spectrum (Fig. 6.29) with $g_1 = 2.047$, $g_2 = 2.103$ and $g_3 = 2.228$. The parameters, $G = 3.105$ and $R = 0.45$, are consistent with the existence of $d_{x^2-y^2}$ ground state in the complex.

In DMF solution at 77 K, an isotropic spectrum was obtained (Fig. 6.30) for the complex **20**. The isotropic spectrum will not give any information about the geometry of the compound. In the frozen solution, the intermolecular interactions are reduced and we expect a well resolved EPR spectrum. The reason for the less informative spectrum may be due to the poor glass formation of the solution and consequent misalignment of tetragonal axes.

133
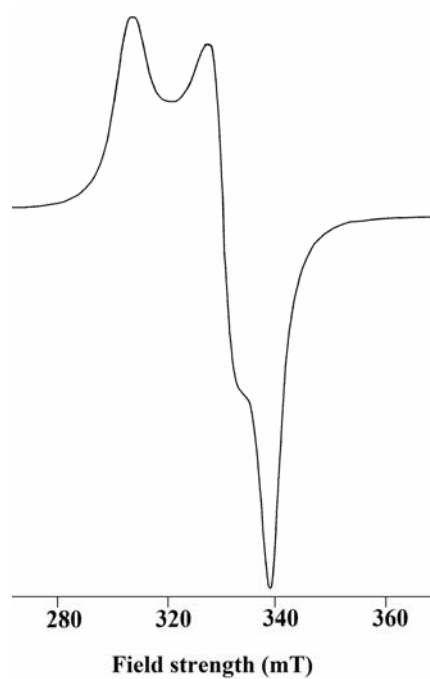
Fig. 6.29. The EPR spectrum of $[Cu(Qn)ClO_4]\cdot H_2O$ (**20**) in polycrystalline state at 298 K.
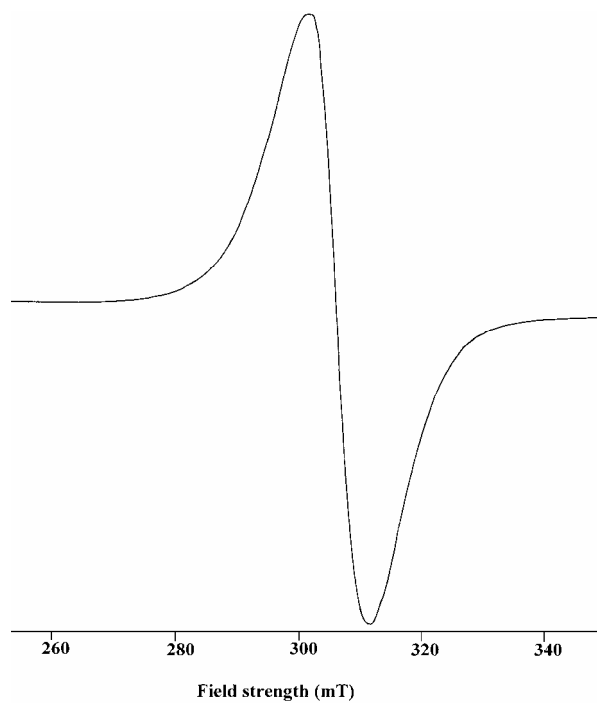
Fig. 6.30. The EPR spectrum of $[Cu(Qn)ClO_4]\cdot H_2O$ (**20**) in DMF at 77 K.

134

The EPR spectrum of $[Cu(Qn)ClO_4] \cdot H_2O$ (**20**) in DMF at 298 K is an isotropic one with $g_{iso} = 2.134$ and $A_{iso} = 59.78 \times 10^{-4}$ cm^{-1}. The four hyperfine lines can be clearly resolved from the spectrum and the spectrum is shown in Fig. 6.31.

Field strength (mT)
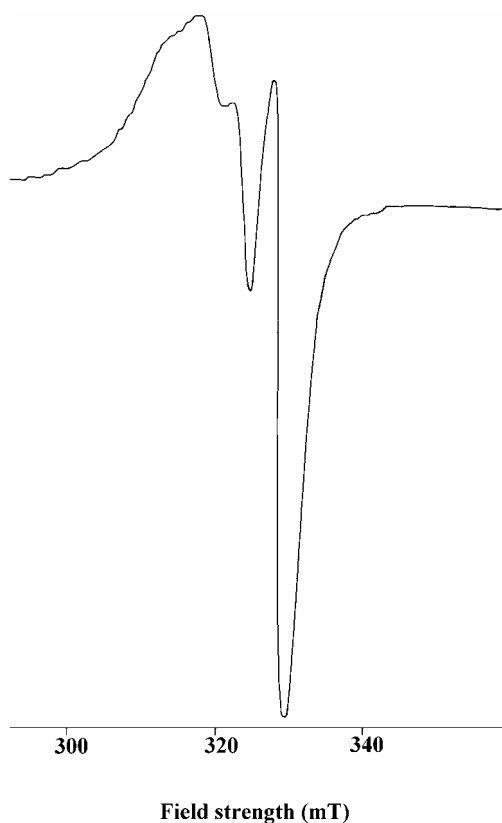
Fig. 6.31. The EPR spectrum of $[Cu(Qn)ClO_4] \cdot H_2O$ (**20**) in DMF at 298 K.

The complexes $[Cu(Qn)NCS] \cdot H_2O$ (**21**) and $[Cu(Qn)N_3] \cdot H_2O$ (**22**) in polycrystalline state at 298 K display exchange coupled EPR spectra with two *g* values (Figs. 6.32 and 6.33). One important factor which affects the line shape of EPR spectra in magnetically non-dilute systems is exchange coupling interaction. If this interaction is greater than thermal energy, partial spin-pairing may occur. As the observed magnetic moments for **21** and **22** are greater than the spin-only value, exchange coupling, if it does occur, must be less than thermal energy. In this case it primarily influences the line shape and does not reduce the magnetic moment below the spin-only value [27].

135
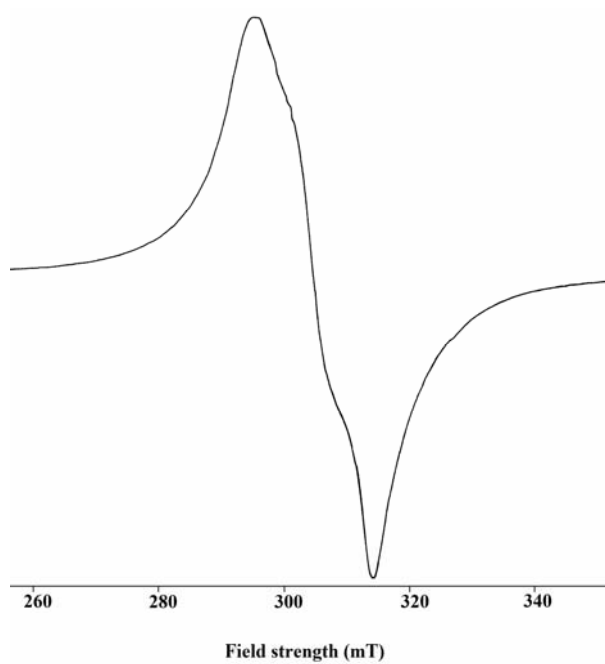
Fig. 6.32. The EPR spectrum of [Cu(Qn)NCS]·H_2O (**21**) in polycrystalline state at 298 K.
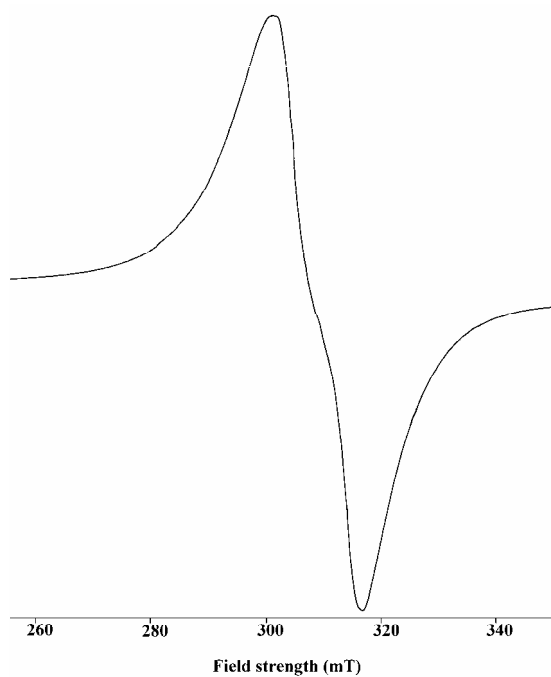
Fig. 6.33. The EPR spectrum of [Cu(Qn)N_3]·H_2O (**22**) in polycrystalline state at 298 K.

136

The compounds **21** and **22** exhibit axial spectra in DMF at 77 K. The EPR spectrum of $[Cu(Qn)NCS] \cdot H_2O$ (**21**) in DMF at 77 K is shown in Fig. 6.34.
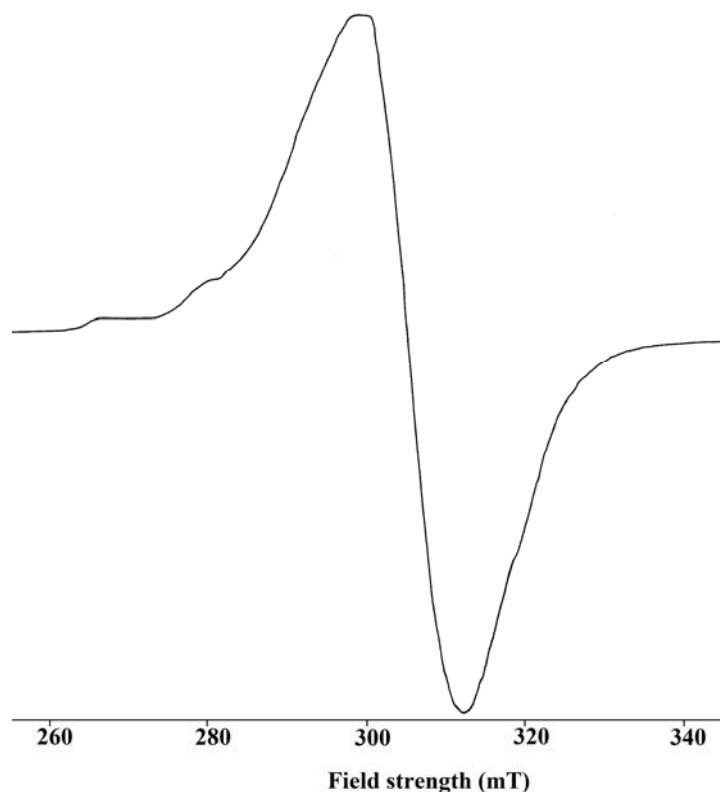
Fig. 6.34. The EPR spectrum of $[Cu(Qn)NCS] \cdot H_2O$ (**21**) in DMF at 77 K.

The EPR spectra of complexes **21** and **22** were also recorded in DMF at 298 K. Both spectra are isotropic and hyperfine structure cannot be resolved.

The EPR spectrum of $[Cu(HQn)Br_2]$ (**23**) is isotropic in the polycrystalline state at 298 K with $g_{iso} = 2.142$. At 77 K in DMF, it gives an axial spectrum (Fig. 6.35).

The g-value of a free electron is a scalar, $g_e = 2.00232$. In a radical species, g becomes a matrix because of the admixture of orbital angular momentum into spin angular momentum through spin-orbit coupling. The components of the g-matrix thus differ from g_e to the extent that p-, d- or f-

137

orbital character has been incorporated and differ from one another, depending on which *p-*, *d-* or *f-*orbitals are involved. The higher *g* value obtained in the present study, when compared to the *g* value of a free electron, indicates an increase of the covalent nature of the bonding between the metal ion and the ligand molecule [30].
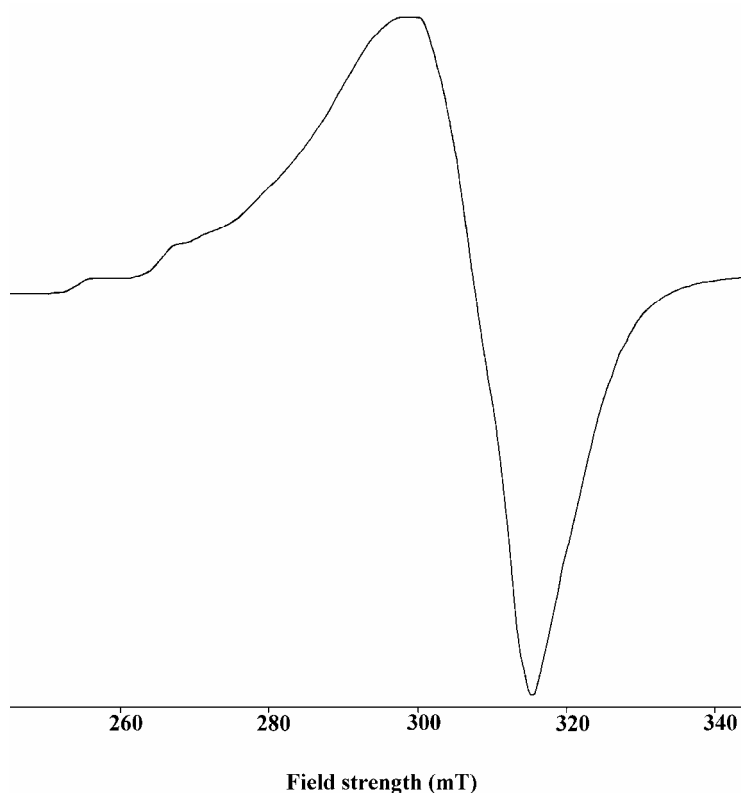
Fig. 6.35. The EPR spectrum of [Cu(HQn)Br$_2$] (**23**) in DMF at 77 K.

The $g_{\parallel}$ values of all the compounds are found to be almost the same, which indicates that the bonding is dominated by the hydrazone moiety. Kivelson and Nieman [31] have reported that $g_{\parallel}$ values less than 2.3 indicate considerable covalent character to metal-ligand bonds, while a value greater than 2.3 indicate ionic character. Here $g_{\parallel}$ values are found to be less than 2.3 for all complexes and hence considerable covalent character is expected to the M–L

138

bond. All the data measured from the EPR spectra of the copper(II) complexes in polycrystalline state at 298 K, in DMF at 298 K and in DMF at 77 K are consolidated in Tables 6.3 and 6.4.

Table 6.3. EPR spectral data of the complexes in polycrystalline state at 298 K.

Compound	g	g_{av}	G	R
[Cu(HQb)Cl$_2$] (**12**)	2.139 (g_{iso})	----	----	----
[Cu(Qb)$_2$] (**13**)	2.177 (g_{iso})	----	----	----
[Cu(Qb)NCS]·H$_2$O (**14**)	2.110 (g_{iso})	----	----	----
[Cu(Qb)N$_3$]$_2$·H$_2$O (**15**)	2.214/2.071 ($g_{\parallel}/g_{\perp}$)	2.119	3.082	----
[Cu(HQb)Br]$_2$Br$_2$ (**16**)	2.142 (g_{iso})	----	----	----
[Cu(HQn)Cl$_2$] (**17**)	2.214/2.131/2.060 ($g_3/g_2/g_1$)	2.135	2.272	0.86
[Cu(Qn)$_2$] (**18**)	2.185 (g_{iso})	----	----	----
[Cu(Qn)NO$_3$]·H$_2$O (**19**)	2.207/2.114/2.057 ($g_3/g_2/g_1$)	2.126	2.460	0.61
[Cu(Qn)ClO$_4$]·H$_2$O (**20**)	2.228/2.103/2.047 ($g_3/g_2/g_1$)	2.126	3.105	0.45
[Cu(Qn)NCS]·H$_2$O (**21**)	2.196/2.067 (g_2/g_1)	----	----	----
[Cu(Qn)N$_3$]·H$_2$O (**22**)	2.174/2.050 (g_2/g_1)	----	----	----
[Cu(HQn)Br$_2$] (**23**)	2.142	----	----	----

The empirical factor, $f = g_{\parallel} / A_{\parallel}$, is an index of tetragonal distortion and the value depends on the nature of the coordinated atom. The distortion from the plane increases with increasing $g_{\parallel}$ values and decreasing $A_{\parallel}$ values. So, the value of $g_{\parallel} / A_{\parallel}$ ratio is a good criterion to determine the distortion level [32]. In all the compounds, except **15**, **16** and **21**, f falls in the range 105−130 cm which shows small to medium distortion. High distortion occurs for the complexes **15**, **16** and **21**, which is evidenced from their f value (Table 6.5).

Table 6.4. EPR spectral data of the copper(II) complexes in DMF at 298 and 77 K.

Compound	DMF solution (298 K)		DMF solution (77 K)		
	g_{iso}	A_{iso} x 10^{-4} cm^{-1}	g	g_{av}	A x 10^{-4} cm^{-1}
[Cu(HQb)Cl$_2$] (**12**) Cu -I	-----	-----	$g_\parallel$ 2.257 $g_\perp$ 2.073	2.134	$A_\parallel$ 214.25
Cu-II			$g_\parallel$ 2.222 $g_\perp$ 2.073	2.123	$A_\parallel$ 179.81
[Cu(Qb)$_2$] (**13**)	-----	-----	$g_\parallel$ 2.163 $g_\perp$ 2.220	2.201	-----
[Cu(Qb)NCS]·H$_2$O (**14**)	-----	-----	$g_\parallel$ 2.212 $g_\perp$ 2.060	2.111	$A_\parallel$ 182.44
[Cu(Qb)N$_3$]$_2$·H$_2$O (**15**)	-----	-----	$g_\parallel$ 2.200 $g_\perp$ 2.067	2.111	$A_\parallel$ 130.1
[Cu(HQb)Br]$_2$Br$_2$ (**16**)	-----	-----	g_1 2.056 g_2 2.180 g_3 2.265	2.124	A_3 158.26
[Cu(HQn)Cl$_2$] (**17**)	2.124	36.39	$g_\parallel$ 2.219 $g_\perp$ 2.093	2.135	$A_\parallel$ 176.11
[Cu(Qn)$_2$] (**18**)	2.136	-----	g_{iso} 2.189	-----	-----
[Cu(Qn)NO$_3$]·H$_2$O (**19**)	2.264	130.32	$g_\parallel$ 2.241 $g_\perp$ 2.121	2.161	$A_\parallel$ 177.86
[Cu(Qn)ClO$_4$]·H$_2$O (**20**)	2.134	59.78	g_{iso} 2.137	-----	-----
[Cu(Qn)NCS]·H$_2$O (**21**)	2.133	-----	$g_\parallel$ 2.241 $g_\perp$ 2.121	2.161	$A_\parallel$ 156.93
[Cu(Qn)N$_3$]·H$_2$O (**22**)	2.190	-----	$g_\parallel$ 2.211 $g_\perp$ 2.103	2.139	$A_\parallel$ 182.39
[Cu(HQn)Br$_2$] (**23**)	-----	-----	$g_\parallel$ 2.280 $g_\perp$ 2.120	2.173	$A_\parallel$ 212.89

In order to understand the nature of metal–ligand bonding in the complexes, various bonding parameters have been evaluated from the low temperature EPR spectra and they are reported in Table 6.5.

The values of magnetic parameters and the energies of the electronic *d-d* transitions have been used for estimating the nature of the chemical bonding between the copper and donor atoms of the ligand. The fraction of unpaired electron density located on the copper ion *i.e.*, the value of in-plane sigma bonding parameter α^2 was estimated from the expression

$$\alpha^2 = -\frac{A_{\parallel}}{0.036} + (g_{\parallel} - 2.0023) + \frac{3(g_{\perp} - 2.0023)}{7} + 0.04$$

where $A_{\parallel}$ is the parallel coupling constant. The metal-ligand bond is purely ionic, if the value of α^2 is unity and it is completely covalent, if $\alpha^2 = 0.5$ [29,33]. The α^2 values for the complexes were calculated and found to be in between 0.5 and 1, which means that the metal-ligand bonds in the complexes under investigation are partially ionic and partially covalent in nature.

The orbital reduction factors $K_{\parallel}$ and $K_{\perp}$ are calculated using expressions:

$$K_{\parallel}^2 = (g_{\parallel} - 2.0023)\frac{\Delta E(d_{xy} \to d_{x^2-y^2})}{8\lambda_0}$$

$$K_{\perp}^2 = (g_{\perp} - 2.0023)\frac{\Delta E(d_{xz}, d_{yz} \to d_{x^2-y^2})}{2\lambda_0}$$

$$K_{\parallel} = \alpha^2\beta^2$$

$$K_{\perp} = \alpha^2\gamma^2$$

where λ_0 is the spin-orbit coupling constant and has a value –828 cm^{-1} for Cu(II) d^9 system, β^2, the in-plane π-bonding and γ^2, the out-of-plane π-bonding.

Hathaway proposed that, for pure σ bonding, $K_{\parallel} \sim K_{\perp} \sim 0.77$; for in-plane π-bonding, $K_{\parallel} < K_{\perp}$ and for out-of-plane π-bonding, $K_{\perp} < K_{\parallel}$. The $K_{\parallel}$ and $K_{\perp}$ values were calculated for the copper complexes and since in all complexes $K_{\parallel} < K_{\perp}$, stronger in-plane π-bonding is proposed in the present compounds [28-30].

Table 6.5. Bonding parameters of the copper(II) complexes.

Compound	α^2	β^2	γ^2	$K_{\parallel}$	$K_{\perp}$	$\dfrac{f}{cm}$
[Cu(HQb)Cl$_2$] (**12**) Cu-I	0.920	0.743	0.782	0.683	0.720	105.35
Cu-II	0.790	0.804	0.912	0.635	0.720	123.58
[Cu(Qb)$_2$] (**13**)	-----	-----	-----	-----	-----	-----
[Cu(Qb)NCS]·H$_2$O (**14**)	0.781	0.847	0.889	0.662	0.694	121.24
[Cu(Qb)N$_3$]$_2$·H$_2$O (**15**)	0.627	1.017	1.163	0.638	0.730	169.11
[Cu(HQb)Br]$_2$Br$_2$ (**16**)	0.819	0.841	1.383	0.688	1.132	143.12
[Cu(HQn)Cl$_2$] (**17**)	0.785	0.803	1.039	0.630	0.815	126.00
[Cu(Qn)$_2$] (**18**)	-----	-----	-----	-----	-----	-----
[Cu(Qn)NO$_3$]·H$_2$O (**19**)	0.824	0.783	1.105	0.645	0.910	126.00
[Cu(Qn)ClO$_4$]·H$_2$O (**20**)	-----	-----	-----	-----	-----	-----
[Cu(Qn)NCS]·H$_2$O (**21**)	0.766	0.923	1.301	0.706	0.996	142.80
[Cu(Qn)N$_3$]·H$_2$O (**22**)	0.799	0.698	1.198	0.558	0.957	121.22
[Cu(HQn)Br$_2$] (**23**)	0.959	0.743	0.967	0.713	0.928	107.10

The $g_{\parallel}$ values in all the complexes are less than 2.3 is an indication of significant covalent bonding in these complexes. Since $g_{\parallel} > g_{\perp}$, distorted square pyramidal structure is proposed for five coordinated complexes and rules out the possibility of a trigonal bipyramidal structure, which would be expected to have $g_{\parallel} < g_{\perp}$ [31,34].

References

[1]   M.A. Ali, D.A. Chowdhury, M. Nazimuddin, Polyhedron 3 (1984) 595.

[2]   C. Gosden, K.P. Healy, D. Pletcher, J. Chem. Soc. Dalton Trans. (1978) 972.

[3]   K.P. Healy, D. Pletcher, J. Organomet. Chem. 186 (1980) 401.

[4]   Z. Huszti, G. Szilagyi, E. Kasztreiner, Biochem. Pharmacol. 32 (1983) 627.

[5]   K.W. Penfield, R.R. Gay, R.S. Himmelwright, N.C. Eickman, V.A. Norris, H.C. Freeman, E.I. Solomon, J. Am. Chem. Soc. 103 (1981) 4382.

[6]   E.L. Ulrich, J.L. Markey, Coord. Chem. Rev. 27 (1978) 109.

[7]   T.B. Murphy, N.J. Rose, V. Schomaker, A. Aruffo, Inorg. Chim. Acta 108 (1985) 183.

[8]   I. Solomon, L.B. La Croix, D.W. Randall, Pure Appl. Chem. 70 (1998) 799.

[9]   K. Pierloot, J.O.A. De Kerpel, U. Ryde, M.H.M. Olsson, B.O. Roos, J. Am. Chem. Soc. 120 (1998) 13156.

[10]   R. Osterberg, Coord. Chem. Rev. 12 (1974) 309.

[11]   D.K. Johnson, T.B. Murphy, N.J. Rose, W.H. Goodwin, L. Picakrt, Inorg. Chim. Acta 67 (1982) 159.

[12]   E.W. Ainscough, A.M. Brodie, A.J. Dobbs, J.D. Ranford, Inorg. Chim. Acta 267 (1998) 27.

[13]   J.D. Ranford, J.J. Vittal, Yu.M. Wang, Inorg. Chem. 37 (1998) 1226.

[14]   W.J. Geary, Coord. Chem. Rev. 7 (1971) 81.

[15]   M. Joseph, M. Kuriakose, M.R.P. Kurup, E. Suresh, A. Kishore, S.G. Bhat, Polyhedron 25 (2006) 61.

[16]   M.B. Ferrari, G.G. Fara, M. Lafranchi, C. Pelizzi, M. Tarasconi, Inorg. Chim. Acta 181 (1991) 253.

[17]   Nakamoto, Infrared and Raman Spectra of Inorganic and Coordination Compounds, 5th Ed., Wiley, New York (1997).

[18]   P.B. Sreeja, M.R.P. Kurup, A. Kishore, C. Jasmin, Polyhedron 23 (2004) 575.

[19]   P.F. Rapheal, E. Manoj, M.R.P. Kurup, Polyhedron 26 (2006) 818.

[20]   K.B. Yatsimirskii, Pure and Appl. Chem. 49 (1977) 115.

[21]   R.A. Bailey, S.L. Kozak, T.W. Michelsen, W.N. Mills, Coord. Chem. Rev. 6 (1971) 407.

[22]   A.M. Bond, R.L. Martin, Coord. Chem. Rev. 54 (1984) 23.

[23]   E. Huheey, E.A. Keiter, R.L. Keiter, Inorganic Chemistry, Principles of Structure and Reactivity, 4th Ed., Harper Collins College Publishers, New York (1993).

[24]   B.J. Hathaway, Coord. Chem. Rev. 53 (1983) 87.

[25]   B.J. Hathaway, D.E. Billing, Coord. Chem. Rev. 5 (1970) 143.

[26]   A.Sreekanth, M.R.P. Kurup, Polyhedron 22 (2003) 3321.

[27]   I.M. Procter, B.J. Hathaway, P. Nicholls, J. Chem. Soc. (1968) 1678.

[28]   M.F. El-Shazly, A. El-Dissouky, T.M. Salem, M.M. Osman, Inorg. Chim. Acta 40 (1980) 1.

[29]   A.H. Maki, B.R. McGarvey. J. Chem. Phys. 29 (1958) 35.

[30]   R. Klement, F. Stock, H. Elias, H. Paulus, P. Pelikan, M. Valko, M. Mazur, Polyhedron 18 (1999) 3617.

[31]   D. Kivelson, R. Neiman, J. Chem. Phys. 35 (1961) 149.

[32]   S.I. Findone, K.W.H. Stevens, Proc. Phys. Soc. 73 (1959) 116.

[33]   B.J. Hathaway, Structure and Bonding, Springer Verlag, Heidelberg (1973) 60.

[34]   J.R. Wasson, C. Trapp. J. Phys. Chem. 73 (1969) 3763.

…..ౚ౬…..

SYNTHESES AND CHARACTERIZATION OF ZINC(II) COMPLEXES OF ACYLHYDRAZONES

Contents

7.1. Introduction

Zinc is present in most body cells of human beings, but its concentration is very low. Zinc(II) ion has been widely found in several metalloenzymes such as zinc-peptidases, human carbonic anhydrase and alkalinephosphatase [1]. Today more than 200 different zinc proteins are known which include numerous essential enzymes [2]. Metallothioneins, proteins containing zinc, remain unique in character and are encountered both in animals and microorganisms [3,4].

The emerging importance of Zn^{2+} in neurological signaling and some proposed functions in biological systems have generated an urgent demand for the development of Zn^{2+}-specific molecular probes and many Zn^{2+} fluorescent sensors have been reported, exhibiting high selectivity and sensitivity over other biologically essential metal ions in specific ranges of concentration [5-7].

The most widely used fluorescent probes for Zn^{2+} are TSQ (*N*-(6-methoxy-8-quinolyl)-*p*-toluenesulfonamide) and its congeners, which are quinoline derivatives

bearing sulfonamide groups that give substantial fluorescence enhancement upon Zn(II) bonding [8]. Recently, new selective Zn^{2+} fluorescent sensors, di(2-quinoline-carbaldehyde)-2,2'-bibenzoyl hydrazone and di(2-quinolinecarbaldehyde)-6,6'-dicarboxylic acid hydrazone-2,2'-bipyridine, have been reported [9].

Complexes of Zn(II) ion are of biological interest, since this metal is involved in many biomolecules. Zinc(II) acts as a Lewis acid and hence it can play a valuable role as a catalyst in hydrolysis reactions. The outer electronic configuration of Zn(II) ion is $3d^{10}$ and due to the presence of filled d sublevel, the bivalent state is highly stable. It shows high flexibility in the structure, coordination mode and coordination number of the complexes produced. The d^{10} configuration does not offer crystal field stabilization, which implies that the stereochemistry of a Zn^{2+} complex depends on the size and polarizing power of this ion. Considering the stereochemistry of the complexes, Zn(II) complexes are observed to be predominantly tetrahedral. Among the less common five-coordinate complexes, trigonal bipyramidal (TBP) geometry occurs more frequently than square pyramidal (SP) [10-12].

This chapter discusses on the syntheses and spectral characterization of zinc(II) complexes of the acylhydrazones derived from quinoline-2-carbaldehyde.

7.2. Experimental
7.2.1. Materials

All the chemicals and solvents used for the syntheses were of analytical grade. Quinoline-2-carbaldehyde (Aldrich), benzhydrazide (Aldrich), nicotinic hydrazide (Aldrich), zinc(II) acetate dihydrate (S. D. Fine), zinc(II) bromide (Riedel-de-Haen), potassium thiocyanate (Merck) and sodium azide (Reidel-De Haen) were used as received.

7.2.2. Syntheses of ligands

Preparation of the ligands were done as described previously in Chapter 2.

146

7.2.3. Syntheses of zinc(II) complexes

7.2.3a. *Synthesis of [Zn(Qb)$_2$] (24)*

HQb·1.5H$_2$O (0.606 g, 2 mmol) was dissolved in methanol (20 ml) by stirring and to this solution, Zn(CH$_3$COO)$_2$·2H$_2$O (0.219 g, 1 mmol) in methanol (20 ml) was added and refluxed the solution for 2 hours. The yellow precipitate of **24** obtained was washed with methanol followed by ether and then dried over P$_4$O$_{10}$ *in vacuo*. Yield: 56.6%. λ_m (DMF): 9 ohm^{-1} cm^2 mol^{-1}. Elemental Anal. Found (calcd.) (%): C, 66.69 (66.51); H, 4.10 (3.94); N, 13.68 (13.69) for [Zn(Qb)$_2$].

7.2.3b. *Synthesis of [Zn(HQb)Br$_2$] (25)*

ZnBr$_2$ (0.225 g, 1 mmol) was dissolved in methanol (20 ml) by stirring, which was added to a solution of HQb·1.5H$_2$O (0.303 g, 1 mmol) in methanol (20 ml). Then the mixture was refluxed for 2 hours. The yellow precipitate of **25** was obtained. The product was washed with methanol followed by ether and then dried over P$_4$O$_{10}$ *in vacuo*. Yield: 68.0%. λ_m (DMF): 17 ohm^{-1} cm^2 mol^{-1}. Elemental Anal. Found (calcd.) (%): C, 41.12 (40.79); H, 2.24 (2.62); N, 8.47 (8.40) for [Zn(HQb)Br$_2$].

7.2.3c. *Synthesis of [Zn(HQn)Br$_2$] (26)*

Compound **26** was prepared by the same procedure as that of compound **25**. Yield: 65.6%. λ_m (DMF): 11 ohm^{-1} cm^2 mol^{-1}. Elemental Anal. Found (calcd.) (%): C, 38.28 (38.32); H, 2.71 (2.41); N, 11.28 (11.17) for [Zn(HQn)Br$_2$].

7.2.3d. *Synthesis of [Zn(Qn)NCS]·H$_2$O (27)*

HQn·1.5H$_2$O (0.303 g, 1 mmol) was dissolved in methanol (20 ml) by stirring. To this solution, Zn(CH$_3$COO)$_2$·2H$_2$O (0.219 g, 1 mmol) and KSCN (0.097 g, 1 mmol) in methanol (20 ml) were added and refluxed the solution for 2 hours. The yellow precipitate of **27** was washed with methanol followed by ether and then dried over P$_4$O$_{10}$ *in vacuo*. Yield: 74.5%. λ_m (DMF): 22 ohm^{-1} cm^2 mol^{-1}. Elemental Anal. Found (calcd.) (%): C, 49.02 (48.99); H, 2.92 (3.14); N, 16.30 (16.80) for [Z(Qn)NCS]·H$_2$O.

7.2.3e. *Synthesis of [Zn(Qn)N₃] (**28**)*

Compound **28** was prepared by the same procedure as that of compound **27**, except that NaN$_3$ (0.065 g, 1 mmol) was used instead of KSCN. Yield: 78.8%. λ_m (DMF): 18 ohm^{-1} cm^2 mol^{-1}. Elemental Anal. Found (calcd.) (%): C, 50.70 (50.21); H, 2.71 (2.90); N, 25.38 (25.62) for [Zn(Qn)N$_3$].

Caution: Although not encountered in our experiments, azido complexes of metal ions with organic ligands are potentially explosive. Only a small amount of the material should be prepared and it should be handled with care.

7.3. Results and discussion

The reaction of quinoline-2-carbaldehyde with hydrazide in 1:1 ratio in methanol gives the corresponding hydrazone. The complexes were prepared by the reaction of the ligand with the metal salts in methanol. Based on the elemental analyses, conductivity measurements and spectral investigations, the complexes were formulated.

Five zinc(II) complexes of hydrazones were prepared and they are found to be yellow in color. In the compounds **25** and **26**, the hydrazone moieties are in the keto form, while in complexes **24**, **27** and **28**, the hydrazones deprotonate and chelate in the enolate form, which is confirmed by the IR spectral data. The molar conductivities of the complexes in DMF (10^{-3} M) solution were measured at 298 K with a Systronic model 303 direct-reading conductivity bridge which suggest that these complexes are non-electrolytes [13].

### 7.3.1. Infrared spectra

IR spectra were recorded on a Thermo Nicolet AVATAR 370 DTGS model FT-IR Spectrophotometer in the range 4000-400 cm^{-1} with KBr pellets and ATR technique at SAIF, Kochi, India.

The IR spectra of the metal complexes were compared with those of corresponding free ligands and significant variations have been observed in the characteristic frequencies upon complexation.

In the IR spectra of ligands and complexes, four bands appeared at *ca.* 1655, 1550, 1360 and 700 cm^{-1} corresponding to amide I [ν(C=O)], amide II [ν(C–N) + δ(N–H)], amide III [δ(N–H)] and amide IV [δ(C–O)], respectively. The band observed in 3420–3423 cm^{-1} range in the ligands and the complex **27** is assigned to lattice water molecule. The C–O stretching modes of the complexes **24**, **27** and **28**, formed due to enolization, appear in the 1325-1330 cm^{-1} range. The ν(N–H) vibration bands of the free ligands and complexes are observed near 3200 cm^{-1}.

The presence of ν(C=O) and ν(N–H) bands in complexes **25** and **26** indicates that the ligand coordinates to the metal in keto form. Also, an intense band located at 757 cm^{-1} is typical of aromatic ring vibrations. As expected, these bands are not much affected by chelation [14]. The IR spectra of complexes [Zn(Qb)$_2$] (**24**) and [Zn(HQb)Br$_2$] (**25**) are given in Figs. 7.1 and 7.2, respectively.
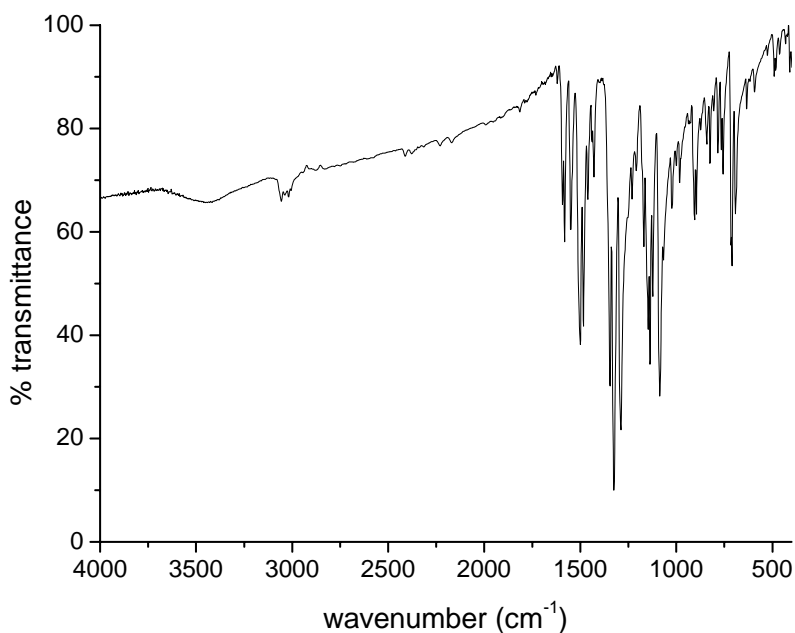
Fig. 7.1. IR spectrum of [Zn(Qb)$_2$] (**24**).

The expected region for zinc-halide stretching frequencies for complexes **25** and **26** is below 400 cm^{-1} which is beyond the scan range.

149

In the thiocyanato complex **27**, the strong band observed at 2096 cm^{-1} corresponds to ν(C=N). Bands observed at 785, 503 and 484 cm^{-1} are assigned to ν(C=S), δ(NCS) and ν(Zn–N), respectively. These facts indicate that thiocyanate group is N-coordinated to the metal [15]. The IR spectrum of [Zn(Qn)NCS]·H$_2$O (**27**) is shown in the Fig. 7.3.
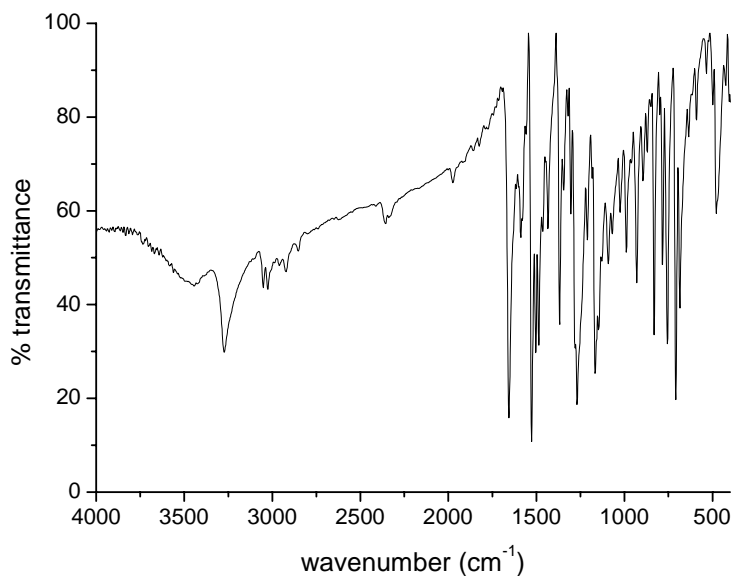
Fig. 7.2. IR spectrum of [Zn(HQb)Br$_2$] (**25**).
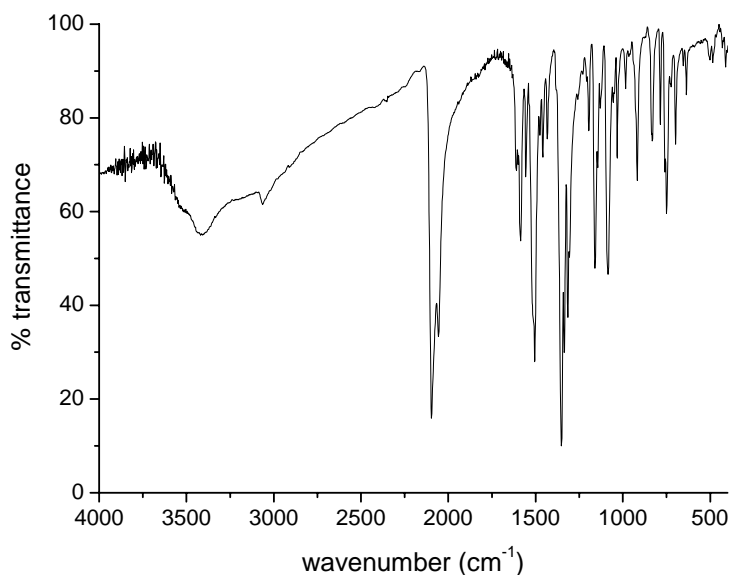
Fig. 7.3. IR spectrum of [Zn(Qn)NCS]·H$_2$O (**27**).

In the azido complex $[Zn(Qn)N_3]$ (**28**), a strong band observed at 2062 cm^{-1} and another one at 1310 cm^{-1} are assigned to ν_a and ν_s of the coordinated azido group. The bands at 635 and 485 cm^{-1} are assigned to δ(N–N–N) and ν(Zn–N$_{azido}$) bands [16]. The spectrum is shown in Fig. 7.4. The selected IR bands of the hydrazones and complexes are represented in Table 7.1.
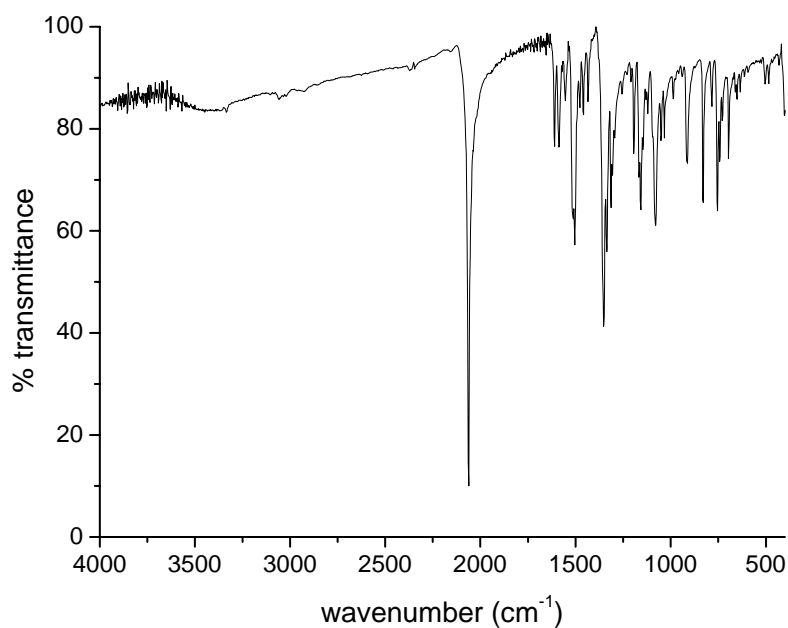
Fig. 7.4. IR spectrum of $[Zn(Qn)N_3]$ (**28**).

Table 7.1 Infrared spectral data of the hydrazones and their zinc(II) complexes

Compound	Amide I [v(C=O)] cm^{-1}	Amide II [v(C–N) + δ(N–H)] cm^{-1}	Amide III [δ(N–H)] cm^{-1}	Amide IV [δ(C–O)] cm^{-1}	v(N–H) cm^{-1}	v(C–O) cm^{-1}	v(N–N) cm^{-1}
HQb·1.5H$_2$O	1655	1560	1358	698	3193	----	1184
[Zn(Qb)$_2$] (**24**)	----	1550	1345	710	----	1325	1208
[Zn(HQb)Br$_2$] (**25**)	1656	1549	1368	708	3170	----	1210
HQn·1.5H$_2$O	1656	1559	1356	695	3173	----	1195
Zn(HQn)Br$_2$] (**26**)	1654	1556	1366	695	3180	----	1209
[Zn(Qn)NCS]·H$_2$O (**27**)	----	1556	1352	698	----	1336	1203
[Zn(Qn)N$_3$] (**28**)	----	1554	1352	696	----	1336	1204

7.3.2. Electronic spectra

The electronic spectra of the ligands and complexes were recorded in acetonitrile solutions on a UVD-3500, UV-vis Double Beam Spectrophotometer. The bands in the range 32000-44000 cm^{-1} are assigned to π-π^* transitions within the ligand moiety. The spectra show bands in the range 27000-32000 cm^{-1}, assignable to n-π^* transitions of the azomethine and amide functions. These intraligand bands are slightly shifted on complexation. The moderately intense broad band observed for the complexes in the region 23000-26000 cm^{-1} is assigned to Zn(II) $\rightarrow$ O transitions. MLCT maxima of the complexes show line broadening which extends to the visible part of the spectrum. This may result from a LMCT band being superimposed on the low energy side of MLCT transitions. No appreciable absorptions occurred below 20000 cm^{-1}, indicating the absence of *d–d* bands which is in accordance with the d^{10} configuration of the Zn(II) ion [17,18]. The electronic spectral data of the ligands and complexes recorded in acetonitrile solutions are summarized in Table 7.2. The spectra are shown in Figs. 7.5 and 7.6.
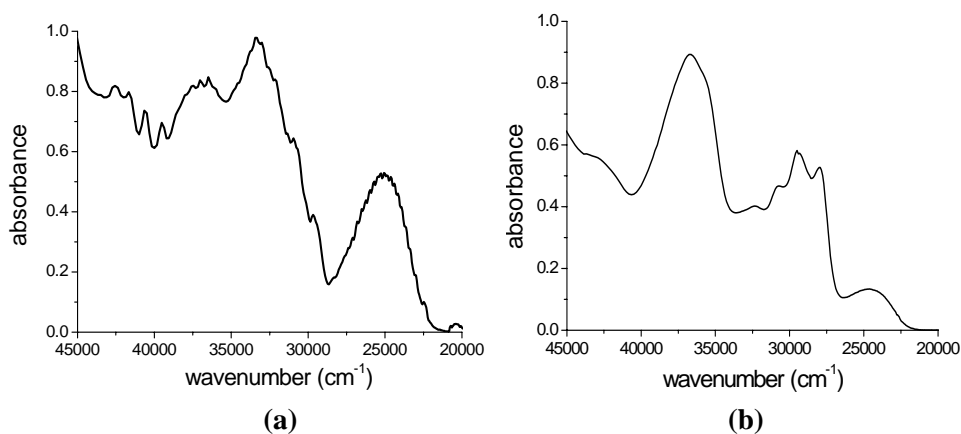
Fig. 7.5. Electronic spectra of (a) [Zn(Qb)$_2$] (**24**) and (b) [Zn(HQb)Br$_2$] (**25**).

(c)

(d)

(e)
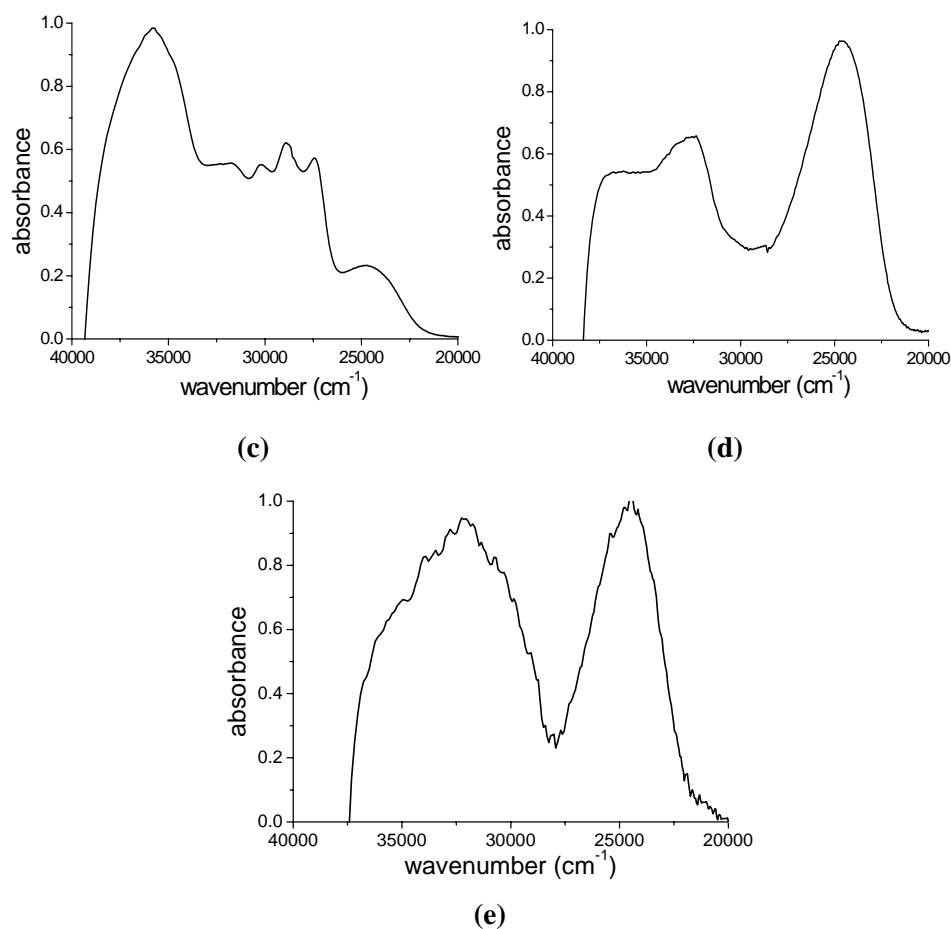
Fig.7.6. Electronic spectra of (c) [Zn(HQn)Br$_2$] (26), (d) [Zn(Qn)NCS]·H$_2$O (27) and (e) [Zn(Qn)N$_3$] (28).

Table 7.2. Electronic spectral data of the hydrazones and their zinc(II) complexes.

Compound	Absorbance λ_{max} (cm^{-1})
HQb·1.5H$_2$O	43790, 41640, 35860, 32580, 31690, 30430, 29130
[Zn(Qb)$_2$] (**24**)	42520, 40780, 39470, 36740, 33260, 30970, 29580, 25110
[Zn(HQb)Br$_2$] (**25**)	43070, 36680, 32400, 30710, 29470, 28030, 24690
HQn·1.5H$_2$O	43920, 41490, 35840, 32580, 31750, 30440, 29150
[Zn(HQn)Br$_2$] (**26**)	35820, 31740, 30180, 28860, 27480, 24750
[Zn(Qn)NCS]·H$_2$O (**27**)	36780, 32760, 28800, 24580
[Zn(Qn)N$_3$] (**28**)	35170, 33820, 32140, 30650, 29010, 24470

154

References

[1]   D.C. Rees, M. Lewis, W.N. Lipscomb, J. Mol. Biol. 168 (1983) 367.

[2]   W. Kaim, B. Schwderski, Bioinorganic Chemistry, Inorganic Elements in the Chemistry of Life, Wiley, New York (1991).

[3]   D. Bryce-Smith, Chem. Brit. 25 (1989) 783.

[4]   B.C. Cunningham, M.G. Mulkerrin, J.A. Wells, Dimerization of human growth hormone by zinc, Science, 253 (1991) 545.

[5]   B.L. Vallee, K.H. Falchuk, Physiol. Rev. 73 (1993) 79.

[6]   C.J. Chang, E.M. Nolan, J. Jaworski, S.C. Burdette, M. Sheng, S.J. Lippard, Chem. Biol. 11 (2004) 203.

[7]   A. Ajayaghosh, P. Carol, S. Sreejith, J. Am. Chem. Soc., 127 (2005) 14962.

[8]   P.J. Jiang, L. Chen, J. Lin, Q. Liu, J. Ding, X. Gao, Z.J. Guo, Chem. Commun. (2002) 1424.

[9]   D.-Y. Wu, L.-X. Xie, C.-L. Zhang, C.-Y. Duan, Y.-G. Zhao, Z.-J. Guo, J. Chem. Soc. Dalton Trans. (2006) 3528.

[10]   Z. Li, Z. –H. Loh, S. –W. A. Fong, Y. –K. Yan, W. Henderson, K. F. Mok, T. S. A. Hor, J. Chem. Soc., Dalton Trans. (2000) 1027.

[11]   S. Padhye, G.B. Kauffman, Coord. Chem. Rev. 63 (1985) 127.

[12]   T. Matsukura, H. Tanaka, Biochemistry 65 (2000) 817.

[13]   W.J. Geary, Coord. Chem. Rev. 7 (1971) 81.

[14]   K. Nakamoto, Infrared and Raman Spectra of Inorganic and Coordination Compounds, 5th Ed., Wiley, New York (1997).

[15]   D.X. West, G. Ertem, R.M. Makeever, Transit. Met. Chem. 10 (1986) 41.

[16]   R. Raina, T.S. Srivastava, Ind. J. Chem. 22A (1983) 701.

[17]   V. Philip, V. Suni, M.R.P. Kurup, Polyhedron 25 (2006) 1931.

[18]   I.-X. Li, H.A. Tang, Yi-Zhi Li, M. Wang, L.-F. Wang, C.-G. Xia, J. Inorg. Biochem. 78 (2000) 167.

…..ജൻ…..

SUMMARY AND CONCLUSION

Coordination chemistry is a challenging field in inorganic chemistry and has evolved as an important subject area in current research activities. The recent surge in the popularity of coordination compounds is their perceived applications in many areas such as catalysis, analytical chemistry and medicine. Coordination complexes show diversity in structures depending on the metal ion, its coordination number and the denticity of the ligands used. The presence of more electronegative nitrogen and oxygen on the ligand is established to enhance the coordinating possibilities of ligands. Hence the coordination chemistry of nitrogen-oxygen donor ligands is an interesting area of research. In this aspect, a great deal of attention has been focused on the complexes formed by transition metal ions with hydrazones.

Hydrazones are compounds derived from hydrazides ($RNH–NH_2$) as a result of condensation with an aldehyde or ketone. Again, attaching groups with potential donor sites increase the denticity of these hydrazones. One such group is the $–C=O$ group which also makes possible an electron delocalization. The presence of potential donor sites in the ketone or aldehyde chosen, gives a multidentate ligand. These can function as chelating agents, complexing with transition or main group metals producing complexes with versatile stereochemistries, applications and with enhanced bioactivity compared to the parental ligands. An attractive aspect of the hydrazones is that they are capable of exhibiting tautomerism. In the solid state, the compound predominantly exists in the keto form, whereas in the solution state the enolate form predominates. Upon metal complexation, the ligand can bind to the central metal ion in keto form or in enolate form depending on the reaction conditions and nature of the ligand.

157

Objectives of the present work

The chemical properties of hydrazones and their complexes are widely explored in recent years; owing to their coordinative capability, their pharmacological activity and their use in analytical chemistry as metal extracting agents. The present work is mainly concerned with the studies on metal complexes of hydrazones derived from quinoline-2-carbaldehyde. Here, quinoline-2-carbaldehyde benzoyl hydrazone (HQb) and quinoline-2-carbaldehyde nicotinic hydrazone (HQn) were selected as ligands. The coordination modes of the ligands with transition metals have been investigated by using different physicochemical techniques.

The chapter wise summary of the thesis is the following:

The thesis is divided into seven chapters.

Chapter 1, entitled 'a concise of acylhydrazones and their metal complexes' describes importance of hydrazones, their mode of coordination and the relevance of present investigation. The details of the different analytical techniques used for the characterization is also presented in this chapter

Chapter 2 explains the preparation of the hydrazones and their physicochemical investigations.

The hydrazones synthesized were:

1. Quinoline-2-carbaldehyde benzoyl hydrazone (HQb)
2. Quinoline-2-carbaldehyde nicotinic hydrazone (HQn)

The acylhydrazones consist of two nitrogen and one oxygen atoms, capable of coordination with the metal ion. They were characterized by ^{1}H NMR, ^{1}H-^{1}H COSY, ^{13}C NMR, ^{1}H-^{13}C HSQC, IR and electronic spectral studies. We could successfully isolate the single crystal of HQb·H$_2$O. The single crystal X-ray diffraction studies of the hydrazone reveal that the molecule is roughly planar and exists in keto form.

Chapter 3 describes the synthesis and characterization of two V(IV) complexes of the acylhydrazones. Both the compounds were characterized by various spectroscopic techniques such as IR, electronic and EPR. The magnetic moments of the complexes were calculated from magnetic susceptibility measurements. The acylhydrazones are found to coordinate in the neutral keto form in one complex and in enolate form in the other one. The EPR spectra of the complexes displayed axial features with eight hyperfine splitting lines.

Chapter 4 deals with the synthesis and characterization of four Mn(II) compounds. The IR, electronic and EPR spectral studies and cyclic voltammetry of all the complexes were done. The magnetic moments of the complexes indicate that they are d^5 high spin system. The acylhydrazones can coordinate either in the keto form or in the enolate form and both types of coordination modes were found in the Mn(II) complexes.

Chapter 5 illustrates the procedure followed for the preparation of the complexes of five cobalt(II) and their physicochemical investigations. The complexes were characterized by IR spectroscopy, electronic spectral studies and cyclic voltammetry. In all the complexes, the acylhydrazones are coordinated in the enolate form.

Chapter 6 deals with the synthesis of twelve Cu(II) compounds and their characterization by IR, electronic spectral studies and EPR. The ligands were found to coordinate in the neutral keto form and in enolate form. The magnetic susceptibility measurements were also done. In the electronic spectral studies, the *d-d* transitions were found to be broad. So the three *d-d* transitions could not be assigned. The IR spectral studies revealed that the azomethine bands are shifted as a result of its coordination to the metal centre. The EPR spectra of the Cu(II) complexes were recorded in polycrystalline state at 298, in DMF at 298 and at 77 K. The *g* values and the various EPR spectral parameters were calculated. The *g* values indicate that in most of the complexes the unpaired electron is situated in the $d_{x^2-y^2}$ orbital.

159

Chapter 7 describes the synthesis and characterization of five Zn(II) compounds using IR and electronic spectral studies. All the Zn(II) complexes are yellow in color and the ligands are found to be coordinated in the enolate form or in keto form.

…..ഇനി…..

SHEEJA S. R
Sreenilayam (H)
Valayanchirangara P.O.
Perumbavoor
Ernakulam   *E-mail: sheejasr@gmail.com*
Kerala-683556   *sheejasr@cusat.ac.in*

JOB PROFILE

Working as lecturer in Chemistry at Government College, Kodanchery, Kozhikode.

ACADEMIC PROFILE

Pursuing Ph.D (Inorganic Chemistry)
(2006 – present)
Topic of work: **Studies on metal complexes with acylhydrazones based on heterocyclic carbonyl compounds.**
Supervising Guide : Dr. M.R. Prathapachandra Kurup
                              Professor
                              Dept. of Applied Chemistry
                              Cochin University of Science & Technology
                              Kochi - 22
                              Kerala, India

Master of Science
Percent –73.7 (2001-2003)
Nirmala College, Muvattupuzha
Mahatma Gandhi University, Kottayam

Bachelor of Science (Petrochemicals)
Percent – 83.7 (1998-2001)
Al-Ameen College, Edathala
Mahatma Gandhi University, Kottayam

Pre-Degree
Percent – 84.8 (1996-1998)
Sree Sankara Vidyapeetham College, Airapurm, Perumbavoor
Mahatma Gandhi University, Kottayam

SSLC
Percent – 84 (1996)
Higher Secondary School, Valayanchirangara, Perumbavoor.

ADDITIONAL QUALIFICATIONS

CSIR-UGC (NET) for Lectureship December 2002
CSIR-JRF (NET) June 2005
Candidate for Shyama Prasad Mukherjee (SPM) Fellowship Test July 2006

RESEARCH EXPERIENCE

- More than four years of research experience in the field of coordination complexes of hydrazones.

TEACHING EXPERIENCE

- Lecturer in Chemistry at Govt. College, Kodanchery (01/06/2010-present)
- Lecturer in Chemistry at Govt. College, Kottayam (17/02/2010-31/05/2010)
- Lecturer in Chemistry at Amrita Viswavidyapeetham University, Amritapuri, Kollam (01/07/2009-15/02/2010)
- Guest lecturer in Chemistry at Sree Sankara College, Kalady (13/01/2004-07/01/2006)

COMPUTING SKILLS

- Expertise in MS-Office
- Chemsketch, origin
- Familiar with crystallographic softwares
- Proficient in EPR simulation pachage

PERSONAL PROFILE

Father's name	H. Raman Namboothiri
Husband's name	Ratheesh P. M.
Date of Birth	15-07-1980
Gender	Female
Marital Status	Married
Nationality	Indian
Languages Known	English, Hindi, Malayalam
Present address	Pakkath Illam
	Thamarassery P. O.
	Kozhikode
	Kerala 673573

RESEARCH PAPERS PUBLISHED/COMMUNICATED

1. Chemistry of molecular and supramolecular structures of vanadium (IV) and dioxygen-bridged V(V) complexes incorporating tridentate hydrazone ligands, N.A. Mangalam, S. Sivakumar, S.R. Sheeja, M.R.P. Kurup, E.R.T. Tiekink, Inorg. Chim. Acta 362 (2009) 4191.

2. Vibrational spectroscopic studies and computational study of quinoline-2-carbaldehyde benzoyl hydrazone, S.R. Sheeja, N.A. Mangalam, M.R.P. Kurup, Y.S. Mary, K. Raju, H.T. Varghese, C.Y. Panicker, J. Mol. Struct., 973 (2010) 36.

3. Mn(II) complexes of some aroylhydrazones with NNO donor sites: Syntheses, a spectroscopic view on their coordination possibilities and crystal structures, N. A. Mangalam, S.R. Sheeja, M.R.P. Kurup, Polyhedron, communicated.

CONFERENCES

International Conference on Coordination and Organometallic Chemistry (ICCOC 2009), Department of Chemistry, Bharathiar University, Coimbatore, India.

…..೮೧…..